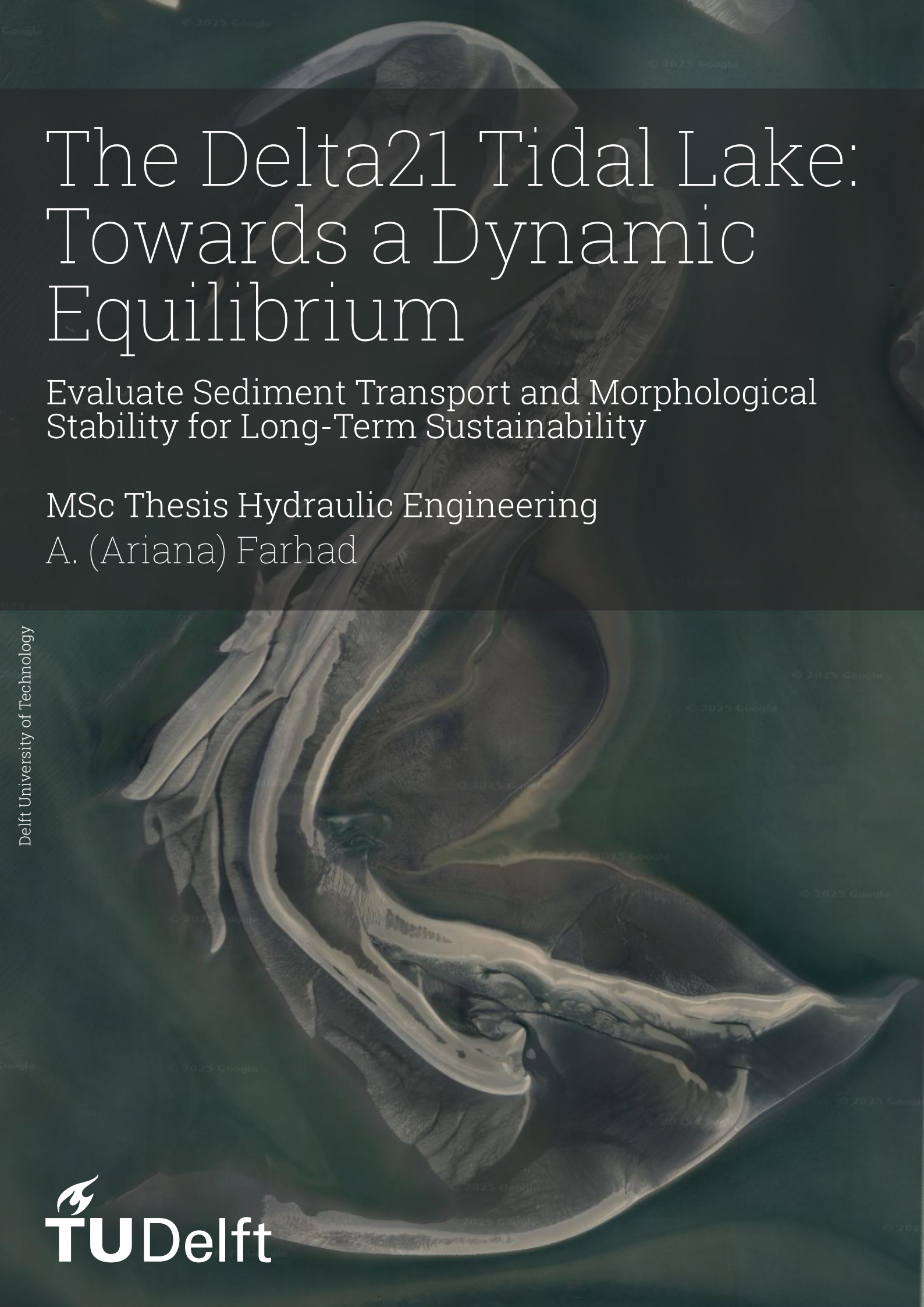

The Delta21 Tidal Lake: Towards a Dynamic Equilibrium

Evaluate Sediment Transport and Morphological Stability for Long-Term Sustainability

MSc Thesis Hydraulic Engineering

A. (Ariana) Farhad

Delft University of Technology

TU Delft

The Delta21 Tidal Lake: Towards a Dynamic Equilibrium

Evaluate Sediment Transport and Morphological Stability for Long-Term Sustainability

by

A. (Ariana) Farhad

to obtain the degree of Master of Science

at the Delft University of Technology,

to be defended publicly on Monday December 15, 2025 at 16:00 PM.

Student number:	5645581	
Project duration:	April 22, 2025 – December 15, 2025	
Thesis committee:	Prof. dr. ir. Z.B. Wang,	TU Delft, chair
	Dr. ing. M.Z. Voorendt,	TU Delft
	Ir. L.E. Panagopoulos	Van Oord
Thesis advisors:	Ir. H.A. Lavooij,	Delta21bv

Cover: Google Earth: Picture of the Hinterplaat

DELTA 21

TU Delft

Van Oord
Marine ingenuity

Acknowledgements

With this research I finish my Master at the Technical University of Delft which I am very proud of. I chose to start studying again after my bachelor because I wanted to dive deep into the knowledge existing about water and the interaction with their surrounding. To fundamentally understand the behavior of water which is all around us. I believe studying natural dynamics makes you appreciate the world around you and let you see the beauty of it. I am grateful for all the interesting lectures and inspiration delivered by TU Delft.

This research would not exist without the idea of Delta21 created by Leen Berke and Huub Lavooij. Thank you for collaborating with students and giving them the opportunity to work on innovative solutions. Therefore also Dick van den Heuvel and Wouter Ockeloen to introduce me to Van Oord and Loukianos Panagolpoulos to supervise me throughout my thesis writing. The weekly meetings helped me to stay motivated during the thesis writing. I felt directly very welcome in this company and have met a lot of other Engineers within Van Oord who took the time to get to know me and gave me advice when needed.

For this research it was my task to organize a committee which I think is something very special. Thank you Zheng Bing Wang and Mark Voorendt for the willingness of guiding me through this thesis writing. I appreciate the knowledge shared and the feedback given.

I want to thank my family, my mother and sister, with all my heart <3. They are my biggest fans and support every step I take. Definitely also my second family, which are my friends. They are the ones who know me the best and were up to date about even the smallest things. One last word of appreciation to my study friends because we share the same experiences for a few years. They made studying enjoyable with a lot of laughs.

A. (Ariana) Farhad
Delft, December 2025

Summary

The goal of this research is to understand the impact of the Delta21 construction on the hydrology and morphology of the current situation. Such understanding helps reveal how the system moves toward a dynamic equilibrium, which is crucial for developing a stable tidal lake. The study employs numerical modeling using Delft3D to simulate the hydrodynamics and sediment transport within the system. The effects of the inlet width and hydraulic forces on sediment transport and bed evolution are investigated to identify how these factors control erosion, sedimentation and long-term morphological changes.

The model focuses on three main hydraulic forces: tidal motion, river discharge, and operational flows from pumps and turbines. To simplify the system, wind and wave effects are excluded, as the Delta21 construction largely protects the tidal lake from incoming waves. A representative tide is imposed, neglecting spring–neap tidal variability, and river discharge is held constant at $1000\,m^3/s$. Pumps and turbines are modeled using maximum discharges rather than realistic fluctuating operations. The sediment transport is limited to sand with a median grain size of $160\,\mu m$, with only a single hydrodynamic layer and one active sediment layer. These simplifications allow the study to capture general morphodynamic trends while recognizing that small-scale and those involving finer sediments or varying tides and river flows, are not resolved.

Results show that inlet dimensions critically control flow velocities and sediment dynamics. Narrow inlets accelerate flow, causing substantial erosion, while wider inlets reduce velocities and promote deposition. Because the inlet is a fixed hard structure, the width cannot adjust naturally; the only way for the system to increase the inlet cross-section is by eroding its bed. The equilibrium depth emerged as a key concept: it represents the depth at which erosion stops. Once this depth is reached, cumulative sediment transport patterns indicate that the system may begin importing sediment from outside, suggesting a potential shift toward flood-dominant behavior. In the simulations, only the 2000 m inlet without river discharge approached equilibrium and showed signs of flood-dominant sediment transport. The 1500 m inlet eroded toward equilibrium but had not yet shifted to flood dominance, while all scenarios with river discharge remained ebb-dominant, exporting sediment.

Future developments, such as sea level rise and increasing extreme river discharges, influence morphological stability. Sea level rise drives long-term sediment loss, whereas extreme discharges induce short-term sediment redistribution inside the tidal lake. These findings highlight the importance of designing inlet dimensions to maintain flow velocities near the critical threshold for sediment transport and of understanding equilibrium depth dynamics to guide the system toward long-term morphological stability.

In conclusion, the research demonstrates that inlet geometry and hydraulic forcing strongly influence the morphodynamic evolution of the tidal lake. Simplified numerical models, informed by natural system analogies, can effectively support the design of engineered tidal lakes and provide insight into the hydrodynamic and morphodynamic processes that control inlet evolution, sediment transport, and overall system stability.

Contents

Nomenclature

Abbreviation	Definition
D21	Delta21 project / coastal system concept
HW	High Water
HWS	High Water Slack
LW	Low Water
LWS	Low Water Slack
M2	Principal lunar semidiurnal tidal constituent

Symbol	Definition	Unit
A	Intertidal flat area in cross-section	[m^2]
A_b	Basin surface area (total)	[m^2]
$A_{b,HW}$	Basin wet surface area at high water	[m^2]
$A_{b,LW}$	Basin wet surface area at low water	[m^2]
A_e	Cross-sectional area of tidal inlet	[m^2]
A_{fe}	Equilibrium tidal flat area	[m^2]
A_s	Subtidal channel area in cross-section	[m^2]
a	Tidal amplitude	[m]
c	Shallow-water wave celerity	[m/s]
C_{od}	Empirical coefficient for outer delta volume relation	[$m^{-0.69}$]
g	Gravitational acceleration	[m/s^2]
h	Water depth	[m]
h_{fe}	Equilibrium tidal-flat height	[m]
P	Tidal prism	[m^3]
P_{ebb}	Ebb tidal prism (including river discharge)	[m^3]
Q	Total discharge (tidal + river)	[m^3/s]
Q_r	River discharge	[m^3/s]
Q_t	Tidal discharge	[m^3/s]
R	Hydraulic radius	[m]
r	Friction coefficient in wave–diffusion equation	[m/s^2]
T	Tidal period	[s]
u	Tidal velocity	[m/s]
$\hat{u}_e$	Amplitude of cross-sectionally averaged entrance velocity	[m/s]
V_c	Channel volume	[m^3]
V_{ce}	Equilibrium channel volume	[m^3]
V_{fe}	Equilibrium tidal-flat volume	[m^3]
V_{od}	Ebb-tidal delta volume	[m^3]
V_s	Intertidal storage volume	[m^3]
α_c	Empirical coefficient for channel–prism relation	[–]
α_f	Empirical coefficient for tidal-flat geometry (0.41)	[–]
α_{fe}	Empirical coefficient for equilibrium tidal-flat height	[–]
η	Oscillatory / tidal water level	[m]
φ	Phase difference between elevation and velocity	[rad]

1
Introduction and Research Approach

1.1. Problem analysis

After the 1953 flood disaster in the Netherlands, a series of Delta Works was built to protect the land in the future. One of these structures is the Haringvliet dam, located in the southwest of the Netherlands. This dam includes large sluice gates (spuisluizen), designed to regulate freshwater outflow and protect inland areas from storm surges and saltwater intrusion (Rijkswaterstaat, 2015). By closing off the estuary from the open sea, the Haringvliet transformed from a tidal estuary into a controlled freshwater basin, which changed the hydrology, morphology, and ecology of the region.

One of the most immediate changes was the loss of natural tidal movement. The estuarine landscape was shaped by a tidal range that once varied by nearly two meters. This range has now reduced to almost zero (Storm et al., 2006). A consequence of this barrier was that the constant mixing process of freshwater from the river and saltwater from the North Sea was disrupted and transformed to a rigid separation of fresh and salt water. The Haringvliet no longer functioned as a true estuary but as a controlled discharge point for river water, where flow was regulated by upstream conditions rather than natural tidal forces. The result is a decrease in biodiversity and a strong reduction in fish migration.

The absence of strong tidal currents and dominant wave forcing resulted in the accumulation of silt and sand, particularly at the mouth of the Haringvliet. Studies have documented that, after closure, sedimentation rates increased, leading to infilling of channels and a reduction in seabed depth (Delta21, 2023). This created the need for continuous dredging of the channel to maintain a certain depth. When analyzing satellite pictures throughout the years after the construction of the Maasvlakte 1, 2 and the Deltawerken, we can clearly see the infilling of the Haringvliet mouth. Figure 1.1 shows the satellite pictures where sediment deposition is growing land inwards.

Figure 1.1: Haringvliet through the years (Google LLC, 2025) Google Earth snapshots from 1984 until 2020 are used to visualize the sediment transport. The construction of the Maasvlakte 2 can be seen and the movement of the sandbanks onshore.

Since the anthropogenic influences, the delta in front of the Haringvliet mouth has been changing towards a new equilibrium. The morphological study done by Arcadis (Arcadis et al., 2024) for this area concludes that the infilling of the mouth will continue because of the wave forcing. From recreational point of view, this means that the beaches in this area, for example Rockanje, will silt up when no action is taken. As the affected area is large, a lot of stakeholders are involved and need to be prepared for a large environmental change.

Over the recent years, Nature-based solutions are becoming more common and defined as an alternative for hard structures along the coast. The effect of working with nature instead of against it becomes more evident and has benefits in different aspects. Nature-based solutions make use of the power of natural systems and can be used to tackle ecological and social problems. By restoring the ecosystems, we strengthen the resilience of the coastline and stimulate sustainable innovations. For this reason it is recommended to design, investigate and implement building with nature solutions.

Deltas around the world are threatened by climate change, leading to extreme river discharges and more frequent storm events in combination with sea level rise and land subsidence (KNMI, 2023). One of the initiatives to address flood protection, renewable energy storage and ecological restoration in the Haringvliet region is the Delta21 project designed by Leen Berke and Huub Lavooij. The project integrates several key components to enhance climate resilience while simultaneously improving biodiversity and sustainable energy production. One of the key elements of the project is the creation of a Tidal Lake (Getijmeer) with a direct connection to the North Sea, reintroducing natural estuarine dynamics and allowing saltwater intrusion in a controlled manner.

The development of the Delta21 project may drastically change the hydrodynamics and morphodynamics in this area and research is needed to understand these changes. The creation of a Tidal Lake with mudflats, creeks and vegetation is highly dependent on the forcings in this area. These forces again depend on the design of the Tidal Lake. For this reason, this report describes the research on optimizing the design of the Tidal Lake to create stable balances in this area.

1.2. Research goal and Research questions

Research goal

The goal of this research is to understand the impact of the Delta21 construction on the hydrology and morphology of the current situation. It is necessary to research the morphological feedback's right after construction and over longer periods as tidal basins are dynamic systems with long response times. Understanding the impact of each element or control in the Delta21 construction on sediment transport, will give direction towards the equilibrium state the new system is moving to. One of the Delta21 project goals is to realize a tidal lake with marshes and tidal flats in salt brackish water, as shown in Figure 1.2. Therefore, understanding the impact of the Delta21 construction on the area will give insight if and how this preferred vision of the tidal lake can be achieved.

Figure 1.2: Vision of the Delta21 tidal lake, older layout by Esmee van Eeden

Research scope

This research does not cover the entire Delta21 project, but focuses on the creation of the tidal lake between the energy storage lake and the Haringvliet. For the tidal lake, the research describes the hydraulic and morphological changes and does not focus on creating a brackish zone or vegetated tidal flats from ecological point of view. The creation of the tidal lake can be achieved by understanding the processes that determine the final equilibrium state. Reaching the final equilibrium state of a system is a long term process which can take several years. Because most changes happen in the first few years after distortion of the system, the maximum morphological research time is narrowed down to 5 years for long-term changes. This reduces the simulation time where predictions for the longer term can still be made.

A combination of literature review and a depth-averaged (2DH) Delft3D model is used to evaluate the system. For this research only the Flow module of Delft3D is used where the effect of waves and wind is outside the scope. The hydraulic forces present in the system will be described and simplified to create simple schematizations of the system. Therefore, this research does not give results based on detailed varying discharges, but constant values. Also the bed composition is simplified to one sediment size neglecting the differences in sediment transport for fine and medium grain sizes.

The Delft3D model helps to understand the effect of the Delta21 project on the area by adding the controls one by one. These results are evaluated but are not used again to optimize the design of the Delta21 construction. For example, the response of the tidal lake to three different inlet sizes are evaluated by comparing it towards each other.

Research questions

The main research question is formulated as:

"How can a dynamically stable tidal lake be developed in the Delta21 project by optimizing inlet (storm surge barrier) size considering long-term morphological evolution under sea level rise and varying river discharge?"

Knowledge-Based sub-questions (Literature Review):

- What are the key sediment transport mechanisms in tidal lakes and estuarine systems?
- What physical relationships describe equilibrium in tidal basins (between tidal prism, basin area, channel volume, and inlet size)?
- How does inlet size (cross-sectional area) influence flow velocities and sediment transport capacity in human-made tidal basins?

Research-Based sub-questions (Modeling and Analysis):

- How does inlet width influence flow velocities and sediment transport capacity in human-made tidal basins?
- How do future developments (sea level rise and extreme river discharge events) impact the morphological stability of the lake?
- What combination of inlet dimensions and sediment placement leads to the fastest development toward a stable tidal system?

The literature review will establish theoretical foundations, while numerical modeling will test different scenarios to evaluate the feasibility of a stable tidal lake.

1.3. Approach and outline of thesis

To answer the main research question, this report is subdivided into simple chronological steps. This structure is shown in Figure 1.3 where the sub-questions can be answered throughout the report. Each step is explained in the text below the figure.

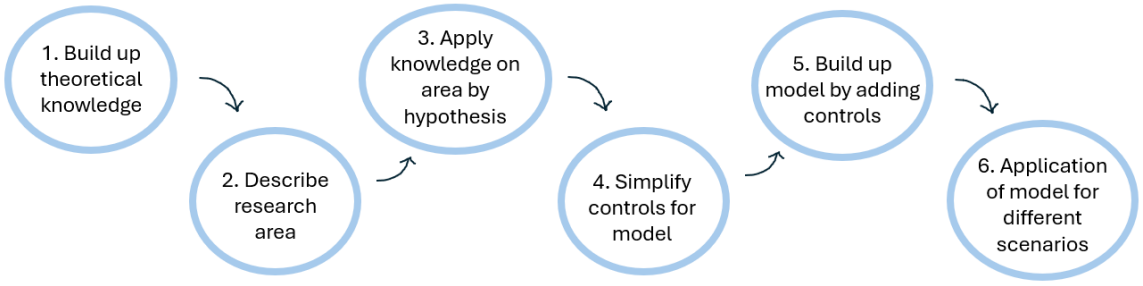

Figure 1.3: Structure of this research to answer all research questions

This research follows a step-wise approach to fully understand the system. In the **first** part the existing theory about the tidal dynamics is described to get a first feeling for these systems. This theory study will help simplify the new coastal system into components that are relevant to understanding the new system. The theoretical background can be found in Chapter 2 and with this knowledge the first two knowledge-based research questions can be answered.

In the **second** part, the research area is described and the Delta21 project is explained. All relevant components (hydrodynamics and morphodynamics) of the current situation are listed and compared to the situation when the Delta21 construction is applied. This part can be found in Chapter 3 and defines the controls in a qualitative manner.

In the **third** part, (Chapter 4), the results of the first and second steps are combined to describe the expected behavior of the system. In the first part of the chapter, different model schematizations are set up to examine this expected behavior. This way, the third knowledge-based research question can be answered.

The **fourth** part (Chapter 5) contains the quantitative simplification of the controls for the model to answer the model-based research question. Description is given of how the numerical model is build up including the computational grid, boundary conditions and sediment transport characteristics. All the different model schematizations are listed. This chapter closes off with a validation of the model for the current situation (without Delta21 construction).

In the **fifth** part (Chapter 6), builds up the model from the current situation by implementing the Delta21 construction and hydraulic forces one by one. During this process, the results are compared to the theory and expected behavior, described in Chapter 4. The first research-based question can be answered.

The last and **sixth** part is for application of the model. The model is used to give suggestions on sea level rise and extreme river discharge. Therefore, this part can also be found in Chapter 6 where the results are presented to answer the second and third research-based questions.

2
Theoretical Background

This chapter describes the existing theory about tidal dynamics to get a first feeling for these systems. This theory study will help simplifying the new coastal system into components which are relevant to understand the new system when the D21 construction is built, which is done in Chapter 5.

2.1. General composition tidal lake

A typical tidal lake has three main components:

- The entrance (inlet)
- ebb-tidal delta (seaward)
- Inner basin including channels and tidal flats (landward)

These components evolve over time and interact with the adjacent coast, forming a dynamic system. During lower tidal waters the flow is concentrated through a main channel (Figure 2.1). The intertidal flats (white area, A in Figure 2.1) store water during high tide and are exposed during low tide, while the active channel (gray area, A_s in Figure 2.1) remains wet throughout the tidal cycle. This results in a larger wet area during high tide with shallow waters above the intertidal flats. The different geometry of surface area and water depths during high and low tides, result in different phase speeds of the tide. This results in different peak ebb and flood flow and the ebb and flood duration. This tidal asymmetry governs sediment transport and depends on factors such as tidal range, channel depth, and the extent of tidal flats.

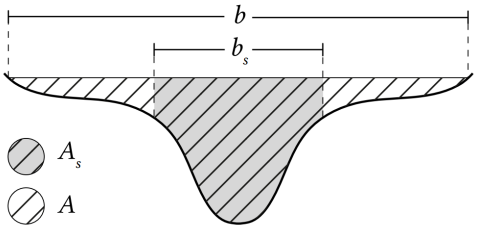

Figure 2.1: parameters cross-section from Coastal Dynamics book (Bosboom and Stive, 2023)

The tidal propagation can be approximated by the balance equations for mass and momentum in x-direction (aligned with the channel axis). After several assumptions, the equation is reduced until it contains elements of the wave equation for inertia in combination with a diffusion equation for friction. The combination or ratio between these elements determine the tidal wave propagation inside the tidal lake.

$$\frac{\partial^2 \eta}{\partial t^2} - gh\frac{\partial^2 \eta}{\partial x^2} + \frac{r}{h}\frac{\partial \eta}{\partial t} = 0 \tag{2.1}$$

in which:

η	Tidal / Oscillatory water level variation	[m]
h	Water depth	[m]
r	Friction coefficient	[m/s^2]
g	Gravitational acceleration	[m/s^2]

In case of funnel-shaped channels inside the tidal lake, the wave energy will converge and let the tidal amplitude increase along the channel axis. The balance of friction and convergence determine the growth or dampening of the tidal amplitude throughout the lake.

The tidal waves entering a basin can either be progressive waves, standing waves or a mixture of the two. In the case of a short basin, where the wave length is much shorter than the basin, the tidal wave is reflected and shows a standing behavior. This result is the same tidal range inside the basin as at open sea. The characteristic of a standing wave is that the water level and flow velocity are 90° out of phase. For a progressive wave, the peaks align (Bosboom and Stive, 2023).

2.2. Tidal Asymmetry

Tidal asymmetry refers to the differences in the shape of a tidal wave along both the vertical and horizontal axes. The tidal wave can be visualized by the water level (vertical tide) or by the current velocity (horizontal tide) with respect to phase, time, or space. Close to the shore, the tidal velocity generally leads the surface elevation, with a phase difference between 0 and $-90°$ ($0 < \varphi < -\pi/2$). In a frictionless situation, the horizontal and vertical tides are in phase, forming a progressive wave. The extreme case of $\varphi = -\pi/2$ occurs when the tidal velocity is in phase with the negative alongshore water level gradient, shown in Figure 2.2 (a).

Friction causes damping of both the tidal amplitude and the velocity, whereas narrowing of channels within a tidal basin can amplify the tide. The net effect is a change in the phase relationship between vertical and horizontal tides, which generally increases inland. This relationship is further complicated by (partial) reflections, which introduce additional phase differences.

For the vertical tide, the propagation speed is slightly higher at high water than at low water due to shallow water effects ($c = \sqrt{g(h+\eta)}$). As a result, the rising (flood) period is generally shorter than the falling (ebb) period. This phenomenon is known as flood dominance. Flood dominance can be reduced by river flow, which enhances seaward velocities. When river input is small, intertidal storage areas play a counteracting role. In tidal basins, intertidal flats periodically dry and flood, causing high tides to propagate slower than low tides due to shallow water depths. This effect can be quantified by the ratio of intertidal storage to channel volume V_s/V_c (Friedrichs and Aubrey, 1988) or by the ratio of wet surface areas at high and low water $A_{b,HW}/A_{b,LW}$ (Dronkers, 1986, 2005).

Sediment transport can be determined by the asymmetry of the horizontal tide. In case of asymmetry around the horizontal (skewness), as an effect of friction, the maximum flood velocity exceeds the maximum ebb velocity. This leads to a residual sediment transport in flood direction (assuming the transport is a power function of the velocity). consequently the area becomes shallower and the channels tend to fill in. The asymmetry around the horizontal, is dominant for medium to coarse sediment and determines the ebb or flood dominance of the system and therefore the net movement of sediment and morphological development over time. This is a feedback mechanism where the basin determines in essence its own evolution.

Asymmetry around the vertical is dominant for fine sediments in the basin as the sediments need time to settle. The sediment deposits when the slack duration is long enough. If the HWS duration is longer than the LWS, there will be a net transport of fine sediments into the flood direction.

Both of the asymmetries are likely to be present at the same time. Figure 2.2 (b) shows a higher maximum ebb velocity than flood velocity (export of coarse sediment) and a longer duration of HWS than LWS (import of fine sediment). In the case of deep channels and large area of intertidal flats, HWS duration is shorter than the LWS duration leading to export of fine sediments. However, the large storage areas (intertidal flats) also accommodate smaller water depths where fine sediments can settle. The result is a net import of fine sediment if the latter dominates which may be one of the reasons why tidal basins contain mostly fine sediments or silt.

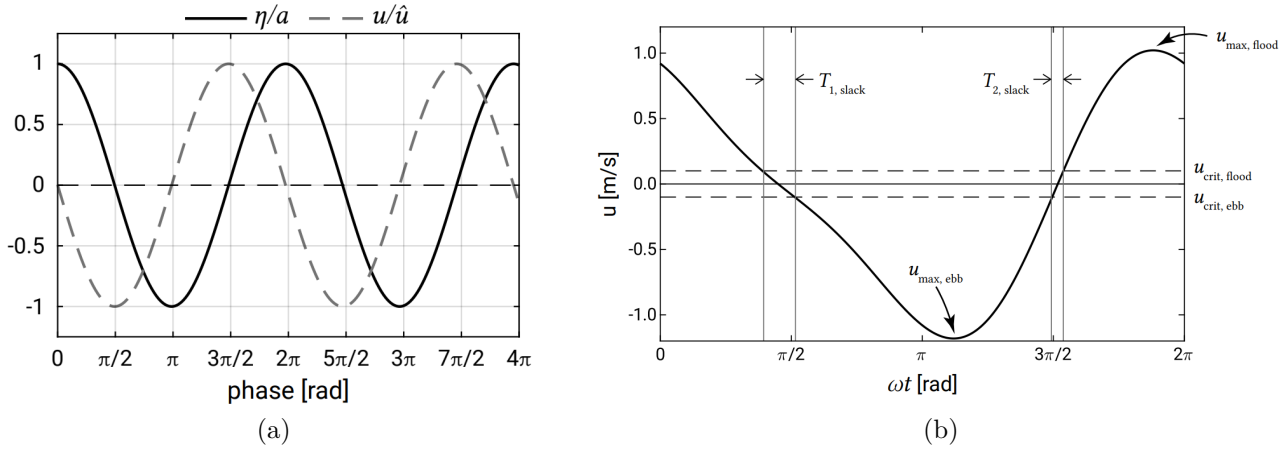

Figure 2.2: Two illustrations from the Coastal Dynamics book of TU Delft (Bosboom and Stive, 2023) (a) 90° phase lag of the surface elevation leading the flow velocity, (b) Skewness and duration asymmetry

2.3. Influence of river discharge

We can define a basin as a short basin when the length of the basin is comparatively small to the tidal wave length $L_b << \frac{1}{4}L$. Along the Dutch coast we experience two high and two low tides every lunar day referring to a semi-diurnal tide. The M2 tide has a period of 12.4 hours and a wave length that decreases as the tide approaches coastal areas. The tidal elevation and velocity are only based on the continuity equation and the discharge is dependent on the volume of water needed to fill the basin (excluding the river discharge). For a short basin, the assumption and simplification is made that there is no variation of tidal amplitude along the channel inside the basin, so we expect that the water level in the basin is equal to the water level of the sea $\partial\eta/\partial x = 0$.

In the case of a river discharge, there is an extra flow through the basin in seaward direction, Figure 2.4. It is therefore not valid to neglect the residual flow coming from the river discharge in the sediment transport formulation by Van De Kreeke and Robaczewska (1993). During flood the infilling of the basin is by the combination of the oscillatory tidal discharge ($Q_t(t,x)$) and the constant river discharge ($Q_r(t,x)$). During ebb, the amount of water leaving the basin is the tidal prism plus the river discharge. This means that the net tide-averaged discharge is not equal to zero (which is the case in absence of a residual current). In general, we can write the water discharge at any cross-section as $Q(t,x) = Q_t(t,x) + Q_r(t,x)$. In case of a constant discharge from the Haringvliet into the tidal basin, the flow graph will look like Figure 2.3. The result is fast infilling of the basin during flood and a longer outflow duration to empty the basin. In general, because of the river discharge, the maximum ebb velocity exceeds the maximum flood velocity leading to a ebb dominance or net transport of sediment in the ebb direction.

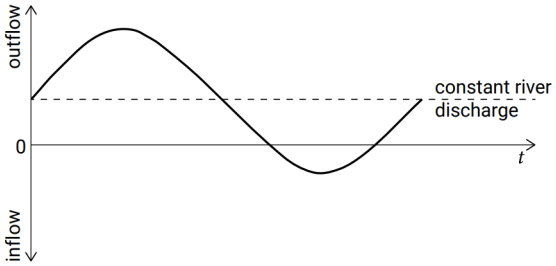

Figure 2.3: Tidal flow and river discharge from Coastal Dynamics book of TU Delft (Bosboom and Stive, 2023)

$$A_b(\eta) \cdot \frac{d\eta}{dt} = Q_t(t,x) + Q_r(t,x) \tag{2.2}$$

The amount of river discharge at the Haringvliet sluices flowing into the tidal basin depends on the amount of water available in the river. In the 'Kierbesluit', the following discharges are determined:

- Low discharges (<1100 m³/s): Sluices remain closed, keeping the Haringvliet predominantly fresh.
- Moderate discharges (>3500 m³/s and <9000 m³/s): Freshwater refreshes the upper layer, aiding desalination.
- High discharges (>9000 m³/s): Sluices fully open, ensuring efficient water discharge to the sea.

(a) (b)

Figure 2.4: Schematization of the filling and emptying of the tidal lake. (a) Schematization during ebb: outward tidal flow and inward river discharge (b) schematization during flood: inward tidal flow and inward river discharge

2.4. Inlet cross-sectional area

The cross-sectional area of the tidal inlet is dynamic as it depends on the hydraulic forces such as tidal currents, storm surges, the tidal prim and littoral sediment transport. Escoffier (Escoffier, 1940) studied the relation of the maximum cross-sectionally-averaged entrance channel velocity u_e to the stability of the inlet. He related the u_e to the hydraulic radius of the channel (R), the cross-sectional area of the entrance (Ae) and the tidal range in the estuary (Δh). These variables are combined into a dimensionless parameter on the horizontal axis of the closure curve, representing the inlet's hydraulic and geometric properties. A larger cross-sectional area generally leads to a higher value of this parameter.The closure curve is shown in Figure 2.5.

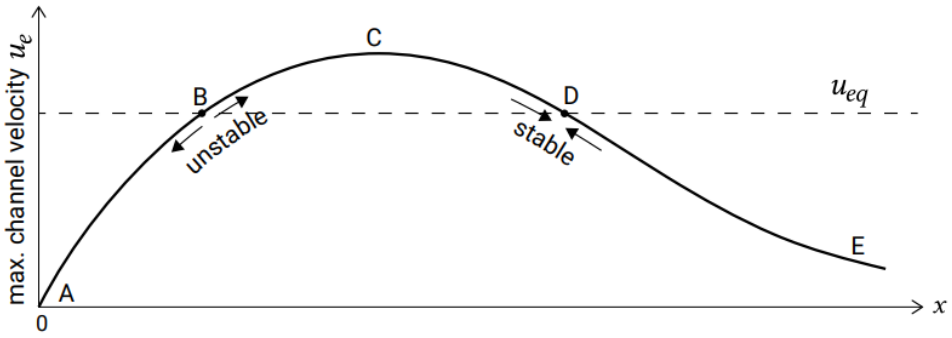

Figure 2.5: Channel velocity geometry relationship (Escoffier, 1940)

The maximum cross-sectionally-averaged entrance velocity in general is related to the tidal prism by Formula 2.3. The relationship assumes a sinusoidal tidal motion and a constant shape while changing in size.

$$P = \int_0^{1/2T} A_e u dt = \int_0^{1/2T} A_e \hat{u} sin(\frac{2\pi}{T}t)dt = \frac{TA_e}{\pi}\hat{u}_e \tag{2.3}$$

where:

P	Tidal prism, volume of water leaving or entering during one tidal cycle	[m^3]
A_e	cross-sectional area inlet	[m^2]
u	sinusoidal tidal motion	[m/s]
$\hat{u}_e$	amplitude of sinusoidal tidal motion	[m/s]
T	period	[s]

And therefore we can say:

$$\hat{u}_e = \frac{\pi P}{A_e T} \tag{2.4}$$

As described in Chapter 2.3, the volume of water flowing into the tidal basin is not the same as the volume of water flowing out. The tidal prism in Equation 2.4 will therefore be replaced by the dominant volume of water leaving the basin during ebb: P_{ebb}.

In the range from A to C the inlet area is so small that the tidal flow is squeezed and the tidal difference inside the estuary is smaller than at sea. In this range, the channel velocity increases for an increasing cross-section. In the range of C to E, the flow is not choked anymore by the cross-section of the inlet and the tidal prism does not change for an increasing cross-sectional area of the inlet. Here, the maximum current velocity decreases for increasing cross-section.

The horizontal dashed line in the closure curve represents the critical maximum velocity for sediment transport, typically around 0.9 m/s for medium sand. This is the critical velocity for sediment to move. Below this value, the flow is too weak to keep the entrance channel open.“In general, the desired inlet cross-sectional area is one where the maximum velocity is just above the critical threshold needed to maintain sediment transport and prevent closure.

Although Escoffier's approach is based on natural inlet systems, the underlying principles are also useful for the design of man-made structures such as storm surge barriers. By ensuring that the flow through barrier openings maintains velocities above the critical threshold for sediment transport, unwanted sedimentation or erosion can be prevented.

2.5. Morphological equilibrium relations

The morphological equilibrium is defined mainly by tidal prism, intertidal area, and channel configuration. The following relations are described by Eysink and Biegel (1992).

Tidal flat area as a function of basin area:

$$\frac{A_{fe}}{A_b} = 1 - 2.5 \cdot 10^{-5}\sqrt{A_b} \tag{2.5}$$

where:

A_{fe}	equilibrium area of tidal flats	[m^2]
A_b	area of tidal basin	[m^2]

Tidal flat height relative to tidal amplitude:

$$h_{fe} = 2\alpha_{fe} \cdot a, \quad \text{with } \alpha_{fe} = \alpha_f - 0.24 \cdot 10^{-9} A_b \tag{2.6}$$

Where:

h_{fe}	equilibrium height of tidal flats	[m]
α_{fe}	empirical coefficient for equilibrium flats	[−]
a	tidal amplitude	[m]
α_f	= 0.41 empirical coefficient for flats	[−]

Tidal flat volume:

$$V_{fe} = A_{fe} h_{fe} \tag{2.7}$$

Ebb-tidal delta volume:

$$V_{od} = C_{od} P^{1.23} \tag{2.8}$$

V_{od}	sand volume stored in the outer delta	[m^3]
C_{od}	empirical coefficient	[m$^{-0.69}$]
P	tidal prism	[m^3]

Channel volume inside the basin:

$$V_{ce} = \alpha_c P^{1.55} \tag{2.9}$$

V_{ce}	equilibrium volume of the channel	[m^3]
α_c	empirical coefficient	[−]
P	tidal prism	[m^3]

These relations help estimate morphological development over time. For example, the Wadden Sea systems show extensive flood deltas when sediment supply is high, whereas wave-dominated systems typically favor ebb-delta growth.

The ideal case for the development of the Delta21 tidal lake is to develop a flood tidal delta that spans a large area inside the lake without infilling of the main shipping channel or recreational beaches. For comparison, the tidal deltas of the Wadden Sea are relatively small with abundant sediment supply which causes the flood tidal delta to span the entire basin.

Another important relation is the volume of the channel inside the basin. Here, it needs to have the capacity for the discharge of the tide and the river.

3
The Delta21 research area

This chapter describes the research area that is located seaward of the Haringvliet. First the current dynamics are explained where the focus is on the interaction of different processes present in this area. Then the hydraulic forces (river discharge, tides and waves) and morphology are described. The aim is to understand the area and how the forces will change when the Delta21 construction is implemented. Therefore also the discharges originating from the pumps/turbines and the inlet are described. Finally the effect of climate change on these forces is explained.

3.1. Current dynamics in research area

Human interventions tend to affect in general the dynamics inside an estuary. In most cases, human interventions push the system out of balance where it needs to find its new dynamic equilibrium for this new situation including the intervention. In the case of the Voordelta, in front of the Haringvlietdam (human intervention), the system is able to restore balances by morphodynamic changes. Due to the reduction of river discharge by the dam, sediment from offshore is transported into the system during flood but is not washed away during ebb. This results in net sedimentation in the Voordelta, a process that is expected to continue in the future (Arcadis et al., 2024) until a new balance is established. This sedimentation could be beneficial for ecology and could eventually lead to the development of a system similar to the Wadden Islands.

To understand these dynamic processes, the estuarine system can be characterized by the following five components, which together determine the overall behavior of the estuary:

- Tide dynamics: ebb and flood flows twice a day
- River dynamics: controlled river discharge from the Haringvliet sluices
- Morphodynamics: transport of sediment inside the Voordelta by tides, waves and river discharges
- Salt and fresh water transition: the gradient of salt concentration shaped by tide and river dynamics
- Supply and conversion of organic matter: supplied by the river and diffused by the tide

Figure 3.1: Abiotic processes PAGW (Arcadis et al., 2024)

In a natural estuary system, these five processes are in balance. It is important to consider the system as a whole: a measure that affects one of the five components will have consequences for the other four components. The construction of the Haringvlietdam has altered river dynamics by regulating discharge, resulting in a wave-dominated estuary. The North Sea has unrestricted access to the Voordelta. However, the influence of the river has largely disappeared. Arcadis recently studied this area and made some conclusions related to the changes after the dam construction (Arcadis et al., 2024). The supply of fine sediment and organic matter from the river has strongly declined, and fluctuations in salt and fresh water have been significantly reduced, especially during periods of low to average river discharge. Only during high discharges (around 50 days per year), a substantial amount of freshwater flows into the area, temporarily creating transitional zones. Erosion and sedimentation in the Voordelta mainly concern the redistribution of older sediment that, prior to the closure, was part of the outer delta extending far into the sea. Over time, this process will gradually stabilize, giving the area more of the characteristics of a shallow coastal lagoon rather than a dynamic river estuary.

3.2. The Delta21 project

The Delta21 project is an alternative to continuous dike reinforcement, offering flood protection, freshwater management, and ecological restoration in line with the NL2120 vision. The project consists of the following main elements:

- A Tidal Lake in front of the Haringvliet mouth with a direct connection to the North Sea, reintroducing natural estuarine dynamics and allowing saltwater intrusion in a controlled manner.
- An Energy Storage Lake offshore of the Tidal Lake which serves as a large-scale pumped hydro storage facility, using excessive wind and solar power for energy storage.
- A Storm Surge Barrier and Pumping System, capable of discharging up to 10 000 m^3/s. PS are also used to discharge excess river water to the sea, providing additional flood safety.

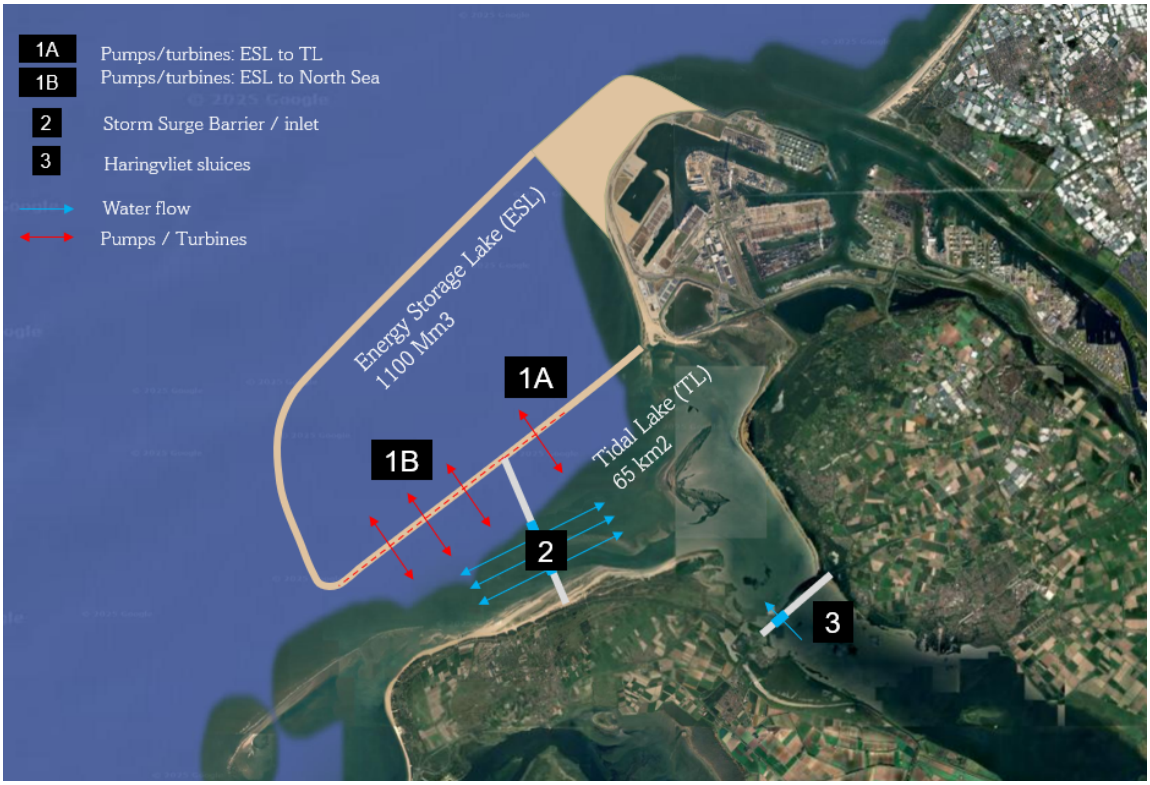

Figure 3.2: Layout April 2025 of the Delta21 project including the expansion of MV3. The Delta21 schematization drawn on a satellite picture of Google Earth (Google LLC, 2025). The hydraulic forces (tide, river discharge and pumps) are listed with numbers in the legend. The arrows indicate the direction of the flow.

The construction of the energy storage lake gives room to create a 65 km^2 tidal lake in the shallow area in front of the Haringvliet locks. The energy storage lake shelters the tidal lake from wave forcing, reducing silting up of the Voordelta. The idea of sheltering is to give back room for nature to develop and restore a salt-brackish zone allowing tidal exchange. This transition zone of salt and fresh water, which was originally in the Haringvliet before construction of the Haringvliet dam, is now moved offshore. This way the Haringvliet can remain a fresh water area. Gullies, banks, and creeks need to transform the tidal lake into a rich natural habitat for flora and fauna. Figure 3.2 shows the plan view of the Delta21 layout, indicating the location of the energy storage lake, tidal lake, the Haringvliet and Maasvlakte 3 expansion. The numbers and colored arrows indicate the location and direction where water can flow in or out of the tidal lake. The blue arrows (location 2 and 3) show the ebb and flood flow direction generated by the tide and the controlled discharge of the river water at the Haringvliet dam. The energy storage lake is closed off from the tidal lake and the North Sea by dikes in combination with the pumps/turbines indicated as red arrows (location 1). In the layout of the Delta21 project, there are two storm surge barriers: the Haringvlietdam (part of the Delta Works) regulating fresh water inflow (location 3) and a new storm surge barrier at location 2 for salt water inflow. The design of the second storm surge barrier (location 2) is open and will depend on balances of fresh/salt water and sediment in- and outflow, as the aim is to create a natural ecosystem. This ecosystem will be exposed to different forcings over time, depending on the controls of the storm surge barriers, pumps, and natural forces. For the following conditions, the function of the Delta21 tidal lake will be explained: normal conditions, high discharges in the Haringvliet, and storm surges.

- During normal wave conditions and night, water is pumped out of the energy storage lake into the North Sea using excessive green energy from wind turbines. Energy is stored in the lake due to the water level difference relative to the North Sea water level. During the day the energy storage lake is filled again with use of the turbines to generate energy. The tidal lake has an open connection with the North Sea where tides can flow in and out (location 2). Fresh water can enter the tidal lake from the Haringvliet where the inflow is regulated by the dams (location 3) depending on the river discharge.
- Due to storm surges the water level and wave height increases. The Haringvliet dam was built as a storm surge barrier and has the capacity to protect the hinterland from these extreme conditions.
- When the discharge in the river is extremely high, the Haringvliet dams (location 3) are open and water can flow via the tidal lake into the North Sea (location 2). When the water level of the North Sea is not increased due to storm surges, no pumps are needed.
- In the case of a combination of high river discharge and a storm surge, the tidal lake will be closed off from the North Sea (location 2). The high river discharge flows through open dams (location 3) into the tidal lake and is pumped via the energy storage lake (location 1A) into the North Sea (location 1B).

Inlet/Storm surge barrier cross-section

The size of the inlet is primarily based on the total discharge produced by the pumps/turbines and river discharge as it needs to have the capacity of discharging this volume. The size (storm surge barrier width) is received from the Delta21 Layout of April 2025 in Figure 3.2. For this research, the width of the inlet is set as a variable because it influences the behavior of the system. It is directly related to one knowledge-based and one research-based sub-question, and has therefore a strong influence on answering the main research question.

This research evaluates only the effect of the inlet width on the tidal lake. No storm surge barrier is placed so sediment can be transported in and out of the tidal lake through the inlet, like a natural system. To make clear conclusions on the effect of the inlet size, extreme decrease and increase of the inlet width is evaluated in this research. A decrease and increase of 50% results in inlet widths of 1000 m and 2000 m respectively. The inlet is dredged until a bed level of 6 m for all three inlet widths.

Discharge by the pumps/turbines

The total volume of water storage capacity inside the energy storage lake is 1100 Mm^3. Because of the use of hydraulic machines, the water level inside the energy storage lake can vary from 3 to 28 m below the surrounding water level. The hydraulic machines can function as pumps (converting green energy into fluid energy emptying the energy storage lake) and as turbines (converting the energy of moving fluid into mechanical energy). To determine values of the discharges resulting from the pumps, it is needed to make a few realistic assumptions. One pump turbine is 20 MW (Mega Watt). For a total capacity of 2 GW (Giga Watt), installation of 100 pump turbines connected to the energy storage lake is required. The total capacity of the Delta21 energy storage lake is 34 GWh (van Cappellen et al., 2024), which results in 17 hours pumping (34 GWh / 2 GW) to empty the whole basin.

To determine the discharge in and out the energy storage lake with the capacity of the pumps, the volume of water inside the energy storage lake is divided over the pump capacity (1100 Mm^3 / (17 * 3600) =) 18 000 m^3/s. This is the full discharge in the extreme situation where the whole capacity (maximum) of the energy storage lake is used. As this is an extreme situation, it is more realistic to look at it in the perspective of which hours in a day empty and when to fill the basin.

So it takes 17 hours to fill or empty the basin. This is more than a tidal cycle of 12 hours and it is not possible to fully fill and empty the energy storage lake within one day. For this research the oscillation of filling and emptying the basin is by the use of time slots. For example, from 06:00 - 18:00 use turbines and from 18:00 - 06:00 use pumps. We assume this is done with a total discharge of 10 000 m^3/s. The second assumption is 1/4 of the pumps is connected to the tidal lake and the other 3/4 is connected to the North Sea. This means at location 1A in Figure 3.2 there is a maximum discharge of 2500 m^3/s and at location 1B a maximum discharge of 7500 m^3/s.

3.3. Hydrodynamics in the Delta21 project

Schematization of the system

The hydrodynamics in the Delta21 layout can be described by looking at the system by the forces. The three main forces are related to the river discharge filling the basin (Q_R), the horizontal tidal flow (Q_T), and the pumps/turbines (Q_P). These pump turbines can be used to pump water from the energy storage lake into the tidal lake or the other way around. The flow directions of the hydrodynamic forcings are schematized in Figure 3.3.

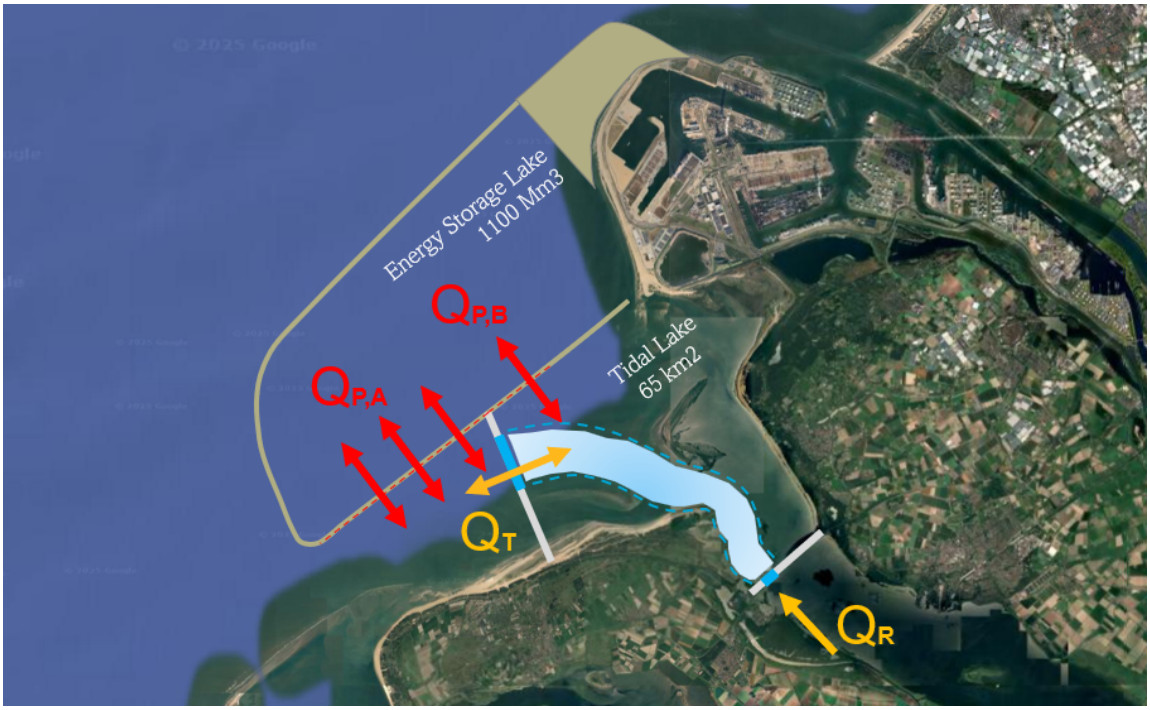

Figure 3.3: Schematization with hydraulic forces Q_P (turbines), Q_T (tides) and Q_R (river)

In a natural tidal basin, the basin fills and empties during one tidal cycle with the water level of the North Sea. In this case, it is the interaction of the three forces that determine the water level inside the tidal basin. The river discharge and pumps can help decreasing the time to fill the basin and increasing the time to empty the basin. As the pumps can also be used as turbines, they can help emptying the tidal lake during ebb. The main hydrodynamic forces in this system are the pumps/turbines, river discharge, tides and (locally generated) waves. Each of these forcings will be motivated separately in this Paragraph.

River discharge

The discharge regulation through the Netherlands is a complex system which is mainly regulated by manmade structures as dams and sluices. Throughout the years Rijkswaterstaat collected data on several locations of for example the discharges. Figure 3.4 shows the two locations indicated in red. For this research we look to the following two locations and their measurements: Haringvliet Binnen and Bovensluis. We use two different datasets which can be compared to each other. The first dataset is named the 'mean surface discharge' (daily discharge) which contains data over 20 years. The second is the 'Discharge' (measured every 10 minutes) for data from 2020 on.

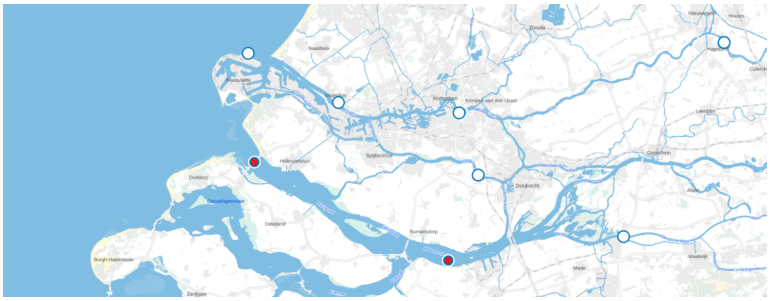

Figure 3.4: In red the locations of measurements by Rijkswaterstaat: Haringvliet binnen and Bovensluis

From the data, we can plot the following graph shown in Figure 3.5. The blue line represents the discharge just in front of the Haringvliet dam and gray the discharge at the Bovensluis. We can assume that the discharge right in front of the Haringvliet dam is the discharge that is going through the dam into the tidal lake. For the last 20 years the plot shows the mean discharge of surface water. This is data that is measured once a day at 12:00 and therefore does not show the differences during the day.

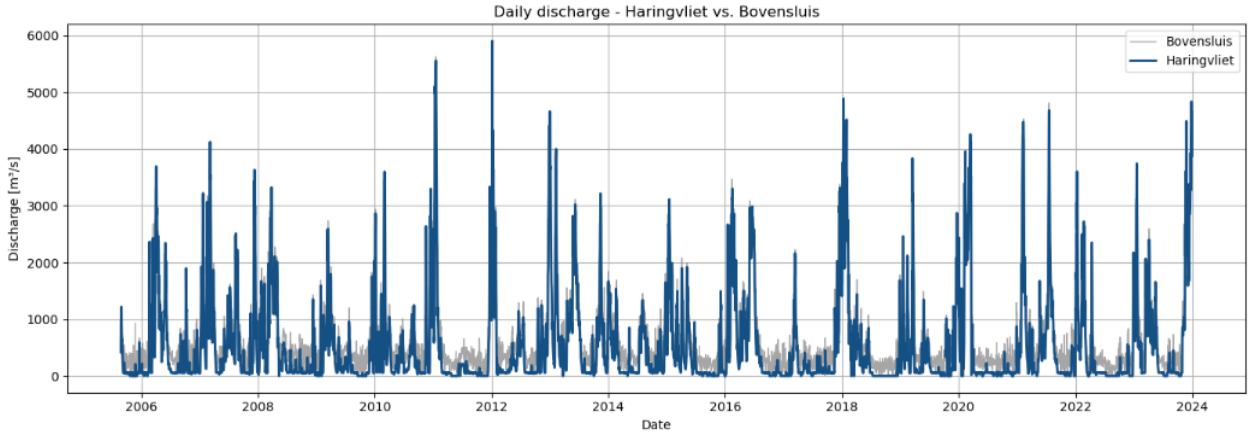

Figure 3.5: Daily discharge at the Maasmonding (bovensluis) and Haringvliet in 2006 and 2023

When we look closer to the discharge volumes, from 2020 on, we have data that is measured every 10 minutes, shown in Figure 3.6. We see higher values as the discharge can show severe changes during the day.

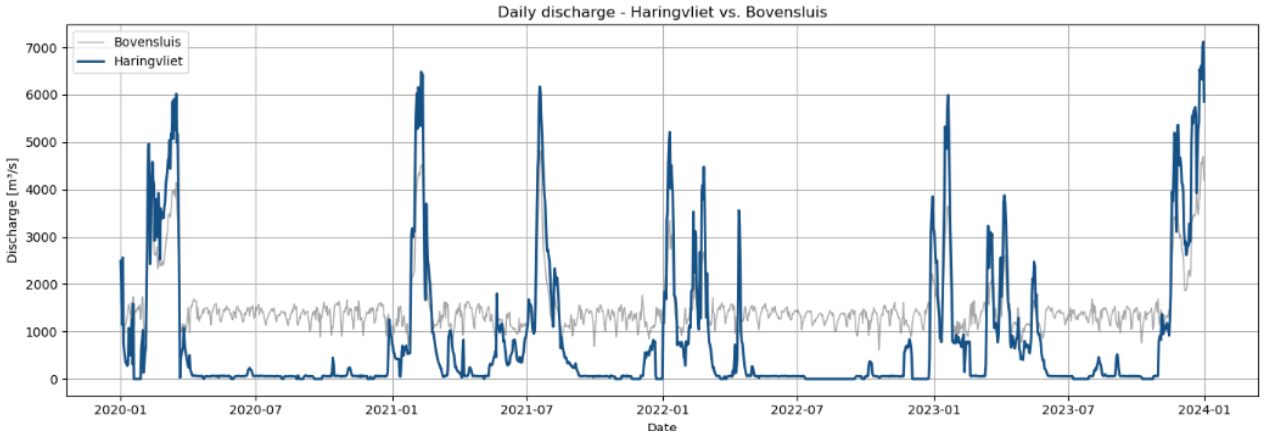

Figure 3.6: Daily discharge at the Bovensluis and Haringvliet in 2021 and 2022

We can immediately notice the correlation between the data measured at the Bovensluis and just in front of the Haringvliet. When there is a peak at the Bovensluis, there is a peak too in front of the Haringvliet. The main difference is that the Haringvliet discharge is zero or near zero when the discharge at the Bovensluis is low. This indicates that the Haringvliet dam is probably closed during these periods.

The correlation of the discharge at the Bovensluis and in front of the Haringvliet dam is shown in Figure 3.7 (a). It shows a clear correlation because the data sets are located at the diagonal, indicating similar values of the discharge at both locations. A slight offset of the diagonal for lower values of the Bovensluis discharge is shown because the Haringvliet is then closed. For higher discharges, the discharges at both locations become more similar.

The frequency of the closing of the Haringvliet becomes clear when the distribution of the discharge is plotted. Figure 3.7 (b) shows the number of days the Haringvliet is closed. This is approximately half of the time when analyzing the data over the past 20 years. We can also see that discharges above 3000 m^3/s do not occur frequently. These insights are very useful to get a feeling of the amount of water flowing through the Haringvliet dam.

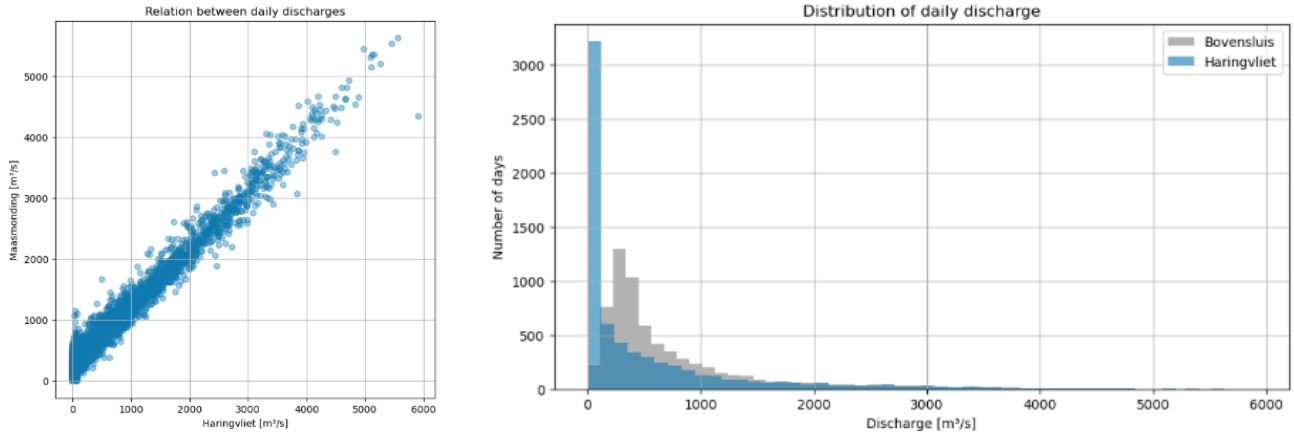

(a) (b)

Figure 3.7: (a) Correlation of the discharges at the Bovensluis and just in front of the Haringvliet dam, (b) Distribution of daily discharges for both the Bovensluis and the Haringvliet dam

River discharge through the Haringvliet sluices

The Haringvliet sluices play a critical role in distributing river discharge between the Nieuwe Waterweg and the Haringvliet. The sluice operation is primarily aimed at maintaining a discharge of approximately 1500 m^3/s through the Nieuwe Waterweg for as long as possible, in order to mitigate salt intrusion in surrounding waterways (Wit et al., 2011). This is particularly important for the Hollandsche IJssel, which contains the principal freshwater intake point for the central-western region of the Netherlands near Gouda. In addition, water level management seeks to prevent the Hollandsch Diep from falling below NAP (Normaal Amsterdams Peil), as this could negatively affect the functioning of the Moerdijk seaport.

When the Rhine discharge at Lobith drops below 1100 m^3/s, the Haringvliet sluices remain completely closed, except for dedicated saltwater and fish migration channels. For discharges between 1100 and 1700 m^3/s, a small flushing opening with a flow of approximately 25 m^3/s is used, provided that the external sea level is lower than the internal water level. This setup results in an average flushing flow of approximately 50 m^3/s per tidal cycle in the western part of the Haringvliet (Wit et al., 2011). Compared to the way larger discharges by the turbines and tidal flow, this value is considered negligible for this research.

When the Rhine discharge increases from 1700 to 9500 m^3/s, the sluices are progressively opened. When the discharge exceeds 9500 m^3/s, the sluices are fully opened. Consequently, the proportion of Rhine–Meuse water discharged via the Haringvliet increases from only a few percent during low-flow conditions to approximately 60–65% during high-flow events. This relative distribution remains nearly constant at even higher discharges (Wit et al., 2011).

The graph of Figure 3.8 shows three lines: LPH'84 (Lozings Programma Haringvlietsluizen 1984), MER (1998) and Kier/HOP (Haringvliet Operationeel Programma 2004).

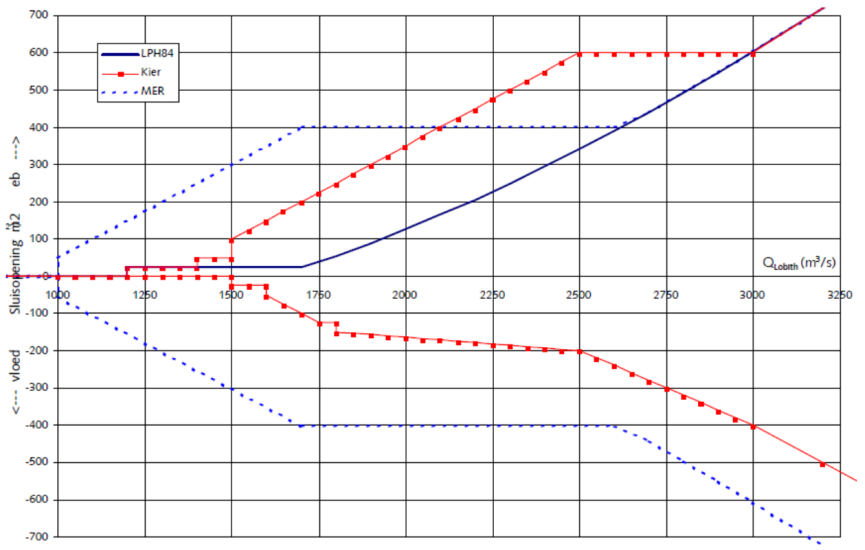

Figure 3.8: Decree on the Management of the Haringvliet Sluices (Waterwet Overheid, 2024)

Until a discharge of 1700 m^3/s at Lobith, the discharge through the Haringvliet is 0 m^3/s as this small flushing due to the 'Kierbesluit' is negligible in the schematization. During extreme cases of high discharge at Lobith of 10 000 m^3/s, the Haringvliet sluices are fully open and 60-65% is flowing through the Haringvliet into the tidal lake which equals 6000 m^3/s. To compare these extreme values, the common discharge which can occur occasionally is set to 1000 m^3/s through the Haringvliet.

Tides

The main tidal constituent along the Dutch coast is the M2 tide (semi-diurnal tide) with a period of 12 hours and 25.2 minutes. This means there are two high waters and two low waters within a 24-hour day, with the high and low tide shifting approximately 50 minutes each day. The M2 tide propagates, under the influence of the Coriolis effect, from South to North along the South-West Delta in a counter-clockwise direction around the amphidromic point shown in Figure 3.9. Along the Dutch coast, the tidal range decreases from about 3.8 m at Vlissingen to 1.4 m near Den Helder. This reduction is likely caused by the decreasing distance to the amphidromic point and the funnel shape of the southern North Sea. The difference in tidal range generates a net current along the Dutch coast from South to North.

The tidal range measured at Haringvliet10, close to the research area is approximately 2 m. These measurements are shown in Figure 3.10 for 42 days.

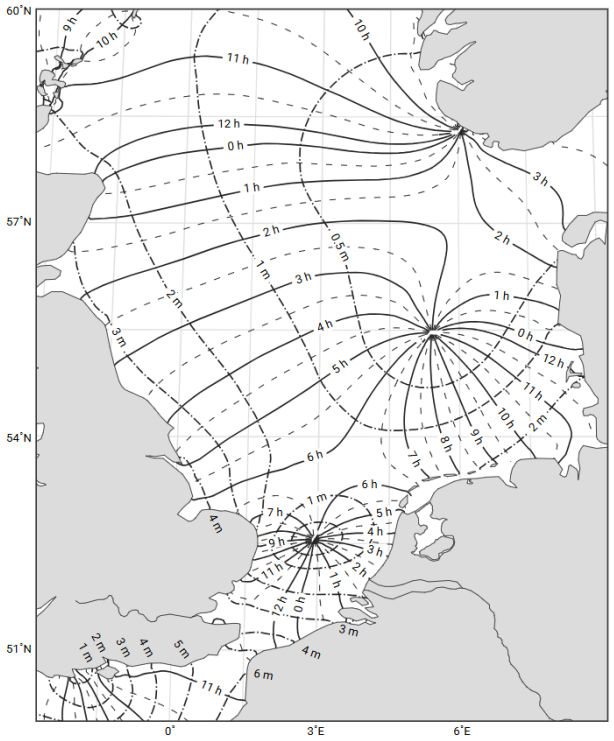

Figure 3.9: Amphidromic points in the North Sea (Bosboom and Stive, 2023)

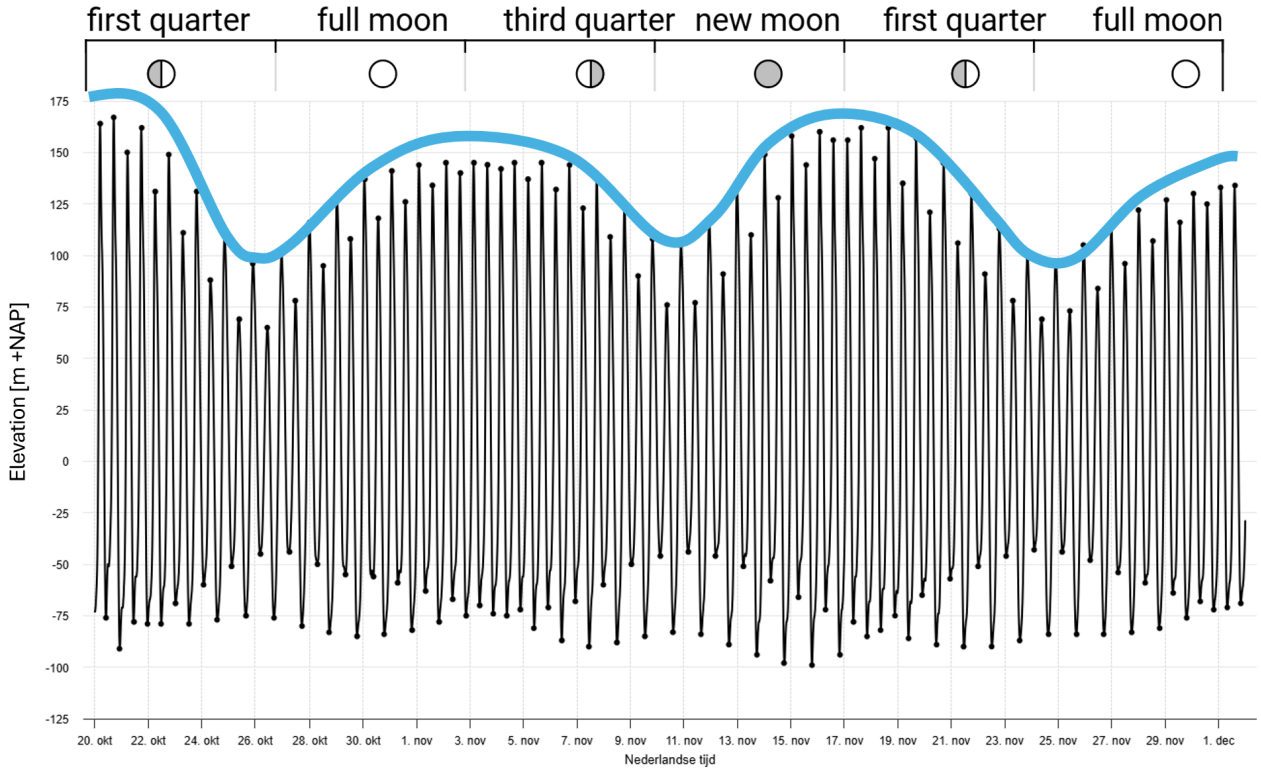

Figure 3.10: Water level measured at station: Haringvliet10. Data collected from October 20th to December 1th (Rijkswaterstaat, 2025b)

Wave climate

The waves entering the Voordelta are mainly wind waves, locally generated in the North Sea. Measurements of the waveheight are received from the measurement station Lichteiland Goeree which is located 30 km from Hoek van Holland. The exact location is pointed on the map shown in Figure 3.11 (a). The data can be collected from the Rijkswaterstaat data source MATROOS which stands for *'Meetdata en Analyse van Tijdreeksen voor Rijkswaterstaat Operationeel en Onderzoek Systeem'* (Rijkswaterstaat, 2025a). From the wind measurements, the wind rose is created for this location, shown in Figure 3.11 (b). The dominant wave direction is clearly South West. The same is for the direction of the waves in Figure 3.11 (c).

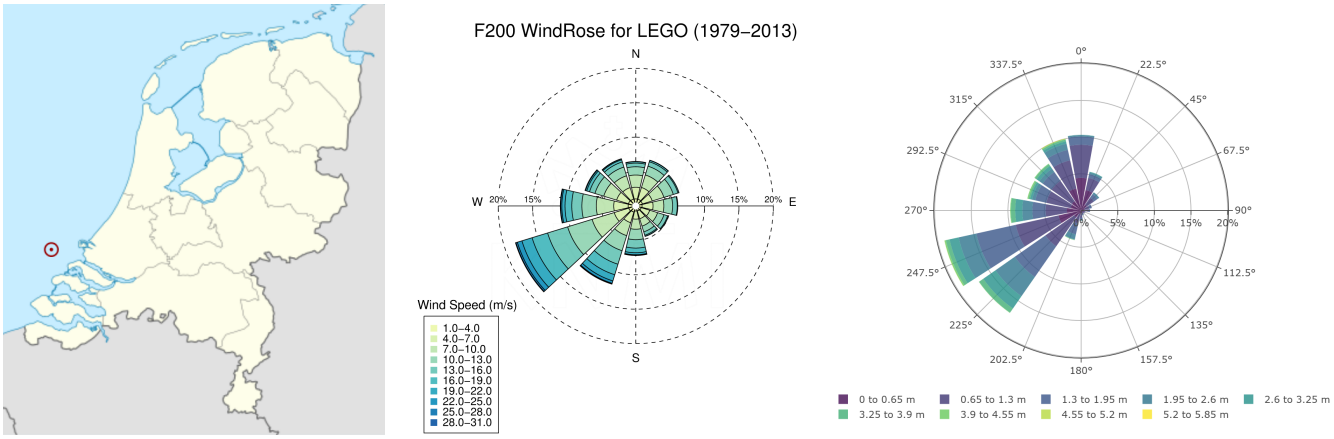

(a) (b) (c)

Figure 3.11: (a) Location of Lichtplatform Goeree measurement station, (b) Windrose of Lichtplatform Goeree, (c) Waverose of South-West delta

3.4. Morphodynamics in the Delta21 project

Bathymetry

Figure 3.12 shows the latest bathymetry measurements from Vaklodingen data of Rijkswaterstaat into the area of the tidal lake. For this research, the bathymetry is subdivided into six different categories. This way we can clearly see the location of the main channel and the intertidal flats.

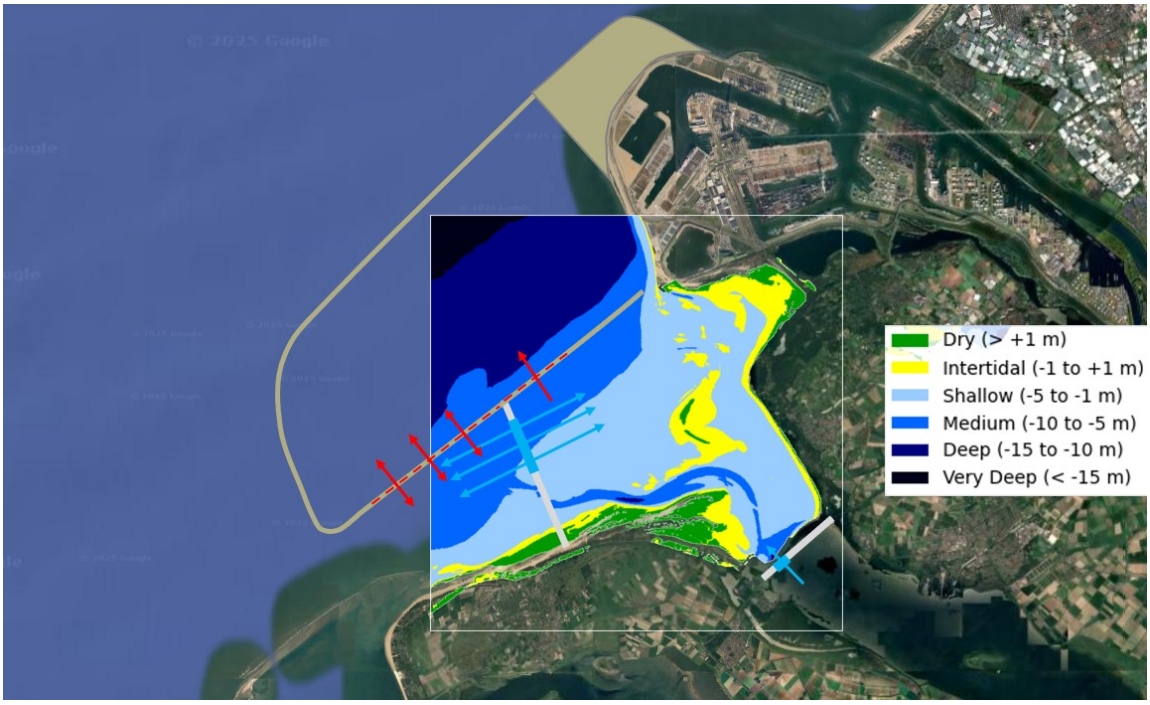

Figure 3.12: Latest bathymetry measured by Rijkswaterstaat (2025c) including the location of the Delta21 construction. The bathymetry is subdivided into six categories by colors indicating for example the location of the intertidal flats or channels.

The intertidal flats are located at the shoreline and in the middle of the tidal lake. The largest sandbank is the Hinterplaat which is according to several studies migrating towards the shore Wateren and Programmatische Aanpak Grote, 2024. The main channel flows from the Haringvliet, along the Kwade Hoek towards the North Sea. As can be seen in Figure 3.12, the location of the Delta21 inlet is located more in offshore direction. The area where the tidal lake will be located is in shallow waters up to 5 m deep. Except for the offshore side of the tidal lake where the water depth can reach up to 10 m.

Sediment characterization

The sediment composition in the mouth area of the Haringvliet mainly consists of sand, with a relatively small fraction of mud. Measurements show that in most channels and intertidal flats, the mud content remains below 10%, while more sheltered zones contain locally higher concentrations between 10–50%. On average, the total mud content in the area is approximately 5–6% (de Vries, 2007; Van Vessem, 1998).

The median grain size (D_{50}) varies depending on the local hydrodynamic conditions. Coarser material, typically between 150–200 µm, is found on the tidal flats, while finer sediments with $D_{50} < 150$ µm are present in the channels. Along the coastal margins, the grain size generally decreases further, often below 125 µm. The upper surface layers of the flats are usually composed of slightly coarser sand with lower mud content than the underlying deposits, likely due to the winnowing of fine particles by wave activity (Van Vessem, 1998).

Data from field surveys indicate that areas exposed to stronger tidal currents maintain coarser grain sizes, whereas finer material accumulates in sheltered regions where hydrodynamic energy is reduced. This spatial pattern results in a gradual fining of sediments from the more energetic outer areas toward the protected inner zones.

Overall, the sediment supply to the Haringvliet mouth is mainly of marine origin, consisting primarily of sand transported along the coast and from nearby offshore deposits. Finer material is partly imported from deeper parts of the North Sea and, to a lesser extent, from the Haringvliet itself (de Vries, 2007; Van Vessem, 1998).

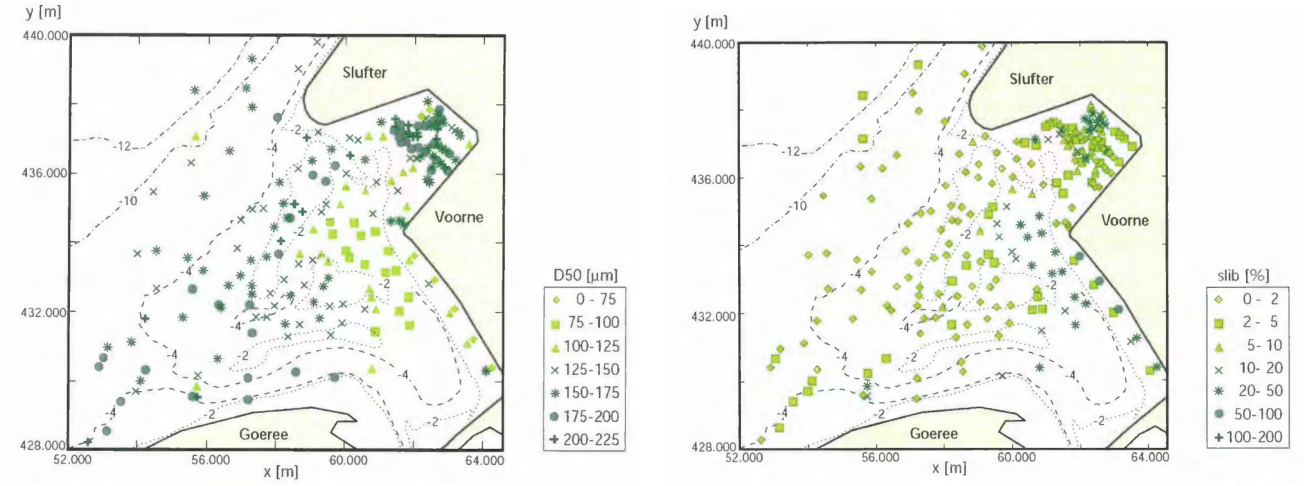

(a) (b)

Figure 3.13: Spacial distribution of median grain size and fine sediments 1994 (Van Vessem, 1998) (a) Distribution by grain size (b) Distribution by mud content in percentage

3.5. Influence of climate change

According to the PAGW reports (Arcadis et al., 2024), restoring estuarine dynamics is essential for the Biesbosch Rhine-Meuse estuary. In exploring potential measures, it is necessary to account for future developments, including sea level rise, extreme river discharges and droughts, increased storm surge frequency, and rising water temperatures. Climate projections from the KNMI'23 scenarios are used to analyze sea level rise and extreme river discharges. Figure 3.14 shows both the observed global temperature increase (black) and the projections of the four emission scenarios. According to the Paris Climate Agreement, global warming should be limited to well below 2° C, with efforts to limit it to 1.5° C by 2050 (KNMI, 2023).

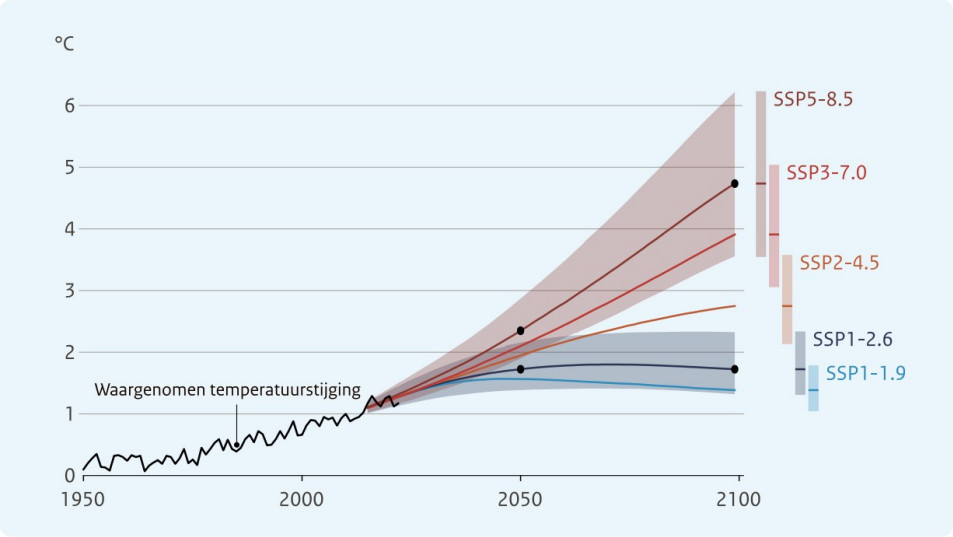

Figure 3.14: Observed global mean surface temperature increase (black line) and projected changes under the Shared Socioeconomic Pathways (SSPs) (colored lines: median; shaded areas: 90% confidence range). Vertical bars indicate the projected global warming levels by 2100 for each SSP scenario. Source: IPCC (Masson-Delmotte et al., 2021), Working Group I, The Physical Science Basis.

Increased extreme discharges and droughts

One of the most direct consequences of climate change in the Dutch delta is the shift in rainfall patterns, which affects both river discharge and water availability. The amount of rainfall is expected to increase in spring, autumn, and particularly in winter. However, summers are projected to become drier, especially in high-emission scenarios (KNMI, 2023). These seasonal differences are illustrated in Figure 3.15.

In the future, the number of light summer rain events will decrease, while the number of heavy rainfall events with high precipitation volumes will increase. This marks a shift toward heavier and more intense rain events (more rainfall within a shorter time). Although KNMI climate models predict an increase in heavy rainfall during summer, the projections carry a high degree of uncertainty. In contrast, the likelihood of extreme droughts is also expected to increase. Under some scenarios, a typical summer may become as dry as what is currently considered an extremely dry summer (KNMI, 2023).

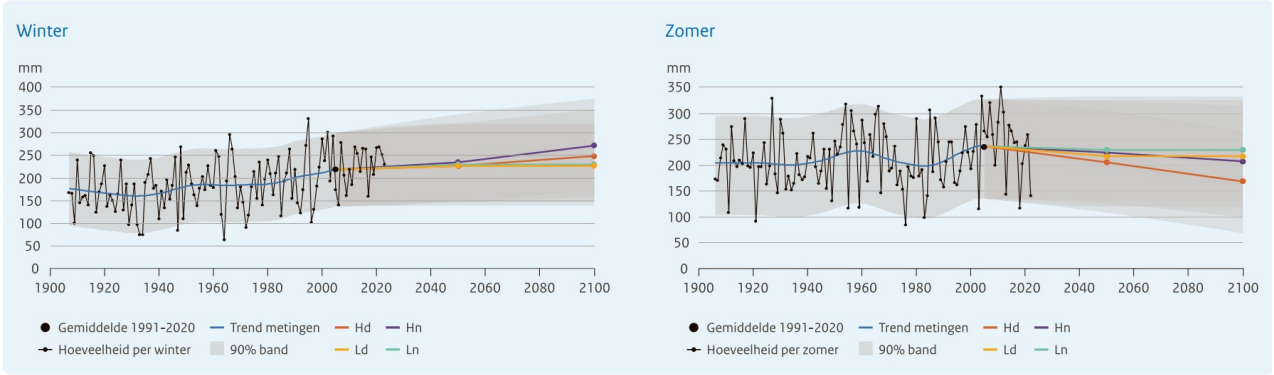

Figure 3.15: Rain predictions in summer (left) and winter (right) in the Netherlands of the KNMI' 23-climatescenarios (KNMI, 2023). The graphs show more rainfall in mm during winter and less rainfall in mm during summer. Source:(Masson-Delmotte et al., 2021)

These hydrological changes have direct implications for the delta's capacity to manage extremes, as freshwater flows through the Rhine and Meuse rivers toward the delta mouth. During periods of high discharge, the system needs enough capacity to transport water to the sea without exceeding dike limits or causing flood risks. In contrast, low river discharge during droughts can lead to freshwater shortages in the delta. This is especially relevant in the Voordelta, where limited inflow can reduce flushing, increase salinity, and put pressure on water availability for nature, agriculture, and drinking water supply.

Sea level rise

According to the Intergovernmental Panel on Climate Change (IPCC), global sea levels may rise up to 1.2 m by 2100. For the Netherlands specifically, the KNMI'23 scenarios project a regional rise of up to 1 m by the end of the century. While this is currently considered manageable, experts warn of a potential acceleration in sea level rise beyond 2100.

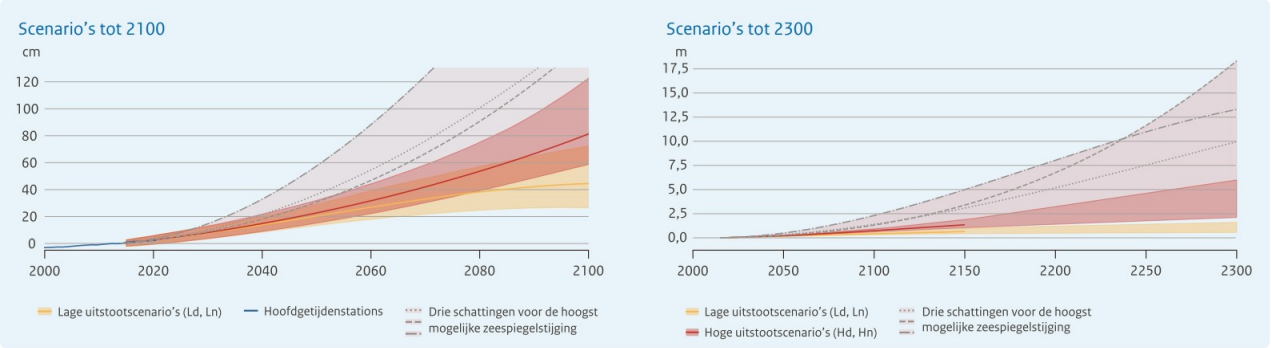

Figure 3.16: Sea-level rise projections for the Netherlands relative to the present level, showing median and 90% confidence ranges for different scenarios up to 2100 and 2300. The dashed lines within the light pink shaded area represent three estimates of the highest plausible sea-level rise. Source: IPCC (2021), The Physical Science Basis (Masson-Delmotte et al., 2021).

The consequences of sea level rise include more frequent closures of the Delta Works. For instance, the Oosterschelde barrier currently closes approximately once per year. In high-emission scenarios, this could increase to three times annually. Increased closure frequency results in higher hydraulic and wave loads on infrastructure and reduces maintenance periods, requiring more precise planning. Moreover, sea level rise leads to increased pressure on dunes, dikes, and storm surge barriers. More frequent pumping will be required as natural water outflow to the sea becomes less effective. Saltwater intrusion into surface and groundwater systems is also expected to increase.

Increased storm surges

While sea level rise is gradual, storm surges will cause temporary high waves and elevated water levels along the coast. Storm surges are the result of strong wind where the duration and direction are important. In the Netherlands, the northwesterly storms have the most impact but these storm frequencies are decreasing. Future storms will not lead to set up of the main water surface but sea level rise will (KNMI, 2023).

Climate change will lead to stronger and more variable hydraulic forces acting on the delta system. Higher river discharges, elevated sea levels, and more intense storms will increase wave impact, flow velocities, and water levels. These shifts must be accounted for in future design and adaptation strategies.

4
Modeling Methodology

The theory of Chapter 2 and the research area description of Chapter 3 leads to this chapter where the knowledge is combined. First, simple modeling schematizations that build up from the current situation are visualized. Then the theory is applied on the research area to describe the expected behavior of the system. This behavior will be examined in Chapter 6

4.1. Modeling schematizations

The approach in this research to understand the effect of the Delta21 construction on the research area, is to start with a schematization of the current situation. The idea is to systematically add the construction or a hydraulic force to the system to see how the system responds. These are in general four different schematizations, namely: the current situation (1), after implementation of the Delta21 construction (2), this system in combination with the pumps/turbines (3) and finally in combination with a river discharge (4). The current situation is modeled to validate the model by comparing it to bathymetry data of Rijkswaterstaat (Rijkswaterstaat, 2025c). The current situation (1) results are also compared in the second stage (2) after implementation of the Delta21 construction. In this comparison the focus is on the flow directions, flow velocities, tidal wave deformation and morphological changes. During the first part of modeling the system, the river discharge is set to zero and the pumps/turbines are not implemented yet. This way, the effect of only the Delta21 construction in the current situation is visible where the focus is on the tidal wave deformation.

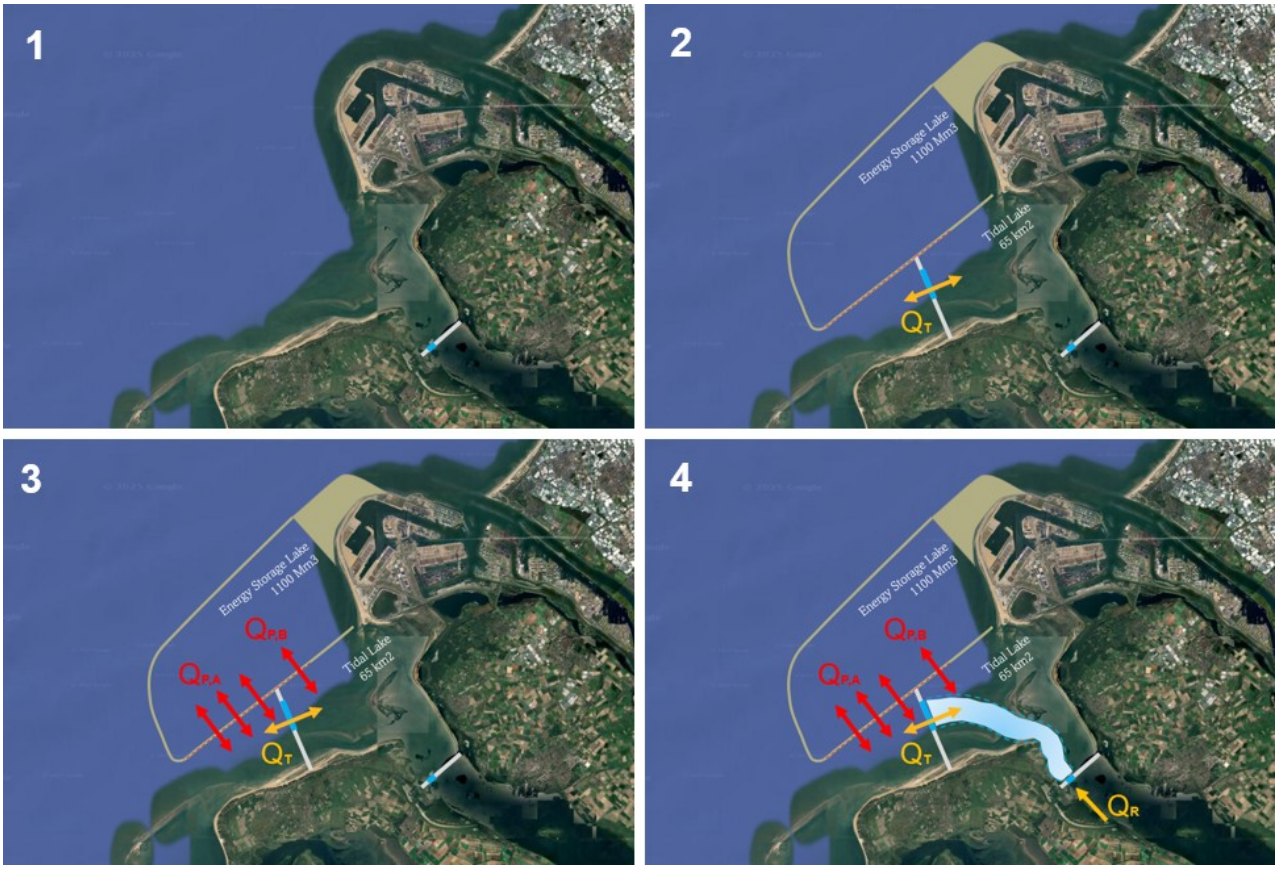

Figure 4.1: Four schematizations drawn on Google Earth screenshots (Google LLC, 2025). These schematizations will be used as input for the Delft3D model. (1) Current situation (2) Including the Delta21 construction (3) Including pumps/turbines (4) Including river discharge

In Section 3.3, the capacity in terms of discharges of the pumps/turbines is described. One way to determine their function is by pumping or turbine in given time slots. For example, from 06:00 - 18:00 use turbines and from 18:00 - 6:00 use pumps. In the third schematization (3) of Figure 4.1, the turbines/pumps are added to the system. Interesting is to see how this changed the system and especially the flow velocities in the inlet. To make clear conclusions, the same run is done by adding and subtracting 500 m to the inlet size.

The final hydraulic force is the river discharge which makes the system complete (4). Looking again at the schematization of the system, repeated in Figure 4.2, different combinations of situations can be made that are representative to understand the system. The turbines which connect the energy storage lake to the tidal lake have the capacity to discharge $Q_{P,B} = 2500$ m^3/s in both directions. For the river, an assumption is made for three relevant scenarios Q_R: no discharge, regular discharge and high discharge. The tidal discharge Q_T is the remaining volume of water needed to fill and empty the tidal lake to match the water level of the North Sea. We use the positive sign to indicate inflow in the tidal lake and a negative sign to indicate outflow of the tidal lake.

Table 4.1 shows, for varying river discharges, the volume of water discharged by the tide into the tidal lake when the pumps/turbines are active. The resulting tidal discharge can be determined by the area of the tidal lake and the tidal range. This is the volume of water which needs to fill the tidal lake during flood and empty the tidal lake during ebb to match the water level outside the tidal lake. For a quick calculation, the area of 65 km^2 is used and a tidal range of 2 m. Division of this volume to half a tidal wave, a discharge of approximately 5000 m^3/s is needed to fill the basin during flood and empty the basin during ebb. The sum of the rows in Table 4.1 is this value where the resulting discharge is positive during inflow and negative during outflow.

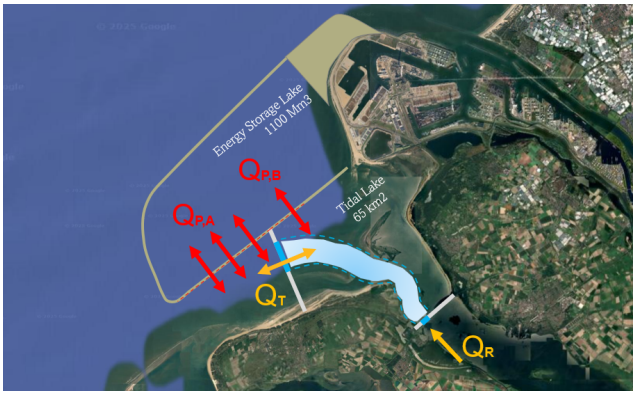

Figure 4.2: Final schematization

	Q_T [m^3/s]	$Q_{P,B}$ [m^3/s]	Q_R [m^3/s]
Flood	+2500	+2500	0
Flood	+7500	-2500	0
Ebb	-7500	+2500	0
Ebb	-2500	-2500	0
Flood	+1500	+2500	+1000
Flood	+6500	-2500	+1000
Ebb	-8500	+2500	+1000
Ebb	-1500	-2500	+1000
Flood	-3500	+2500	+6000
Flood	+1500	-2500	+6000
Ebb	-13500	+2500	+6000
Ebb	-8500	-2500	+6000

Table 4.1: Discharges related to the final schematization

4.2. Interaction between the M_2 tide and the S_1 signal

As described in Chapter 3, the main tidal constituent is the M2 tide (semi-diurnal tide) with a period of 12 hours and 25.2 minutes. The interesting thing is that the pumps/turbines of the Delta21 construction do generate a wave too as the pumps are operating in a repeating cycle. The pumps are filling the energy storage lake in 12 hours and emptying in 12 hours resulting in a 24 hours cycle. This can be compared to a S1 tidal wave which has also a period of 24 hours (Figure 4.3).

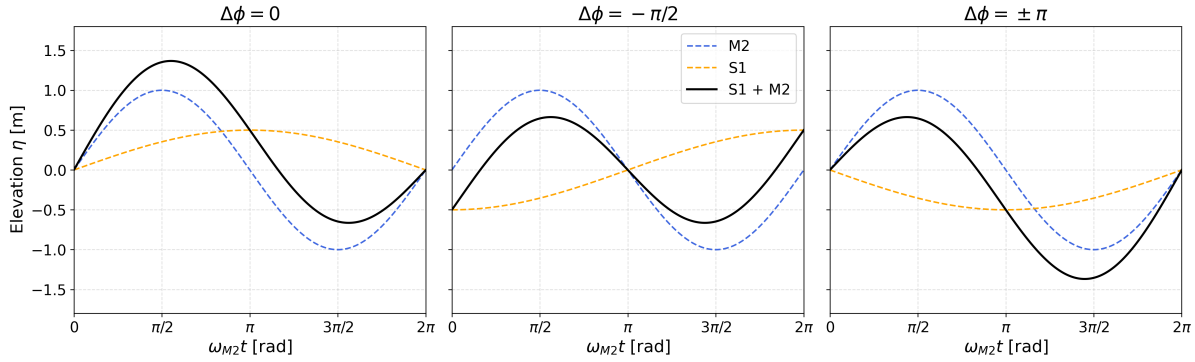

Figure 4.3: Interaction between the astronomical M_2 tide (semi-diurnal, $T_{M2} \approx 12.42$ h) and the diurnal S_1 signal generated by turbine/pump operation ($T_{S1} \approx 24$ h). Each panel shows the superposition of M_2, S_1, and their combined elevation signal for different relative phase differences $\Delta\phi = \phi_{S1} - \phi_{M2}$: (a) $\Delta\phi = 0$ rad (in phase), (b) $\Delta\phi = -\pi/2$ rad (S_1 lags M_2), and (c) $\Delta\phi = \pm\pi$ rad (out of phase). When the two components are in phase, constructive interference amplifies the tidal range, while out-of-phase conditions lead to destructive interference and reduced amplitude. Intermediate phase differences introduce temporal asymmetry and modulation of the high and low water levels.

The superposition of two harmonic constituents with different frequencies can be written as

$$\eta(t) = a_{M2}\cos(\omega_{M2}t - \phi_{M2}) + a_{S1}\cos(\omega_{S1}t - \phi_{S1}), \tag{4.1}$$

where a and ϕ denote amplitude and phase, and ω the angular frequency. Because $\omega_{S1} \approx \frac{1}{2}\omega_{M2}$, the resulting signal exhibits a clear envelope or "beating" pattern, characterized by slow oscillations of the tidal range over several tidal cycles (Bosboom and Stive, 2023).

Depending on the relative phase difference $\Delta\phi = \phi_{S1} - \phi_{M2}$, the M_2+S_1 interaction can cause:

- periodic strengthening or weakening of the total tidal amplitude,
- slight asymmetry between the rising and falling stages of the tide,
- and temporal shifts in the timing of high and low water levels.

When the S_1 signal is in phase with M_2, the tidal range in enhanced, leading to stronger velocities and larger surface gradients. Conversely, when the signals are out of phase, the effective tidal amplitude is reduced as shown in Figure 4.3.

4.3. Inlet stability

One variable that is still open in the design of the Delta21 tidal lake is the dimension of the inlet or storm surge barrier. This is because the inlet depends on the flow velocity through the opening and therefore the design of the full tidal lake including pumps, discharge and storage area. To understand and say something about the inlet, we first simplify the schematization until we only have the tidal and river forces.

The hydrodynamics in the Delta21 layout can be described by looking at the system during ebb and and during flood. In both cases there is a constant river discharge filling the basin (Q_R). The main difference is the direction of the horizontal tidal flow (Q_T) which causes inflow in the basin during flood and outflow of the basin during ebb. The flow directions are schematized in Figure 4.4 (a) and (b).

(a) (b)

Figure 4.4: (a) Schematization ebb (b) schematization flood

During one tidal cycle, the basin fills and empties to match the water level of the North Sea. The river discharge helps decreasing the time to fill the basin and increases the time to empty the basin. The main hydrodynamic forces in this system are the river discharge, tides and (locally generated) waves.

During ebb, the river discharge and volume of water to empty the basin flows in the ebb channel, trough the inlet into the North Sea. The channel and inlet need to have the capacity to transport this volume of water. To ensure this capacity is reached over the whole tidal cycle, the focus is on the maximum volume of water. The influence of river discharge on the tidal prism was explained in Chapter 2 by looking at the volume of water that flows in and out during one tidal cycle.

If we look at the graph of Figure 4.5, we see the peak flow is during ebb. This figure shows a simplified schematization of the tide. If the maximum flow velocity is during ebb, it can be concluded that the system is ebb dominant and there is a net sediment transport in ebb direction followed by the theory explained in Chapter 2: Theoretical Background.

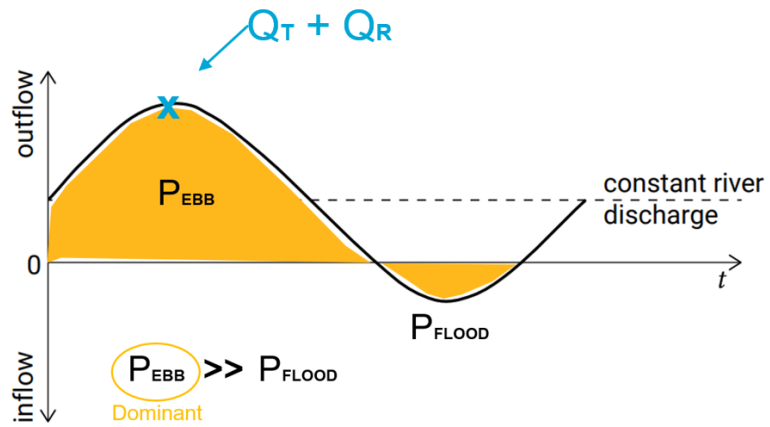

Figure 4.5: Tidal flow and river discharge from Coastal Dynamics book of TU Delft (Bosboom and Stive, 2023)

Only, the Delta21 construction includes pumps and turbines that generate a discharge into and out of the system. This will cause distortion in the simplified sinus wave that is represented in Figure 4.5. Therefore, the use of a Delft3D model helps to visualize the actual discharges when the three hydraulic forces (tide, river and pumps) are applied to the system.

First, the Delta21 construction will be implemented in the Delft3D model to see how the tidal wave is shaped at the inlet. From this information, the volumes of water entering and leaving the basin are derived. The maximum volume of water leads then to the maximum velocity inside the inlet. As described in Chapter 2, the Escoffier's graph can give insight on the dimensions of the inlet related to the flow velocity. If the inlet cross section is too small for the volume of water needed to flow in to keep the water level the same as outside, the flow is squeezed. There can be a smaller tidal difference / range inside the basin as there is not enough time in one tidal cycle to empty the basin. This smaller tidal range is not beneficial from environmental point of view, looking at ecology and volume of tidal flats. If the inlet is too large, the flow velocity decreases and the tidal prism does not change. The decrease of flow velocity results in sedimentation until the flow velocity is high enough to start moving sediment and keep the inlet open. The ideal cross-section of an inlet is determined by the flow velocity through the inlet. If it is near the stable point D indicated in Figure 4.6, the flow is not squeezed and not over dimensioned.

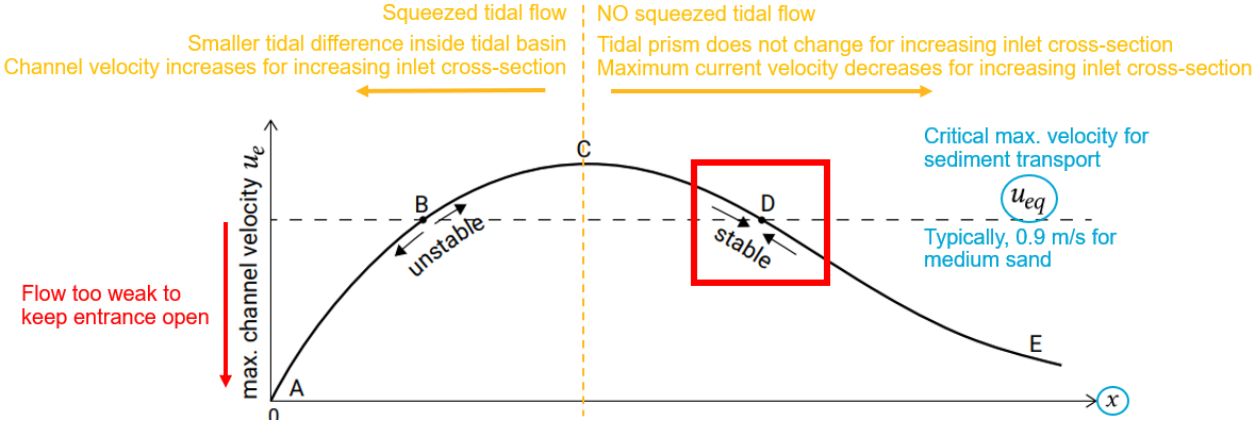

Figure 4.6: Channel velocity geometry relationship (Escoffier, 1940)

As the inlet of the Delta21 project will be a hard construction (because it also needs to function as storm surge barrier during extreme storms) the size is fixed. The inlet will not naturally adapt with erosion (or sedimentation) to its equilibrium cross-section but needs to be determined beforehand. In this research the tidal inlet size of 1500 m is used as a starting point as this was described in the latest layout. The inlet is dredged until a water depth of 6 m and no bed protection is used. It is chosen to not include the bed protection to see how the system responds (erosion or sedimentation) to a fixed inlet width. The expected behavior that is described until now can then be checked by increasing and decreasing the inlet width. To see clear results, different simulations are set up where the inlet width will change to 1000 m and 2000 m.

4.4. Dynamic equilibrium

The final step in this research is to look into the (preferred) dynamic equilibrium of the system as a whole. In other words, how to reach an optimal design schematization of the Delta21 project where morphological changes are minimized and tidal flats are stable in the tidal lake. With the theoretical knowledge and use of Delft3D, the inlet size and use of pumps are studied. They interact with each other until an equilibrium over longer time is reached. This interaction or loop is visualized in Figure 4.7.

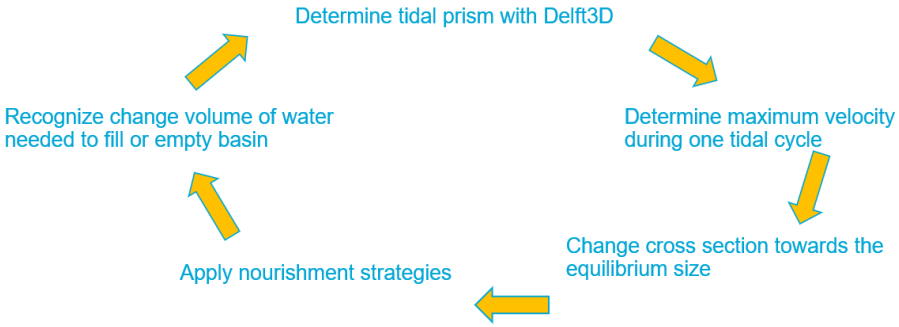

Figure 4.7: Schematization of the tidal prism change over time.

To gain a first-order understanding of how the Delta21 tidal lake might evolve morphologically, the empirical equilibrium relations were evaluated using the present-day basin characteristics. The equilibrium relations described in Chapter 2 and simplified basin dimensions of Chapter 3 are used. Although the system is not yet in equilibrium, these estimates provide a reference for the expected proportions of tidal flats, channel volumes, and tidal deltas.

Table 4.2: Estimated equilibrium properties of the tidal basin (Area $A_b = 65$ km^2, tidal amplitude $a = 1$ m, tidal prism $P \approx 1.04 \times 10^8$ m^3)

Parameter	Value	Unit	Fraction of Basin/Prism
Basin area, A_b	6.5×10^7	m^2	100% (baseline)
Tidal amplitude, a	1	m	-
Tidal range, $2a$	2	m	-
Tidal prism, $P = 2aA_bf$	1.04×10^8	m^3	100% (baseline)
Tidal flat area, $A_{fe} = A_b\left(1 - 2.5 \cdot 10^{-5}\sqrt{A_b}\right)$	5.7×10^7	m^2	88% of A_b
Tidal flat height, $h_{fe} = 2\alpha_{fe}a$	0.79	m	-
Tidal flat volume, $V_{fe} = A_{fe}h_{fe}$	4.5×10^7	m^3	43% of P
Ebb-tidal delta volume, $V_{od} = C_{od}P^{1.23}$	2.5×10^7	m^3	24% of P
Channel volume, $V_{ce} = \alpha_c P^{1.55}$	3.7×10^7	m^3	36% of P

These are the equilibrium proportions which the basin wants to reach. Whether the basin can reach these proportions depends on sediment transport patterns. Comparing the equilibrium tidal flat area of 88% to Figure 3.12, it can be concluded that the system should import large amounts of sediment from outside the system to reach this equilibrium state. To realize this sediment import, the system needs to have a flood dominant character.

4.5. Sea level rise and extreme discharges

Sea level rise can put extra pressure on the system as the tidal flats need to grow with the water level to avoid loss of intertidal flat area. It is therefore interesting to look if the system can build up this growth by itself. Another result of climate change is the extreme discharge events. This results in large discharge volumes into the system which can lead to high velocities and therefore sediment movement. The response of the system to one of these events is therefore interesting to investigate further.

5
Model Setup and Validation

In this Chapter, the setup of the model schematizations (described in Chapter 4) are translated to the Delft3D setup. The boundary conditions (hydraulic forces described in Chapter 3) are simplified as the idea is to understand the overall effect of these forces. These forces are implemented one by one in the system where Table 5.2 gives an overview of the model runs used for this research. Finally, the model is validated to make sure it is suitable to use for this research.

5.1. Model setup

Numerical model choice: Delft3D

Delft3D is an integrated computer software suite for 3D computations of coastal, river and estuarine areas. The Delft3D suite is composed of several modules. The modeling study of this research is executed by using the Delft3D-FLOW module. It is a multi-dimensional hydrodynamic and transport simulation program which calculated non-steady flow and transport resulting from tidal and meteorological forcing. The Delft3D FLOW model is used in 2DH where the depth is averaged and only one layer is used. In Delft3D the models bathymetry can be updated to create a morphodynamic model where the bed level changes the influence the hydrodynamics. This way it is possible to achieve equilibrium conditions.

The model that is used for this study results from the thesis research of de Vries (2007) on the morphological modeling of the Haringvlietmonding. This again is a follow-up of previous studies done in this area related to the morphological changes due to the Maasvlakte-2 construction. The previous research was done to understand the impact of the Maasvlakte-2 on the flora and fauna where the results can be found in several Environmental Impact Assessment (EIA) reports. As there were still differences comparing the model results and the observations, de Vries (2007) made an upgrade of the morphological model, for example by implementing wave-asymmetry transport correctly. This model is used as basis for this research where the newest data is implemented and will be explained in this chapter.

Bathymetry

The data used for the bathymetry in this area is a combination of two datasets. From the Haringvliet sluices until the Moerdijkbrug, upstream of the river. Geoweb contains the most recent measured bottom level on behalf of Rijkswaterstaat. The data is expressed in meters relative to NAP and the value for each square meter is based on the average of all points measured within that square meter (Rijkswaterstaat, 2024). The measurements of the coastal area are also received from Rijkswaterstaat Vaklodingen dataset which are measured in 2024 (Rijkswaterstaat, 2025c). The two datasets are merged and cropped in QGIS, shown in the left plot of Figure 5.1. To ensure the boundary conditions have a sufficient distance from the research area, the offshore area is filled with data from 2014 and finally smoothened in QUICKIN.

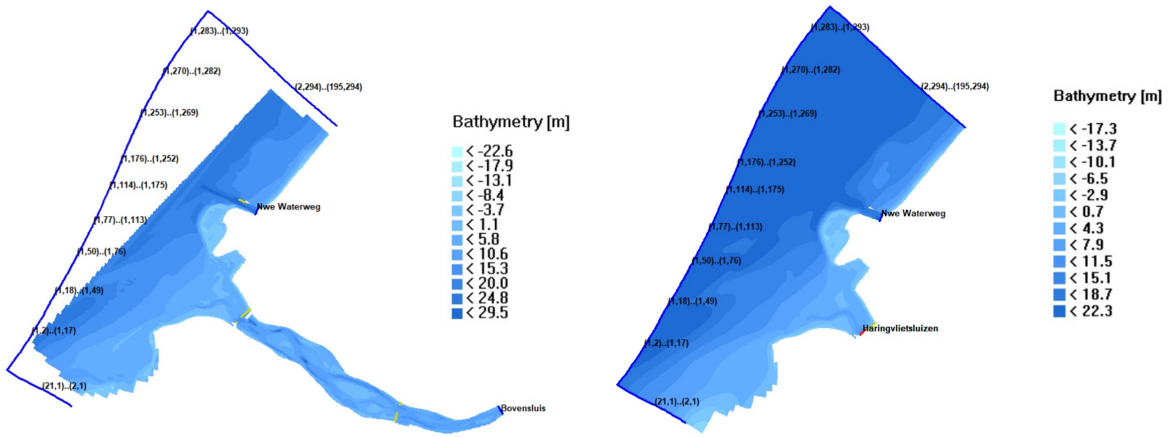

Figure 5.1: Bathymetry overview of the research area (a) First incomplete dataset (b) Complete bathymetry, merged with the second data set

Computational grid

The computational grid used for the FLOW-model within Delft3D is shown in Figure 5.2. The grid consists of the Dutch coast between Brouwersdam at the south and Noordwijk in the North. The boundary conditions are this way far enough from the area of interest to avoid boundary disturbances. Also the grid cells are not too small to avoid long computational time. The resolution is getting higher in the area of interest (order of 50x50m^2) and lower in the North-Sea (order of 600x600m^2).

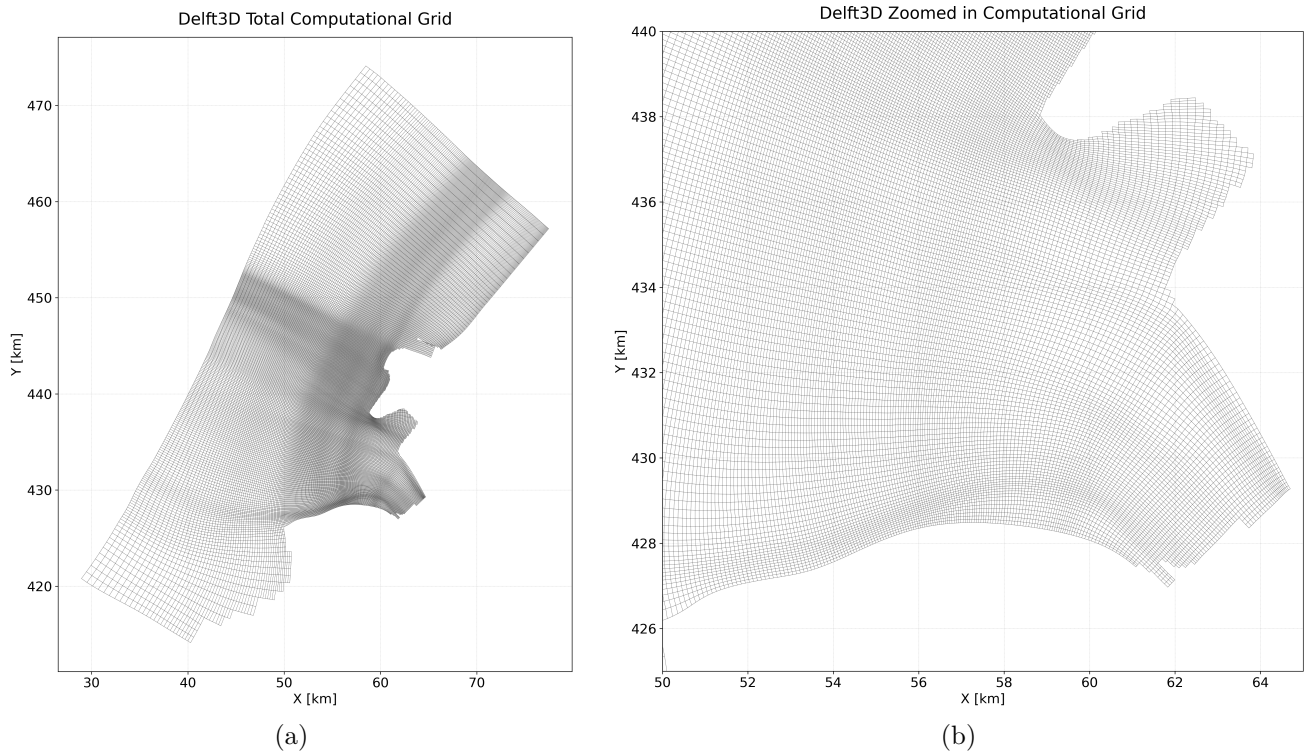

(a) (b)

Figure 5.2: (a) full computational grid (b) Tidal lake computational grid (zoomed in)

Boundary conditions

In the model, three different boundary conditions are specified for the flow module: water level boundary, Neumann boundary and discharge boundary. Figure 5.3 shows where these boundaries are applied.

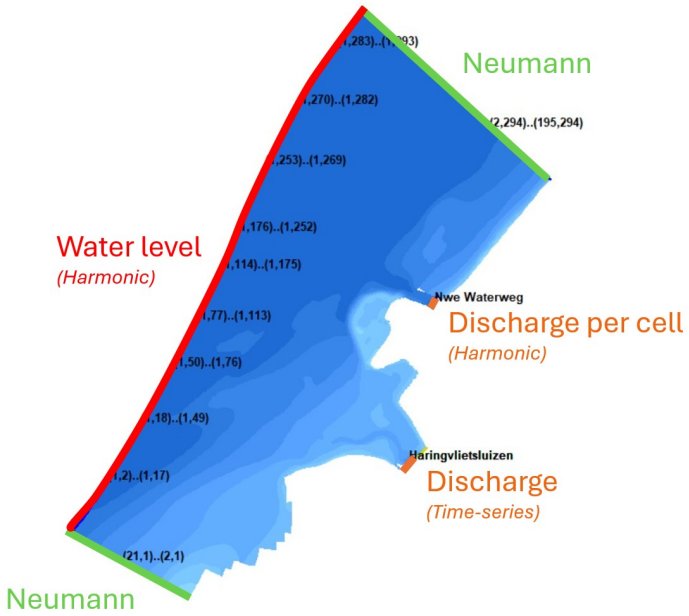

Figure 5.3: boundaries of the model (river discharges and water levels)

The tide is caused by regular astronomic phenomena (excluding meteorological effects as storm surges), and can therefore be predicted by harmonic analysis. It is the sum of the tidal constituents where each frequency ω_n is known. Only the phase angles α_n and amplitudes a_n are site-specific. The water level at a certain location is described as a function of time:

$$\eta(t) = a_0 + \sum_{n=1}^{N} a_n cos(\omega_n t - \alpha_n) \tag{5.1}$$

where:

η_t	= measured (or predicted) tidal level with reference to a fixed level	m
a_0	= mean level	m
a_n	= amplitude of component number n	m
ω_n	= angular velocity of component number n	1/h
α_n	= phase angle of component number n	-
t	= time	h
N	= number of harmonic components	-

During one year of water level measurements, most of the tidal constituents are captured except for the constituent with a period of 18.6 yr. As one year of water level data in a model requires a lot of computational time, it is preferred to only look at the constituents that can be representative for the long term forcing. In the model that is used for this research, the alongshore water level boundary is already determined by a representative tide and validated. This morphological representative tide is implemented as a harmonic boundary condition that consists of eight tidal components (M2,M4,M6,etc.). To check the representative tide used, it is plotted against the recently measured water level at the Haringvliet10 measurement station already shown in Figure 3.10.

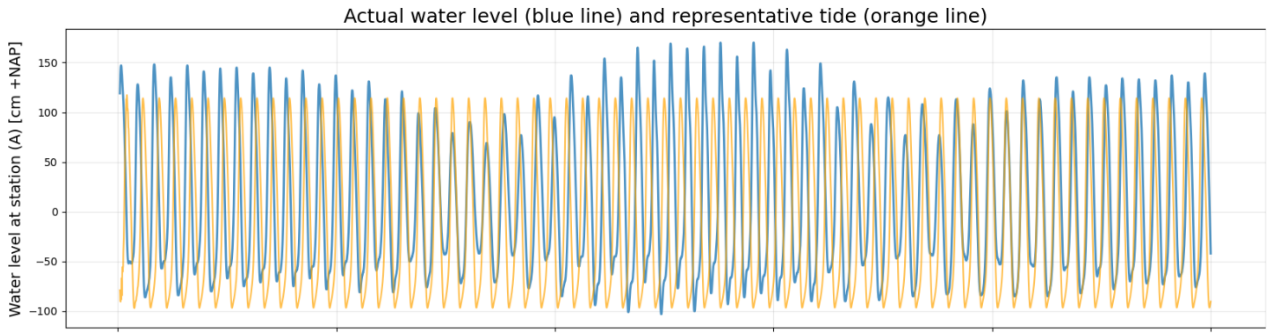

Figure 5.4: Water level measured at Haringvliet10 (blue line) and representative tide at observation point (A) (orange line).

At the cross-shore boundaries, the Neumann boundary conditions are applied. Instead of a fixed water level, alongshore water level gradients are imposed. The gradient is assumed to be fixed over the lateral boundary and will only vary over time by the tidal wave tavelling along the coast.

The alongshore water level gradients are determined by a reduction of the general water level formulation at the longshore boundary (equation 5.1).

$$\frac{\partial \eta}{\partial x}(t) = \sum_{n=1}^{N} \frac{\eta_{n,2}\cos(\omega_n t - \alpha_{n,2}) - \eta_{n,1}\cos(\omega_n t - \alpha_{n,1})}{\Delta x} = \sum_{n=1}^{N} \frac{\eta_{n,3}\cos(\omega_n t - \alpha_{n,3})}{\Delta x} \tag{5.2}$$

where:

$\frac{\partial \eta}{\partial x}(t)$	= water level gradient	m/m
η_1, η_2, η_3	= amplitude of tidal wave in point 1, 2 and 3	m
ω	= frequency of tidal component	
α_1, α_2	= phase of tidal wave in point 1 and 2	-
Δx	= distance between point 1 and 2	

The river discharge of the through the Haringvlietdam is simplified. Most of the time the Haringvliet dam is closed and the discharge through the Haringvliet remains zero. The dam is closed off by the use of thin dams in Delft3D. For regular discharges which will be run for longer simulations, the discharge is simplified to a discharge of 1000 m^3/s through the Haringvlietdam. In case of extreme discharges, the sluices are fully open and a discharge of 5000 m^3/s is released from the river into the tidal lake for a short period.

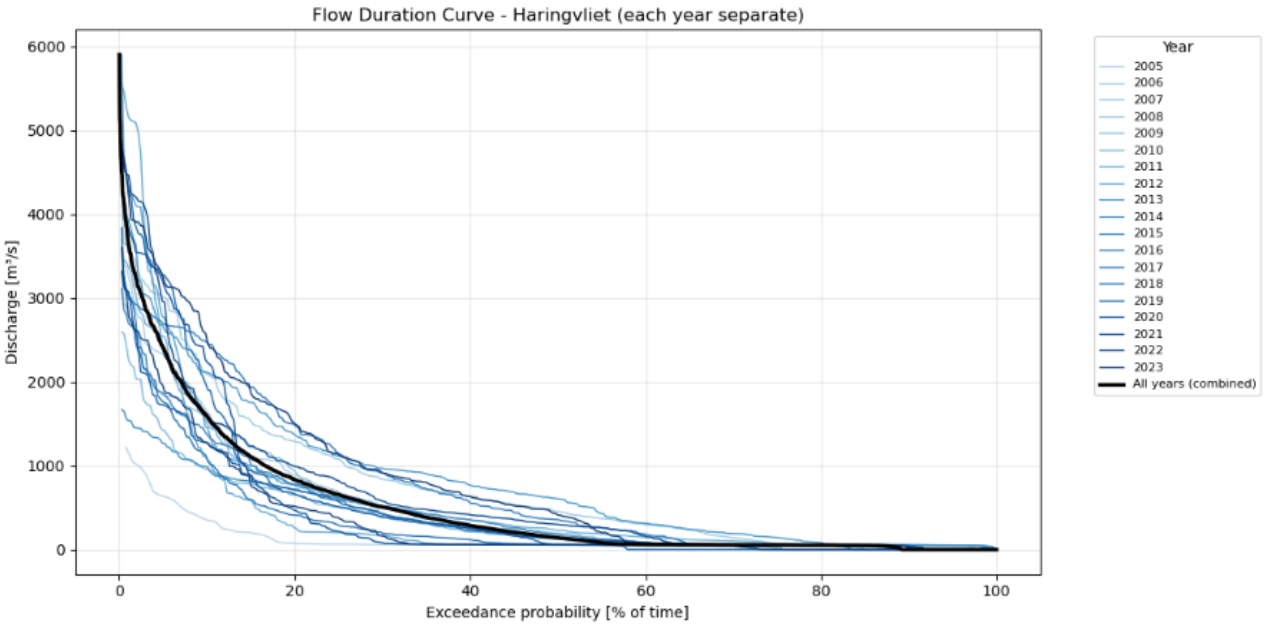

Figure 5.5: Daily discharge at the Maasmonding (bovensluis) and Haringvliet in 2021 and 2022

Table 5.1: Chosen steady discharges for Delft3D scenarios.

Chosen steady discharges for Delft3D		
$Q = 0$ m^3 s^{-1}	–	Closed-sluice baseline
$Q = 1000$ m^3 s^{-1}	–	Representative sustained high-flow (above typical regime)
$Q = 5000$ m^3 s^{-1}	–	Short-term extreme opening

Sediment transport

The total sediment-transport module in Delft3D computes both bed-load and suspended-load transport of non-cohesive sediments (Deltares, 2025). Bed-load transport is calculated using the Van Rijn (2007a) empirical formulation based on instantaneous bed shear stress (currents + waves), whereas suspended-load transport is solved via an advection–diffusion equation for sediment concentration in the water column (Van Rijn, 2007b).

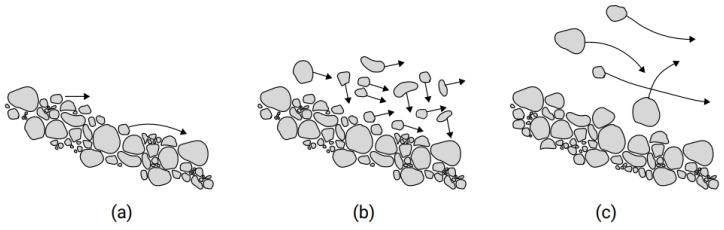

Figure 5.6: Different modes of sediment transport:(a) bed load at small shear stresses; (b) sheet flow (often considered as bed load at higher shear stresses); (c) suspended load (Bosboom and Stive, 2023).

In our model, a single sand fraction ($D_{50} = 160$ μm) is used. Although Van Rijn's empirical bed-load formula is typically calibrated for coarser sands (200–1000 μm), the method remains acceptable for finer sand in this case, where suspended-load transport is expected to dominate.

At the inland open boundary, a zero-gradient (Neumann) condition for sediment concentration is applied ($\partial c/\partial n = 0$), ensuring that the inflowing sediment concentration matches the local domain value.

Only one sediment fraction is considered, which is a simplification given that Delft3D supports multiple fractions. However, this approach suffices to capture the bulk sand dynamics in the study area.

The total sediment transport vector $\mathbf{S}_{\text{tot}}$ is computed as the sum of the bed load and suspended load components in both the u- and v-directions:

$$S_{u,\text{tot}} = S_{u,\text{bed}} + S_{u,\text{susp}} = \text{SBUUA} + \text{SSUUA}, \tag{5.3}$$

$$S_{v,\text{tot}} = S_{v,\text{bed}} + S_{v,\text{susp}} = \text{SBVVA} + \text{SSVVA}. \tag{5.4}$$

The total transport magnitude is then calculated as:

$$|\mathbf{S}_{\text{tot}}| = \sqrt{S_{u,\text{tot}}^2 + S_{v,\text{tot}}^2}, \tag{5.5}$$

and the transport direction (angle with respect to the x-axis) as:

$$\theta = \tan^{-1}\left(\frac{S_{v,\text{tot}}}{S_{u,\text{tot}}}\right). \tag{5.6}$$

The quantities $S_{u,\text{tot}}$ and $S_{v,\text{tot}}$ have units of $\text{m}^3/(\text{s m})$ (volumetric transport rate per unit width). As these values are integrated over the total simulation period, we get a volume per meter m^3/m or simply m^2. Figure 5.7 (a) shows the bed load transport, Figure 5.7 (b) the suspended load transport and Figure 5.8 the total sediment transport.

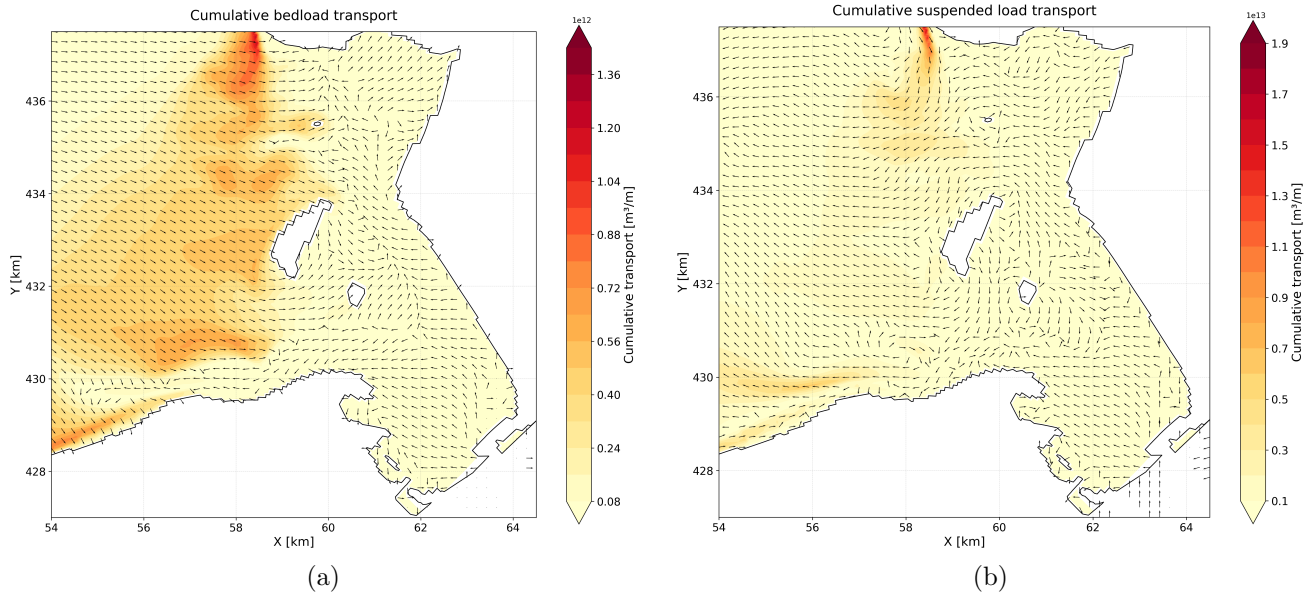

Figure 5.7: (a) Cumulative bed load transport (b) Cumulative suspended load ransport

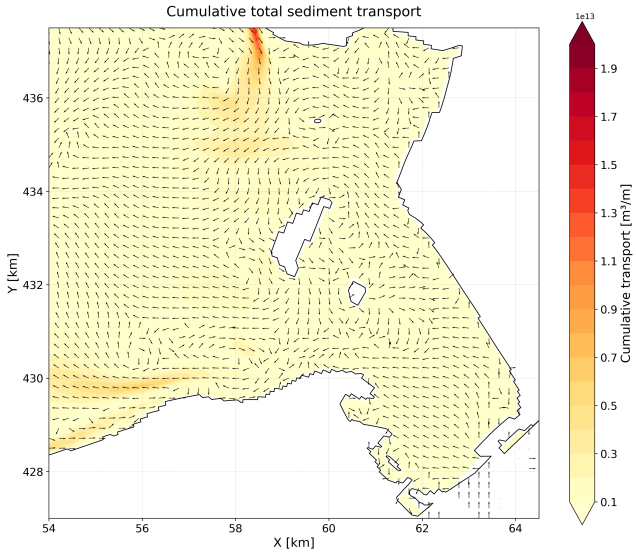

Figure 5.8: Cumulative total sediment transport

Constructions

The energy storage lake will be constructed by dredging the lake and placing the sand at the outer edges of the energy storage lake as a dike ring. In the model, the bed level of the dike ring is increased to a max value of -5 m, which is 5 m above mean sea level. There is a slight slope defined at the sea side of the dike ring to avoid sharp gradients and unrealistic results. The light blue area in Figure 5.9 shows the dike ring around the energy storage lake which has the same height as Maasvlakte 2.

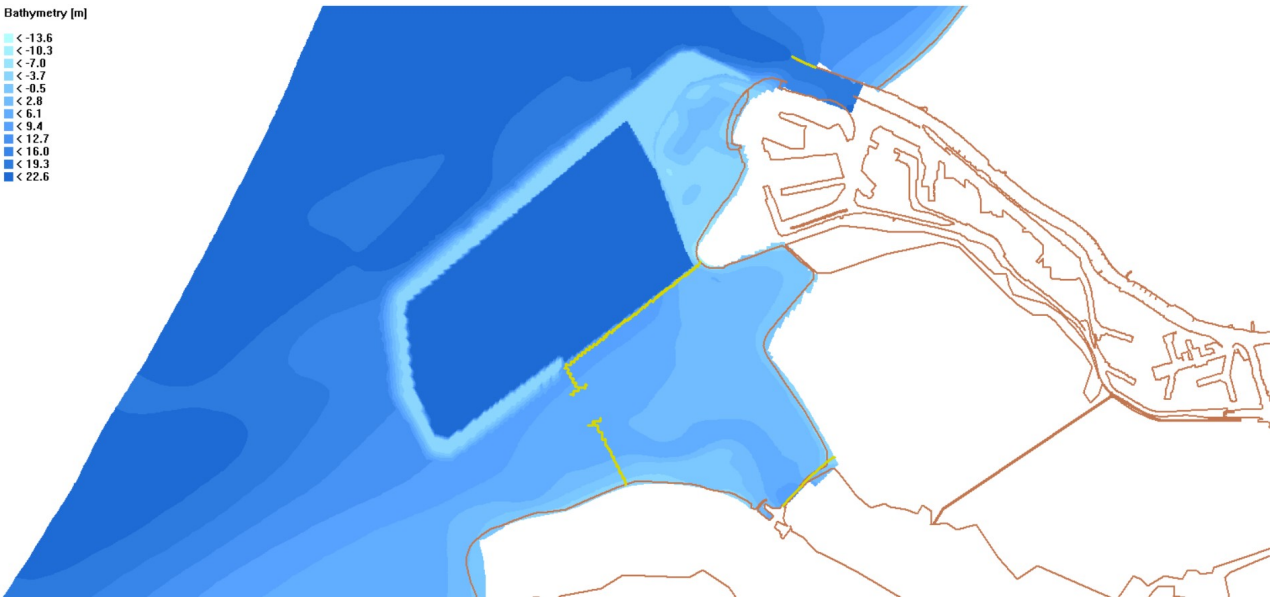

Figure 5.9: Visualization of the Delta21 construction in Delft3D. In blue the bathymetry (light blue around the energy storage lake and Maasvlakte is above sea level). The yellow lines represent thin dams where no water can flow through.

The tidal lake is semi-closed off by thin dams and land boundaries. As mentioned before, the tidal lake has an open connection with the North Sea by a storm surge barrier. The design and therefore the size of the cross-section is still a variable in the Delta21 design. As a storm surge barrier is a hard structure, the inlet can not change its size as is the case for a natural system. Therefore it needs to be determined beforehand. For this research it is interesting to investigate the effect of changing the inlet size.

Pumps and turbines

The pumps and turbines are implemented in Delft3D using discharges. As can be seen in Figure 5.10, 1/4 pumps are connecting the energy storage lake with the tidal lake and 3/4 of the pumps are connecting the energy storage lake with the North Sea. The total discharge of all the pumps together is 10 000 m^3/s. The steps towards these values are described in Chapter 3.

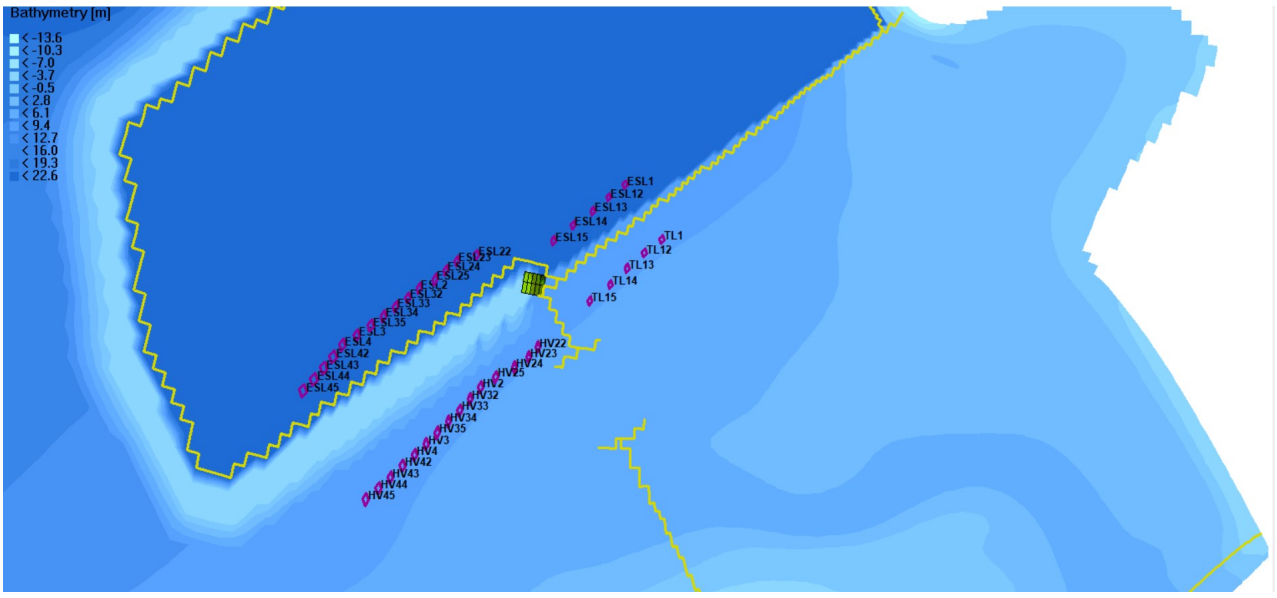

Figure 5.10: Visualization of the Delta21 construction in Delft3D including pumps. The pumps/turbines are implemented in Delft3D as discharge points.

The operating times of the pumps and turbines are described as follows. During night, the need of energy is minimum and excess green energy from wind moles are used to pump the water from the energy storage lake into the North sea and tidal lake. The daily pumping time is predefined and starts at 18:00 and ends at 06:00. During the day, this stored energy in the lake can be used by filling the energy storage lake again with turbines and receive the energy. The operation times are shown in the plot of Figure 5.11 relative to the water level. The implementation of the pumps and turbines in Delft3D can be done by using the in-out type of discharge.

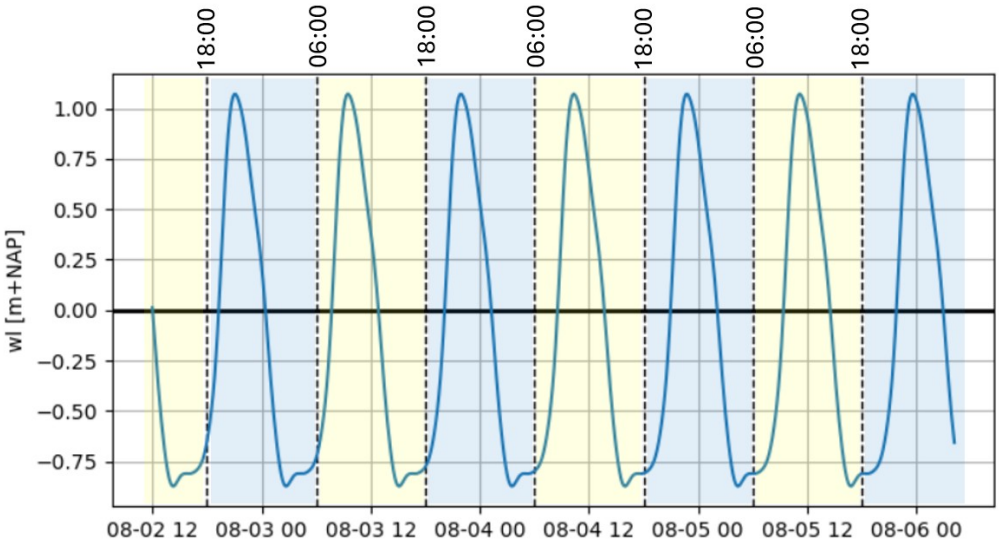

Figure 5.11: Schedule of the pumps/turbines The water level in the tidal lake is plotted with the pump operation (blue) turbine operation (yellow)

5.2. Model runs

Different schematizations

For this research, the four different schematizations shown in Figure 4.1 will be analyzed in two different scenarios. For the Netherlands we can divide this in normal conditions (around 9 months a year) and storm conditions (around 3 months a year). The different scenarios are fully calculated in Delft3D for six weeks. These six weeks include one week of spin-up, one spring-neap tidal cycle and one extra week. This period should be representative to use a MorFac for longer morphological simulation results.

Schematization	**Computational time**
1A - Current situation	366 days run, MorFac = 1
1B - Current situation	37.5 days run, MorFac = 10
1C - Current situation	12.2 days run, MorFac = 30
1D - Current situation	7.3 days run, MorFac = 50
2A - Delta21 construction	37.5 days run, MorFac = 10
3A - Delta21 construction, pumps/turbines and inlet size 1	37.5 days run, MorFac = 10
3B - Delta21 construction, pumps/turbines and inlet size 2	37.5 days run, MorFac = 10
3C - Delta21 construction, pumps/turbines and inlet size 3	37.5 days run, MorFac = 10
4A - Delta21 construction, pumps/turbines, river discharge and inlet size 1	37.5 days run, MorFac = 10, Q = 1000 m^3/s
4B - Delta21 construction, pumps/turbines, river discharge and inlet size 1	11 days run, MorFac = 1, Q = 5000 m^3/s
4C - Delta21 construction, pumps/turbines, river discharge and inlet size 2	37.5 days run, MorFac = 10, Q = 1000 m^3/s
4D - Delta21 construction, pumps/turbines, river discharge and inlet size 2	11 days run, MorFac = 1, Q = 5000 m^3/s
4E - Delta21 construction, pumps/turbines, river discharge and inlet size 3	37.5 days run, MorFac = 10, Q = 1000 m^3/s
4F - Delta21 construction, pumps/turbines, river discharge and inlet size 3	11 days run, MorFac = 1, Q = 5000 m^3/s
5A - Delta21 construction, pumps/turbines, SLR and inlet size 2	37.5 days run, MorFac = 10

Table 5.2: Delft3D runs Overview and description of all the model runs used for this research.

Run 3A and 3B will give the flow velocity in the inlet. If this is around 1 m/s, the erosion / sedimentation can be checked for this situation. When the flow velocity in the inlet is much lower or higher, the inlet dimensions need to be checked and adjusted.

Also from these runs it is interesting to check the sedimentation and erosion differences over the years. How is sediment moving and is there a net sediment import or export in the tidal lake. This can be done by determining the volumes of different classifications and see how they change over the years.

Overall observation points and cross sections

Throughout the simulations, the same observation points and cross sections are used for a reliable comparison. These observation points are shown in Figure 5.12.

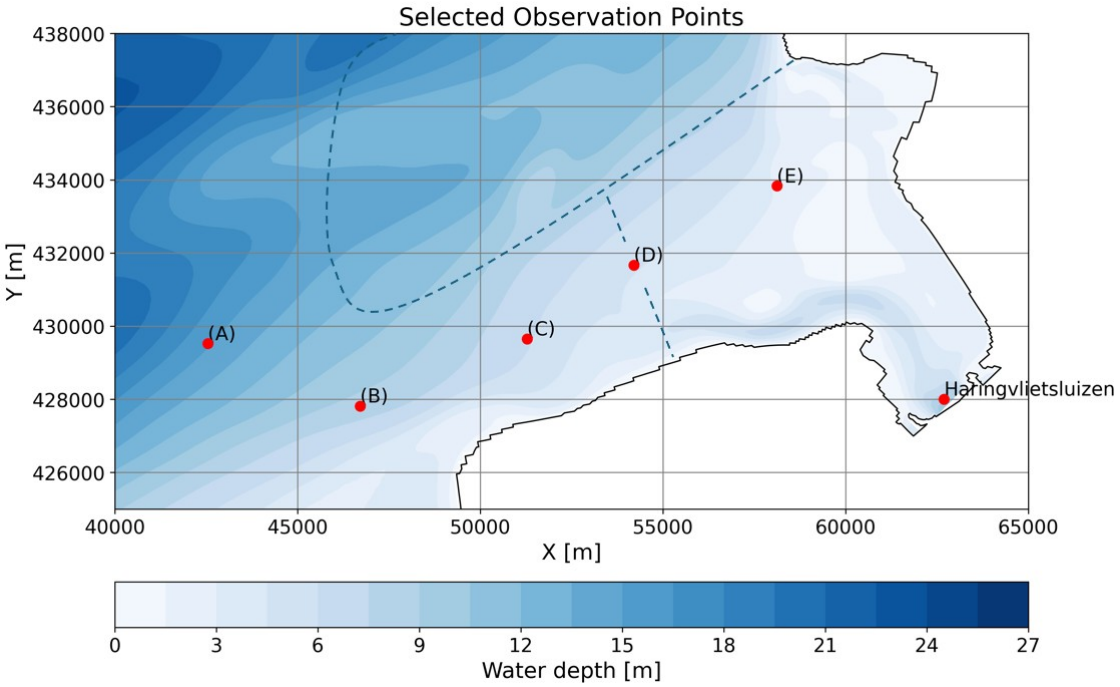

Figure 5.12: Observation points in Delft3D. Plotted on the water depth with the location of the Delta21 construction shown as a dashed line.

Observation points (A), (B), (C), (D) and (E) are interesting to visualize the changes in the shape of in the tidal wave when propagating into the tidal lake. Point (A) is the most offshore location where the effect of the Delta21 construction is expected to be minimum. Point (D) is exactly inside the inlet where the tides flow in and out during one tidal cycle. Point (E) is located more or less in the middle of the tidal lake. Points (B) and (C) represent the points in between to ensure the points have equal distances.

Computational time

After determination of the boundaries, the spin-up time is checked by plotting the output of the tidal wave after running the model. Figure 5.13 shows the shape of the water level, mainly caused by the tidal forcing. We can see the spin-up is around 2 till 3 tidal cycles. For convenience, the default of 720 min is doubled to 1440 min (24 hours). This means that sediment transport rates are not computed until this specified time.

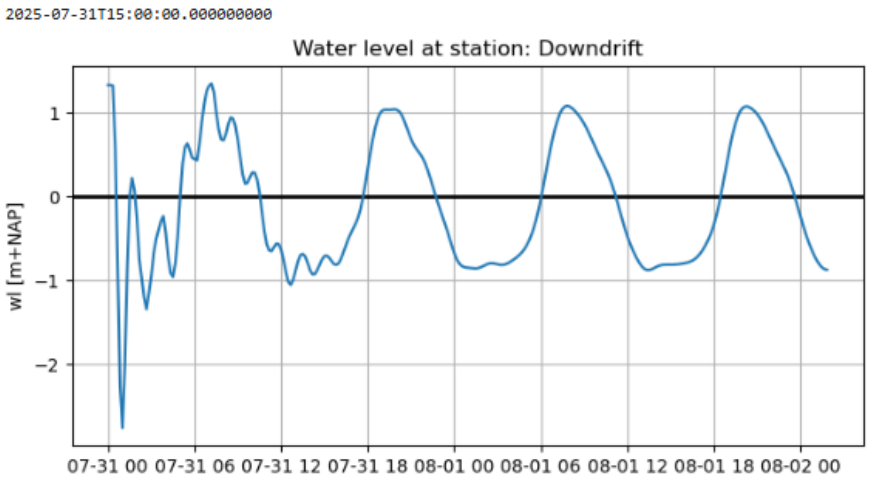

Figure 5.13: spin up for the hydraulic forces, around 3 cycles

In general, morphological developments take place on a time scale several times longer than the flow changes. Especially in this model, because we do not include the spring-neap tide and use a constant discharge. To speed up the morphological changes, we can make use of the "morphological time scale factor". This factor simply is multiplied by the erosion and deposition fluxes from the bed to the flow at each computational time-step. It is important to check the maximum factor that can be used without affecting the accuracy of the model. This can be tested by varying the factor and looking at the differences in sedimentation and erosion. One of the main problems that can occur in this case is the availability of sediment inside the system. We therefore want to reduce the morphological factor and run the model as long as possible.

To see the difference by the use of a morphological time factor, we run the same model without Delta21 layout for 1 year result with morfac=1, 10, 30 and 50. The reason the days are for example 37.5 in stead of 36.5 is because of the 24 hour spin-up. The results of the use of different morfac's are briefly explained in Chapter 6.

5.3. Validation

Detailed wave parameters of previous studies

This paragraph describes the method used to evaluate the accuracy of the model by comparing it to the physical world. The model itself has been used for several studies before (by Roelvink (1999) and Steijn et al. (2001)) and has improved over time. Previous students have used this model for their research too (de Vries (2007), Colina Alonso (2018), Zaldivar Piña (2020) and van Horick (2023)).The model that is used for this research was received from a previous student who validated the model by comparing it to the actual available bathymetry of Vaklodingen datasets from Rijkswaterstaat (Zaldivar Piña, 2020). The idea is to use the 2015 measured bathymetry and run the model for three years including the tide and waves. The final bathymetry from the models output can be compared to the actual bathymetry measured in 2018. The comparison is done by visualizing the final bathymetry and the cumulative sedimentation/erosion pattern (final minus initial bathymetry). This is done by the previous study and the results are shown in the first two columns of Figure 5.15.

Validation of the model can only be done for the current situation, without Delta21 construction. The difference, compared to the used model for this research, is the inclusion of the Wave-module to reconstruct the current situation. The first step is to define the WAVE conditions for Delft3D as in the current situation waves cannot be neglected. If the model results when waves are included show similarities to the model results of the previous student, we assume that the model is more or less well received. For the next part when we include the Delta21 construction we can exclude the WAVE module as the area of interest is mostly sheltered by the energy storage lake. In addition to this, the hydraulic forces will be included stepwise, so that the results can be compared relatively to each other.

The wave climate used in previous studies is shown in Table 5.3. The wave climate was based on the schematization of de Vries (2007), who reduced long-term measurements at the Europlatform station (52.00° N, 3.28° E) into a representative set of offshore wave conditions. Each condition is defined by a fixed significant wave height, peak period, wave direction, wind speed and wind direction, and is associated with a proportional duration over the year. These representative conditions were converted into a continuous time series for Delft3D. The relative frequency of each wave condition was translated into time blocks (in minutes) and assigned sequentially. Although the series is based on one year of offshore wave statistics, the conditions were compressed into a 36.5-day forcing period for use in the model. To obtain morphological evolution over a three-year period (2015–2018), a morphological acceleration factor of 30 was applied.

Table 5.3: Overview of the wave and wind parameters used for validation

WC	Hs [m]	Tp [s]	Dir [°]	Wind vel. [m/s]	Wind dir [°]	Weight factor [-]	Duration [days/yr]	No. Mor. [-]	Tides MF [-]
70	2.99	7.78	323.7	12.7	310.2	0.045 65	50	4	24.1880
40b	1.99	6.35	231.6	11.6	225.9	0.026 01	28	2	27.5573
102	4.48	9.52	276.2	17.8	277.3	0.002 28	2	1	4.8276
89	3.98	8.98	247.5	18.1	253.0	0.005 79	6	1	12.2700
43	1.99	6.35	277.4	10.8	271.2	0.088 27	97	7	26.7239
8a	0.48	4.45	292.9	4.2	240.0	0.238 27	261	17	29.7048
64	2.98	7.77	231.6	15.2	225.6	0.031 61	35	3	22.3274
40a	1.99	6.35	231.6	11.6	225.9	0.173 88	190	12	28.3464
8b	0.48	4.45	292.9	4.2	240.0	0.238 27	261	17	29.7048
36	1.47	6.05	352.9	6.4	345.9	0.147 40	161	11	28.3984

The results of the model when these wave conditions are used (by Zaldivar Piña (2020)) are shown in the second column of Figure 5.15. The upper plot shows the cumulative sedimentation and erosion pattern after three morphological years. The lower plot shows the final bathymetry calculated by the model. These two plots are compared to the first column of Figure 5.15 which are results of real measurements made by Rijkswaterstaat.

Sedimentation and erosion patterns

The model is run without waves Figure 5.14 (a) and with the inclusion of the simplified waves 5.14 (b). In the plot without waves the Haringvliet is open but the discharge is set to zero. This means water can flow into the Haringvliet during flood.

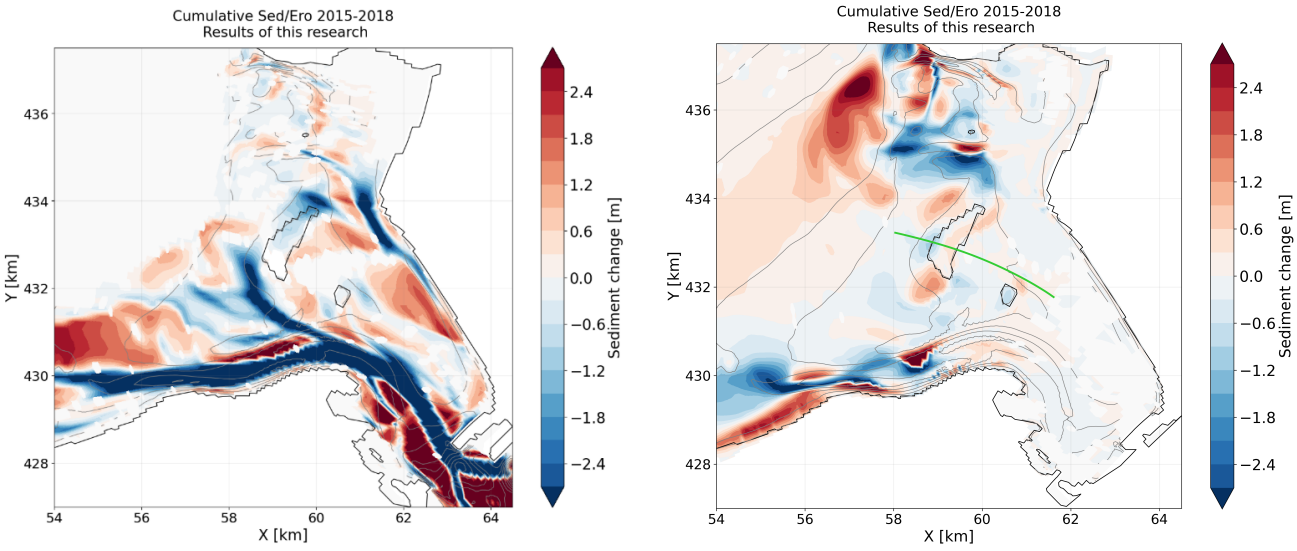

Figure 5.14: (a) Model results with an open Haringvliet and no waves (b) Model results with a closed Haringvliet and inclusion of the waves presented in Table 5.3.

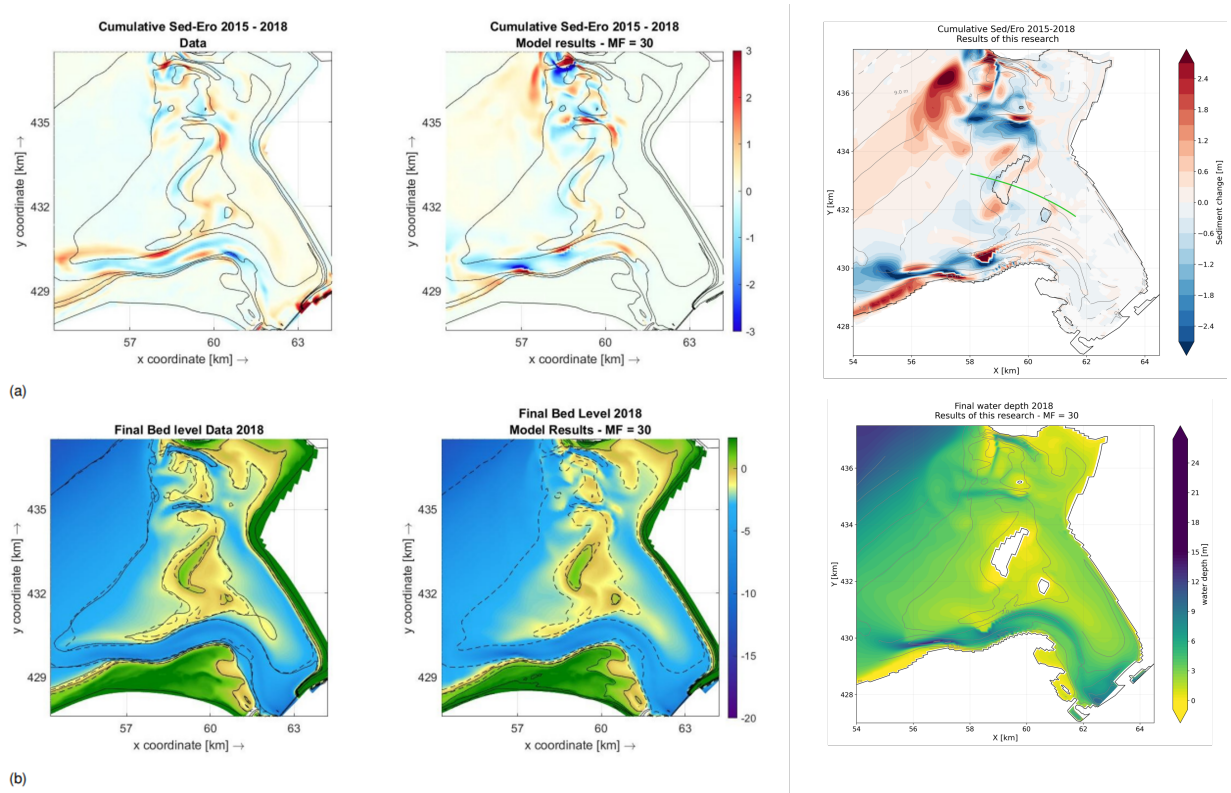

Figure 5.15: Long term validation of the model. Validation method in previous thesis study of Zaldivar Piña, 2020 for the period 2015 - 2018 with a constant morfac of 30. The columns respectively represent the cumulative sedimentation / erosion and final bathymetry of: available data, previous thesis and this research.

The third column of Figure 5.15 shows the results of the model that is used for this research. The overall comparison can be done between the three cumulative sedimentation erosion patterns. Erosion is found at the sea side of the delta when observing the actual data whereas sedimentation is found when the model is used. This incorrect prediction was already known for the model. The first element we can observe is the

movement of the Hinterplaat towards the shore. The initial and final cross section of this sandbank is shown in Figure 5.16. Erosion at the seaside of the Hinterplaat and sedimentation at the other side is due to water overflowing the Hinterplaat. Another comparison is by looking at the main channel Slijkgat. Overall, the main channel shows erosion pattern with local sedimentation areas along the sides. These sedimentation locations are comparable but show higher values in the model used for this research. These higher values are especially along the channel and in the northern side of the plot. This inaccuracy is something that we need to keep in mind.

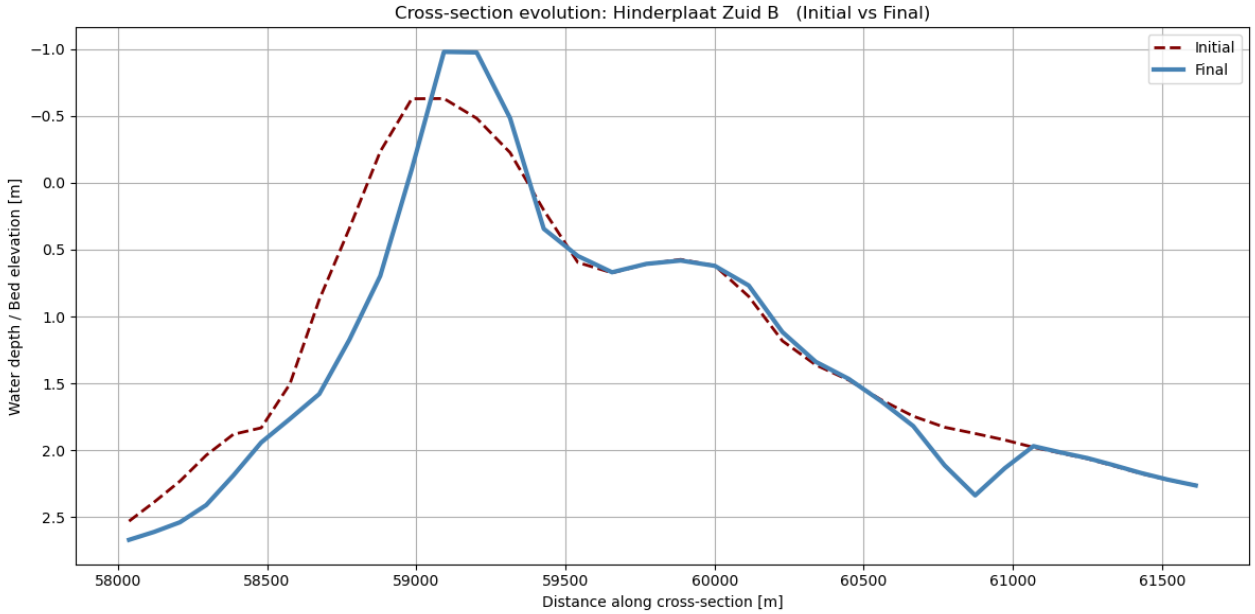

Figure 5.16: Hinterplaat cross section

Calibration

Model calibration is needed to ensure that the model resembles the reality as close as possible. This is done by adjusting the input parameters to reproduce physical phenomena. As described in the beginning of this chapter, the model is used in previous studies and many calibrations have been carried out (Roelvink, 1999, Steijn et al., 2001, de Vries, 2007, Colina Alonso, 2018). Recommendations are written in previous models to improve the models morphodynamic predictive performance. Most of these recommendations are related to the WAVE-module and the sand mud interaction which are not used in this study. Therefore improving the morphodynamic performance is not within the scope of this project. The main idea is to build up the model by including the controls one by one. This way it is possible to only look at the relative effects of each control on the system.

6
Model results and scenario analysis

In this chapter the results of the model runs (Table 5.2) are presented including an analysis. Figure 6.1 shows again the four different schematizations which resembles the way this Chapter is organized. Each section has the focus on one schematization to build up the model from the current situation. This chapter concludes with application of the model to test the response of the system to Sea level rise and extreme river discharges.

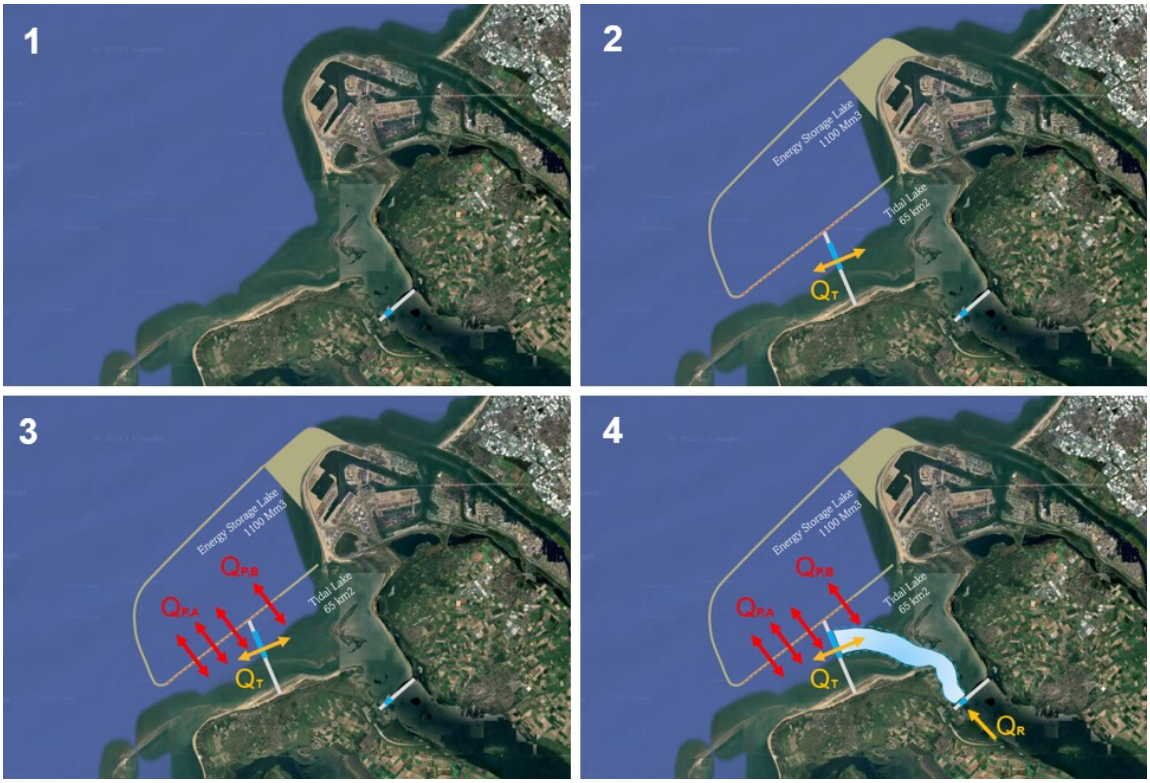

Figure 6.1: Four different schematizations used for this research where the Delta21 construction and the hydraulic forces are visualized on a Google Earth screenshot (Google LLC, 2025).

6.1. Model schematization 1: current situation

Model schematization 1A and 1B both represent a simplification of the current situation, without the Delta21 construction. The only hydraulic force is the tide, defined at the boundaries, as we set the river discharge to zero. This first run is to understand the flow patterns during one tidal cycle and the morphological changes over one year. In the first plot on the next page, we can see the water level change over two days at location (E) which is just offshore the Hinterplaat. It shows the semi-diurnal tide which has around two peaks and two troughs a day. At these peaks and troughs, the water level reaches its highest or lowest point and shifts between increasing and decreasing water level. The relation between the water level and the velocities depends on the character of the tide. For progressive waves the maximum velocities are found under the crest of the wave (Bosboom and Stive, 2023) and for standing waves this phase difference is 90°. Figure 6.2 shows the water level in the upper plot and the flow velocity in the lower plot. At the time steps where we have the output data of the History and Map files of Delft3D, a snapshot is made to visualize the flow velocities at that specific moment in one tidal cycle. The vertical lines indicate these locations with a time step of two hours.

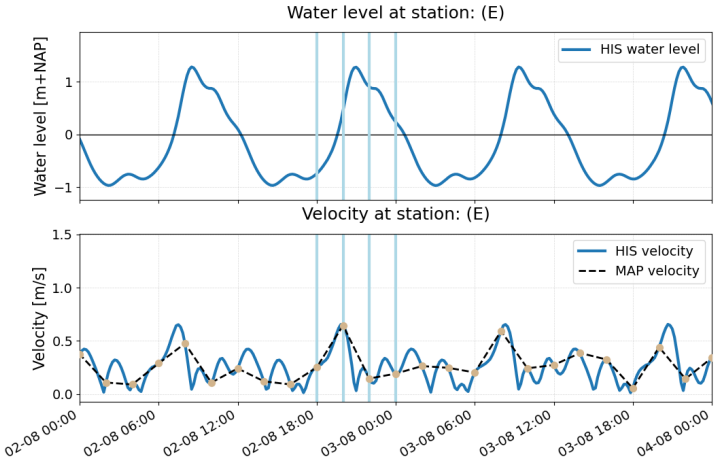

Figure 6.2: location phases 1

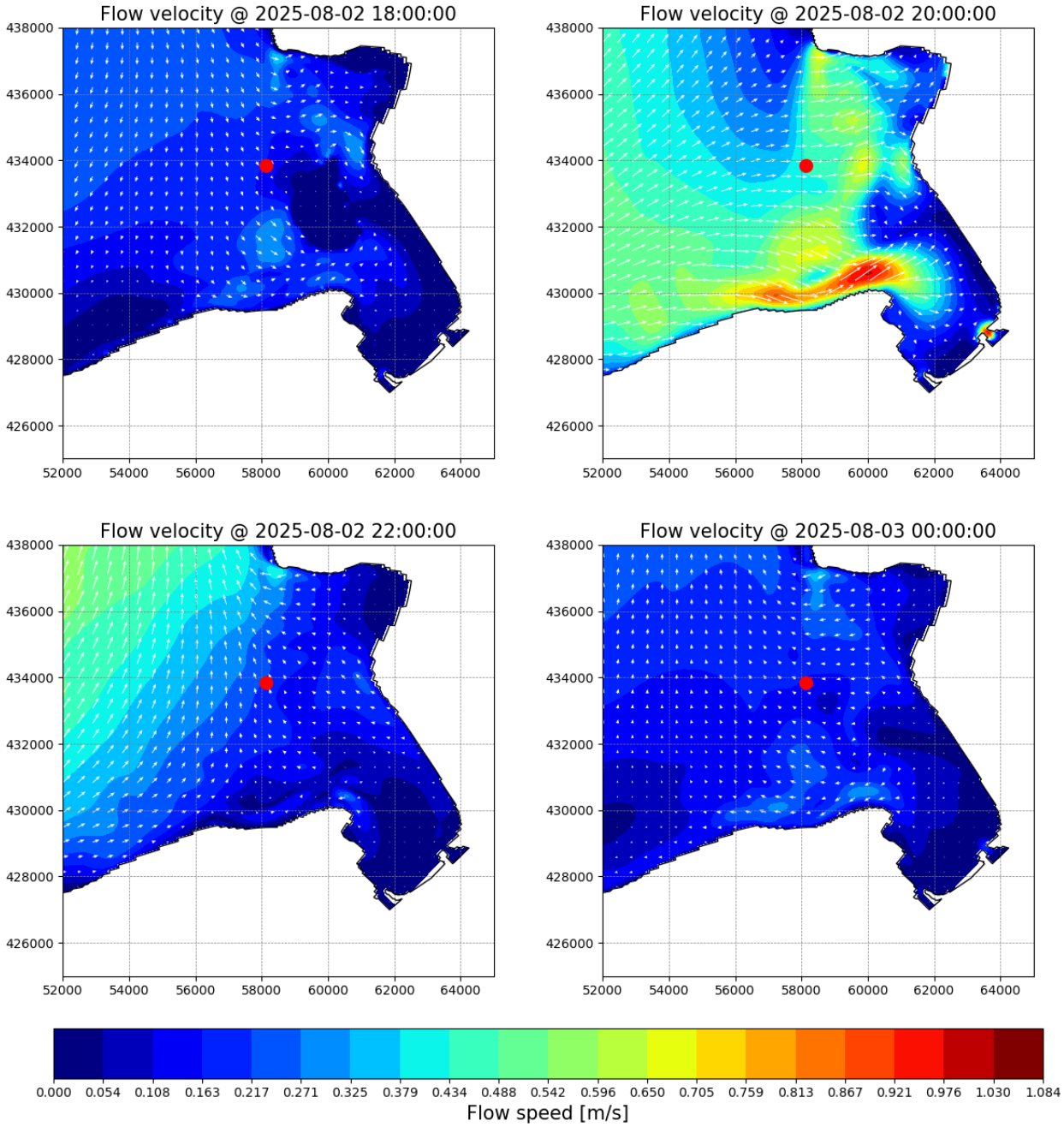

Figure 6.3: phases1B

Interesting is to compare the graphs of the water level and velocity to the 2D flow velocity maps at the four time steps. This is a method to check if the map matches the expectations. The first distinction between the four time steps of the graph in Figure 6.2 is that the first two chosen time steps are during water level rise and the last two time steps during water level fall.

A rising water level will fill the coastal area with water and increase the wet area. Looking at the first plot, we see that the flow velocity vectors are pointing towards the shore and the Hinterplaat is above water level. During this time, the water level is NAP - 0.75 m and is around its lowest point when the intertidal areas should emerge. If we compare this with the second time step, two hours later, the graph shows that the water level increased and the flow velocity is maximum. The increase in water level shows less dry areas in the map and water flows over the intertidal Hinterplaat. As the water level is rising, the directions of the flow are still towards the shore filling the coastal area. During this time, the flow velocity is maximum. The colors indicate the locations and magnitude of the flow velocity. The highest flow velocities are in the Slijkgat tidal channel. This is the deepest channel of the Voordelta where the most volume of water, including river discharge, flows through. An explanation for these high flow velocities can therefore be flow concentration in the Slijkgat channel as the Voordelta is mainly a shallow area.

The two plots below in Figure 6.3 are the flow velocities during water level fall. The water flows out of the Voordelta in offshore direction. The third plot is right after the water level peak when the water level is still high.

Movement sandbanks / tidal flats

The graph below, Figure 6.4 shows the water level or tidal wave in the six observation points. The location of these observation points are shown in Figure 5.12. At these observation points the tidal waves are almost identical. This makes sense as the observation points are close to each other and the tidal wave reaches each observation point around the same time. Only at the Haringvliet sluices, there is some deformation in the shape of the wave. This is probably due to the irregular bathymetry in front of the Haringvliet sluices.

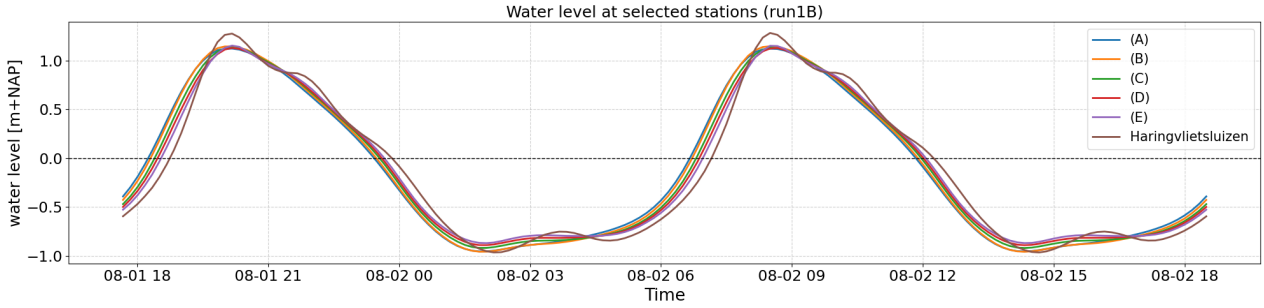

Figure 6.4: Water level at the six observation points (Locations in Figure 5.12)

One difference between the observation points for this schematization is the water depth. The water depth is decreasing from observation point (A) (most offshore) to observation point (E) (most onshore) . When waves are propagating towards the shore they start shoaling. This process is characterized by asymmetry around the horizontal and vertical as described in the Theoretical Background in Chapter 2. The asymmetry around the horizontal is skewness where we can see peaking of the wave crest and flattening of the trough. Looking at the colored lines of Figure 6.4, the decrease in water depth results in more flatten troughs.

The other asymmetry is around the vertical where we can see a faster increase of the water level (rise) compared to the decrease of the water level (fall). So the wave crest moves faster than the wave trough and therefore results in a pitched-forward wave shape. This relative steepening of the face while propagating towards the shore is a result of the decreasing water depth. It is described by the speed of non-linear shallow water waves: $C_{crest} = \sqrt{g(h+a)}$ and $C_{trough} = \sqrt{g(h-a)}$. This effect can also be seen in the graph of Figure 6.4 when we look at the colors of the different observation points and their water depths. The more the tidal wave travels onshore, the more asymmetry it shows.

Comparison morphological scale factor

Finally, model schematization 1 (current situation) is used to make an analysis on the morphological scale factor (morfac). This is done by comparing the morphological results (sedimentation/erosion patterns) using different values for the morphological scale factor. Figure 6.5 (a) shows the sedimentation/erosion pattern for a full simulation period of 365 days. The two red lines indicate the locations of two cross sections. Starting with comparing a scale factor of 10, which is an important one as this morphological scale is used often in this

research. The idea is to reduce the modeling time from 365 days to 36.5 days using a morfac of 10. Figure 6.5 (a) shows the result when using a morfac of 1 and Figure 6.5 (b) shows the difference when a morfac of 10 is used. What can be seen is that the difference in erosion and sedimentation does not exceed 20 cm. The difference is mainly in the main channel where the sedimentation/erosion values are largest.

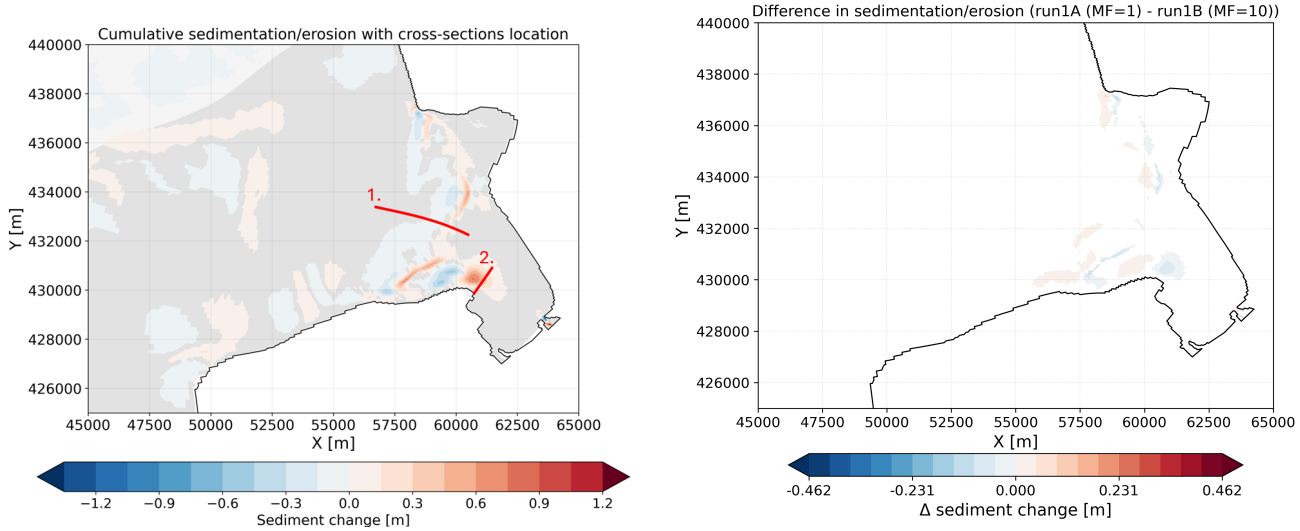

(a) (b)

Figure 6.5: (a)365 days run Morfac=1 (b)difference 36.5 days run Morfac=10)

For longer term simulations, comparison with higher morfac values are necessary. When the model is run for 36.5 days, the morphological responds can be increased to three years when using a factor of 30 and five years when using a factor of 50. For this reason it is interesting to see the effect when these values are used. To make a valid comparison, the erosion sedimentation patterns are plotted for one morphological year. In Figure 6.6 (a) and (b) the differences between the 365 days run and the runs with morfac = 30 and 50 are plotted respectively.

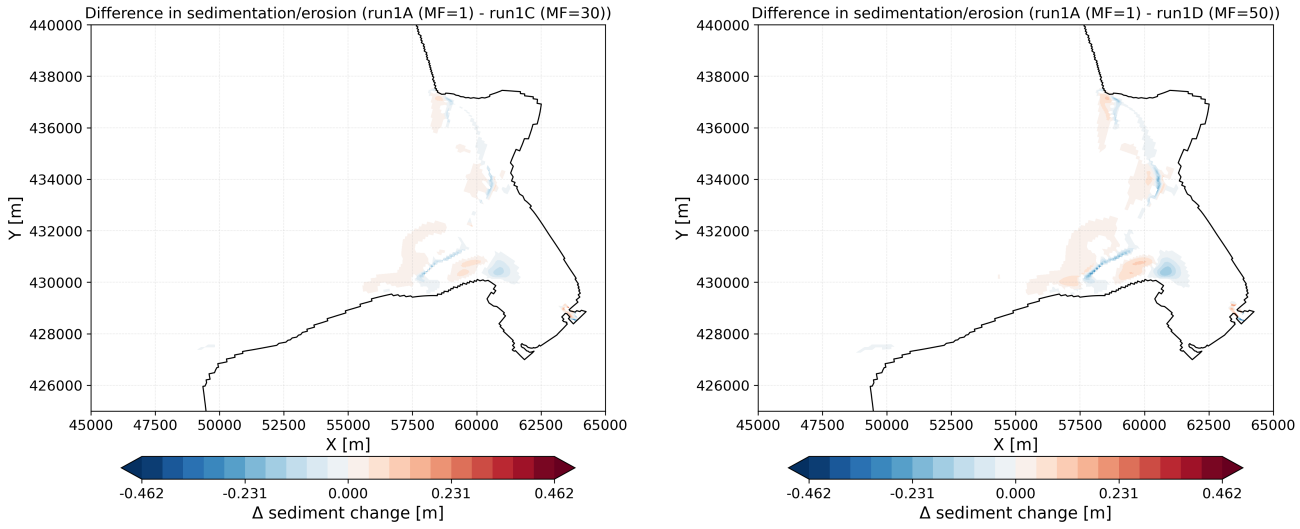

(a) (b)

Figure 6.6: (a)12.2 days run Morfac=30 (b)7.3 days run Morfac=50)

As in this schematization the only hydraulic force is the tide, movement of the sediment bank can be analyzed. In general, waves push sediment onshore by their skewness so the net sediment transport is towards the coast. This was described by the theory explained in Chapter 2. One of the interesting cross-sections is the one through the intertidal sandbank named Hinderplaat. This cross-section is indicated in Figure 6.5 in red (1.). The initial and final cross-section are shown in Figure 6.7. The left side of the plot is located in the offshore direction and the right side of the plot in onshore direction. It is clear from the graph that the peak of the sandbank moved in onshore direction and increased its height.

The final cross-sections of the Hinterplaat, in case of four different morphological factors are visualized by use of different colors. The blue line represents the case when a morphological factor of one is used which implies the actual result. When including a morfac, we want the result not to deviate too much compared to this situation. First thing that we can notice is that the differences are relatively small. At the crest of the sandbank we only see a maximum difference of 30 cm. This difference is increasing by increasing the morphological factor. Also the shape of the final cross-section does not show extreme differences.

Figure 6.7: Cross-sections of the Hinterplaat when different morphological factors are used. The black dashed line represents the initial cross-section and the colored lines the final cross-section after one year morphological time.

Another interesting cross-section is the Slijkgat channel indicated in Figure 6.5 (a) as cross-section (2.). Also here the overall shape does not change and the maximum difference is not higher than 15 cm.

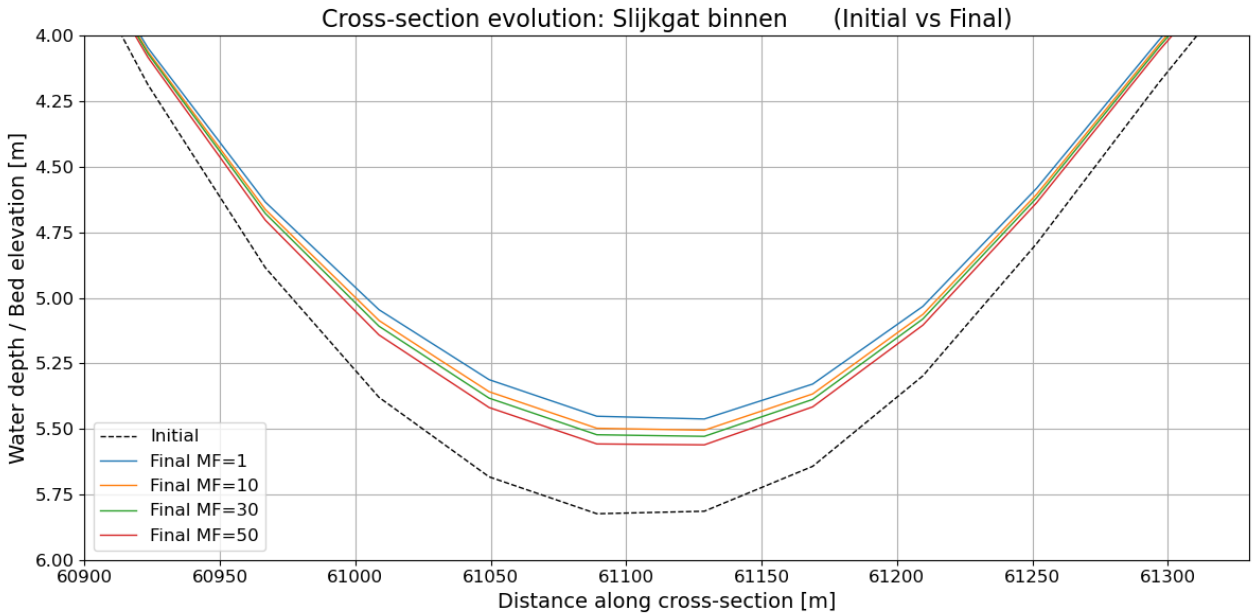

Figure 6.8: Cross-sections of the Slijkgat (main channel) when different morphological factors are used. The black dashed line represents the initial cross-section and the colored lines the final cross-section after one year morphological time.

The conclusion can therefore be made that all the morfac values show reliable results. For this research it is chosen to use a maximum value of 30 to reduce small deviations as much as possible.

6.2. Model schematization 2: including Delta21 construction

In this next schematization, the Delta21 construction is implemented and the hydraulic forces stay the same. No pumps are activated yet. Figure 6.10 shows the energy storage lake, surrounded by the dike. Part of the dike is indicated in a white color as it reaches above the maximum water level. The other parts of the Delta21 construction are modeled using thin dams which are not visible in this plot. The inlet width is set to 1500 m with a dredged depth of 6 m. The bathymetry is not changed at the other locations to analyze the effect of the Delta21 construction on the hydrodynamics and morphodynamics. The four plots show again the depth averaged flow velocity including vectors at the same time steps as used before. But this time we see differences in water level and flow velocity compared to Figure 6.2.

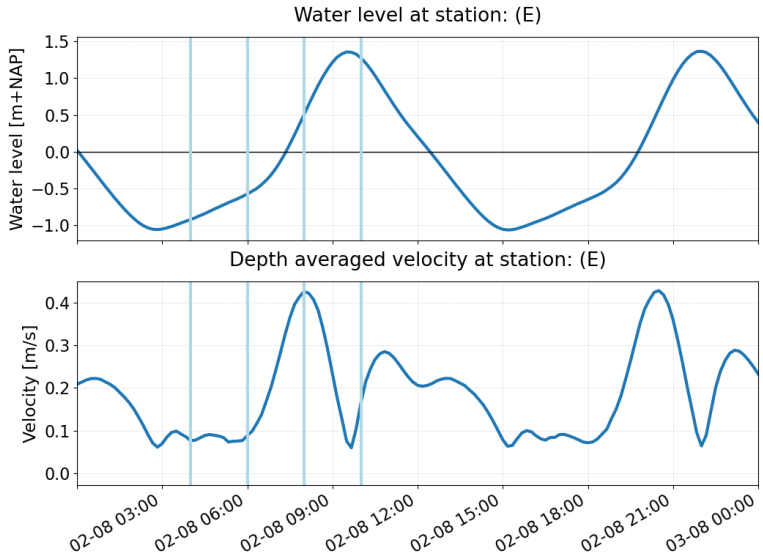

Figure 6.9: Water level and depth average velocity at observation point (E) which is located inside the tidal lake

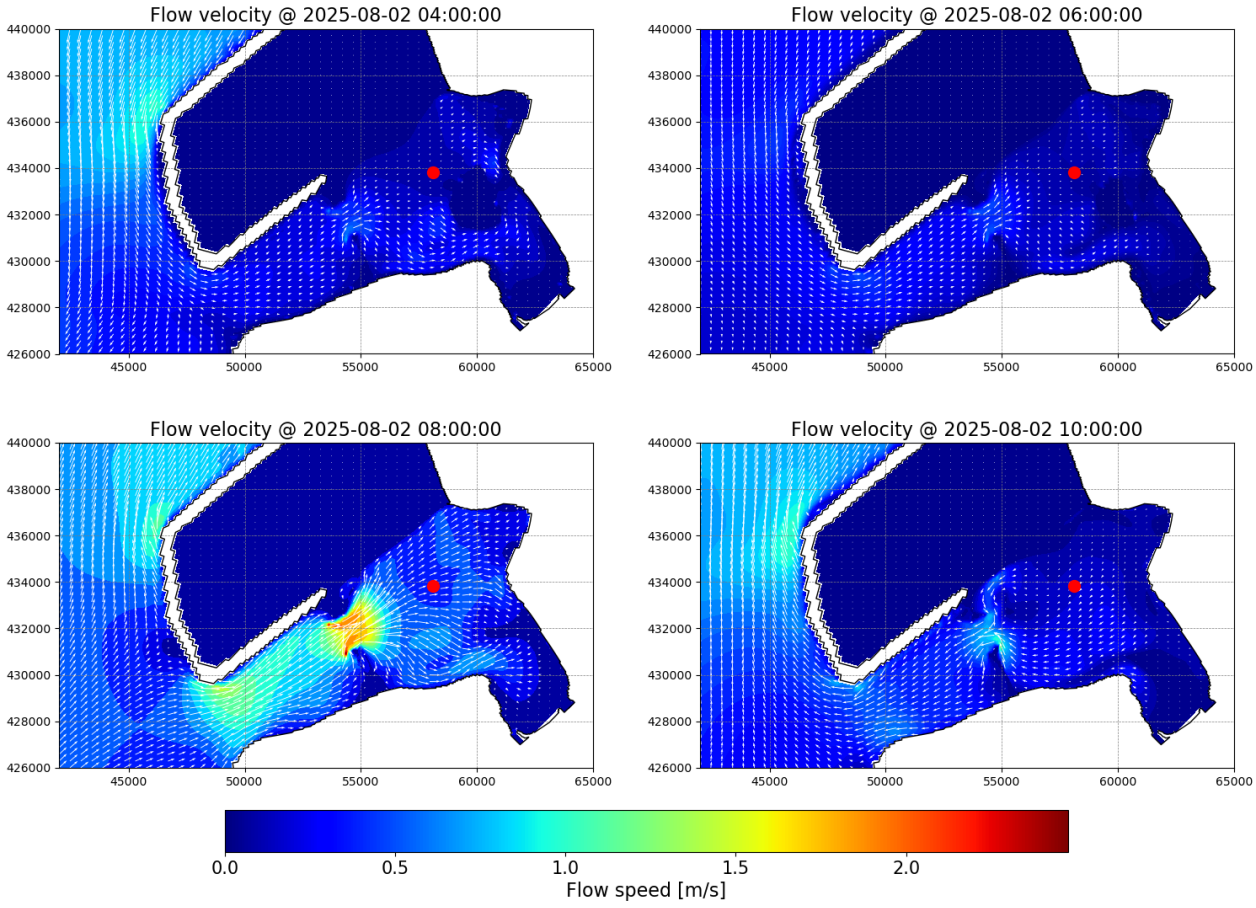

Figure 6.10: Depth averaged velocity with vectors indicating the flow direction

The first plot shows the situation when the water level is low but starts rising. The tidal lake starts to fill in and water is flowing around the Hinterplaat as it is above the water level. The flow velocity is increasing because of contraction inside the inlet but also around the Hinterplaat. The main water flow is through the Slijkgat channel. It is the deepest channel where during low water, most of the water is flowing through. In the second plot, two hours later, the same flow pattern is observed. The water level increased a bit but no major differences.

Two hours later, the maximum flow velocity is reached at almost all locations on the plot. The velocity inside the inlet reaches 2 m/s and the tidal lake is filling at maximum rate. The water starts flowing over the Hinterplaat and other shallow areas. During these high velocities it can be observed that not only in the tidal inlet the velocity is high, but also in the corner of the energy storage lake near Goeree. An increase of flow velocity can lead to erosion so this area needs attention when analyzing the system as a whole.

The fourth and last plot shows the flow velocities during ebb. Water is flowing through the inlet out of the tidal lake emptying this area. Just before the water flows out of the tidal lake near the inlet, the construction is not streamlined and the flow needs to switch direction fast and increases the flow velocity.

We can again look at the tidal wave at locations (A), (B), (C), (D), (E) and Haringvlietsluizen. The water level is plotted in Figure 6.11 against each other, the same way as the case without Delta21 construction in Figure 6.4. The tidal wave shifts along the horizontal time axes. This makes sense as the propagation of the tidal wave follows the observation points respectively. Besides this shift in time, amplification of the crest can be observed.

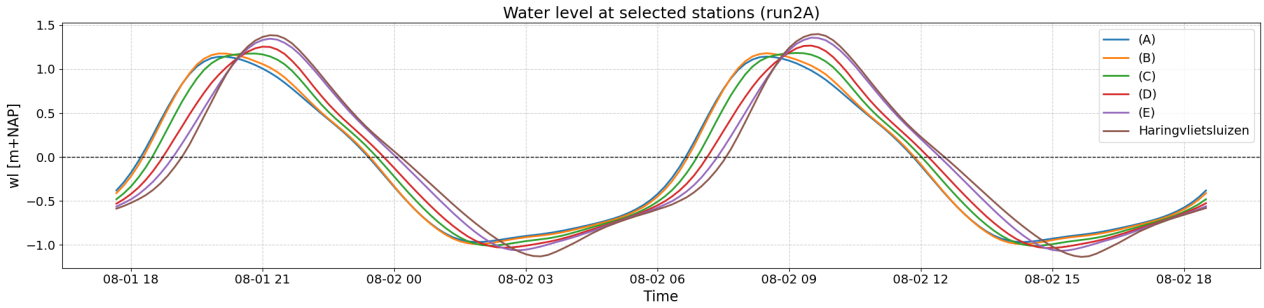

Figure 6.11: Water level at the six observation points (Locations in Figure 5.12)

Interesting is to look at the phase differences for the case with the Delta21 construction and the case without Delta21 construction. As described in the theoretical background of Chapter 2, we expect the tidal wave behave as a progressive wave in the case of no Delta21 construction. The plot of Figure 6.12 shows the water level and velocity without Delta21 construction at observation point (D) located inside the tidal inlet. The tidal wave at observation point (D) can only be effected by the Maasvlakte but this effect is expected to be minimum. It needs to be noted that the velocity is plotted with only positive values. Therefore the division between ebb and flood currents is made when the velocity reaches zero. For a progressive wave, the peaks align between the water level and velocity which is also visible in the plot.

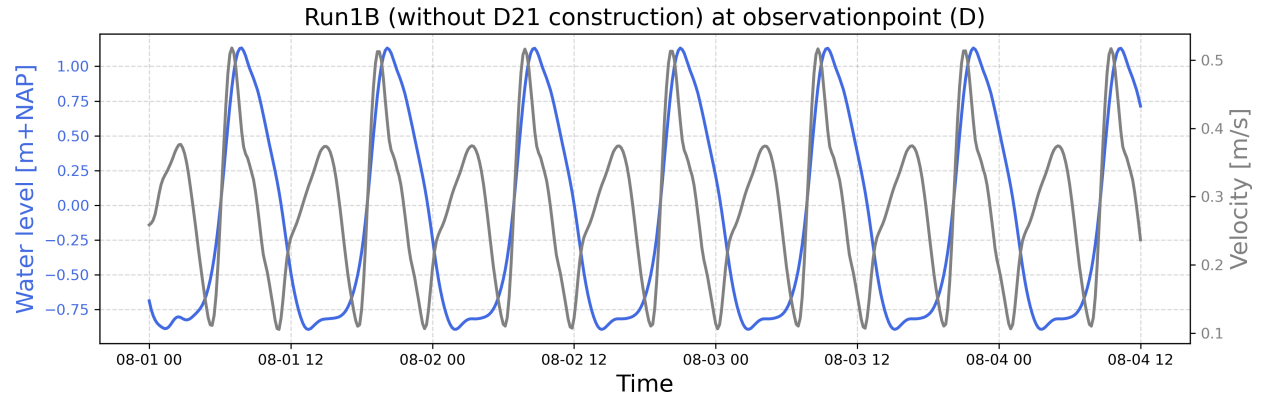

Figure 6.12: Water level and velocity in phase indicating a progressive wave.

If compared to the case with Delta21 construction, a shift in the phase difference is expected. The water level and velocity are shown in the plot of Figure 6.13. This graph indicates a standing behavior of the tidal wave as the peaks of the velocity aligns with the moment in time when the water level reaches zero. Also, this 90 degree phase difference was expected and described in the theoretical background of Chapter 2 and visualized in Figure 2.2 (a).

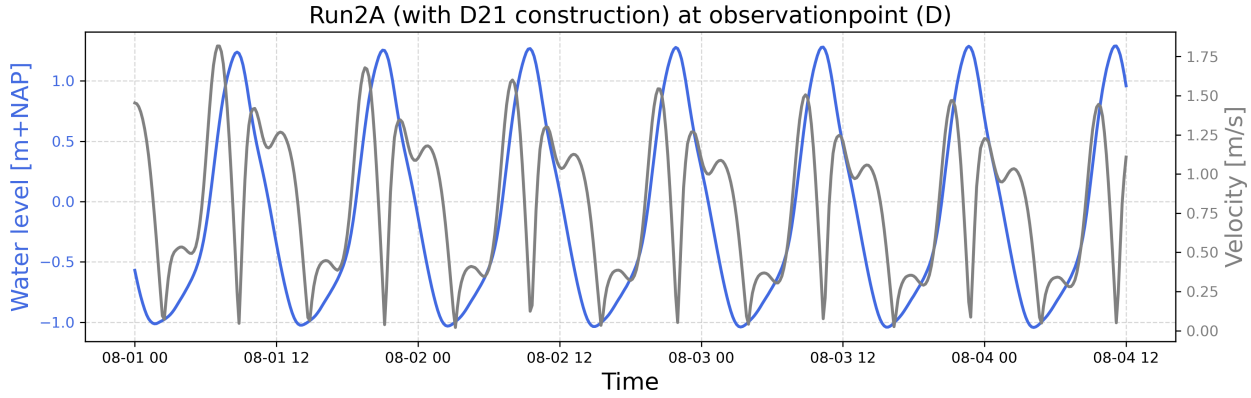

Figure 6.13: water level and velocity 90 degree out of phase indicating a standing wave.

Sediment transport is directly related to the velocity and the plot of Figure 6.14 shows this relation by overlapping the two results inside the tidal lake. The red dashed line is the velocity as in Figure 6.13. Now both bed load and suspended load transport are added in the figure in U and V direction. First thing that can be noticed is the dominance of the suspended load over the bed load sediment transport. The light and dark blue colors indicate the suspended sediment and as the u and v components are shown separately, positive values are in flood direction and negative values in ebb direction. It is clear that the transport is directly related to the velocity as they have the same shape in the figure. What can be seen is that the suspended load starts moving when it reaches a velocity of around 0.16 m/s. Below this value there is no sediment transport. What also can be seen are the higher transport rates at the start of the simulation that is decreasing each tidal cycle. This can be the result of erosion that is leading to a higher water depth and less bed shear stress.

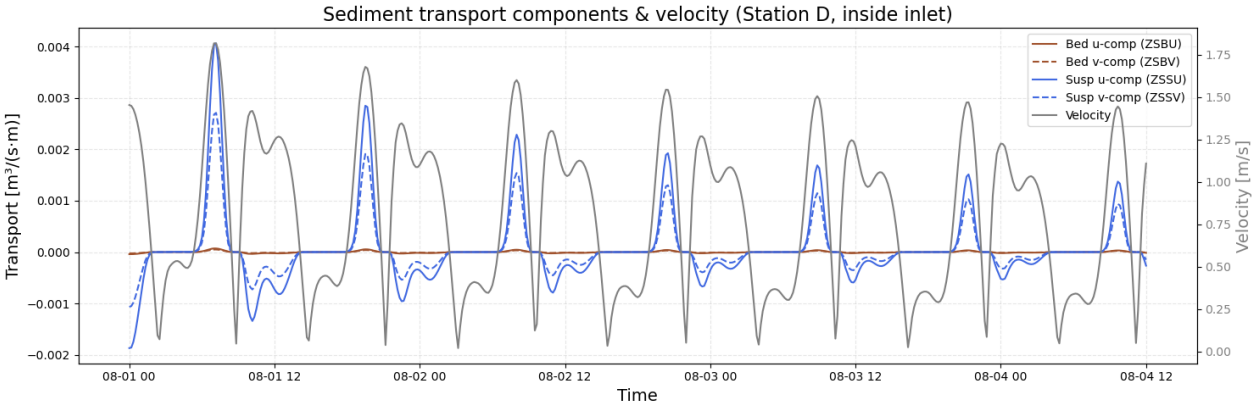

Figure 6.14: Bed load transport (brown lines) and suspended sediment transport decomposed (blue lines) in u and v direction on the left y-axis. The depth averaged velocity is shown in a red colored dashed line on the right y-axis. On the x-axis time. Observation point (E) is located inside the tidal lake.

If this total sediment transport (bed load and suspended load) is integrated over the whole simulation period, it will result in the cumulative sediment transport. This is shown in Figure 6.15 (a). In this situation only the Delta21 construction is placed in the research area without pumps/turbines and river discharge. The colors in this figure show the transport over one year in m^2 x 10^{12}. The arrows in the figure are normalized and only show the direction of the resulting transport.

The location of the tidal inlet shows the highest values of sediment transport. This is a result of the high flow velocities that were shown in Figure 6.10 where the lower left plot is during these high velocities. The tidal inlet shows more than 10 times of sediment transport compared to the rest of the area. There is a clear division in the inlet where the vectors show opposite directions. At the offshore side, the sediment is transported in outward direction At the side of the tidal lake the sediment is transported into the tidal lake.

More offshore of the tidal inlet, the vectors are directed towards the inlet indicating sediment transport towards the tidal lake. At the point where the these opposite directed arrows meet (x=52 500, y=431 000), an ebb tidal delta is expected to grow. Inside the tidal lake most of the vectors are directed in flood direction. Sediment is transported towards the coastline inside the tidal lake.

What can be concluded from this graph is that there is no sediment from outside the tidal lake, transported into the tidal lake. Only the sediment close to the inlet will be transported away from this location until the flow velocity decreases. This decrease of sediment transport in direction of sediment transport, leads to accumulation of sediment. On the other side, increase of sediment transport in the direction of the flow velocity leads to erosion.

This leads to Figure 6.15 (b), the cumulative sedimentation/erosion. This figure is created by subtracting the initial bed level from the final bed level. When the velocity gets higher than the threshold value for sediment transport, the bed starts to erode. It was already noted that the velocity inside the inlet is reaching 2 m/s which results in erosion inside the inlet. After contraction of the inlet, the flow has space to spread and decreases its velocity. This decrease in velocity will lead to sediment deposition.

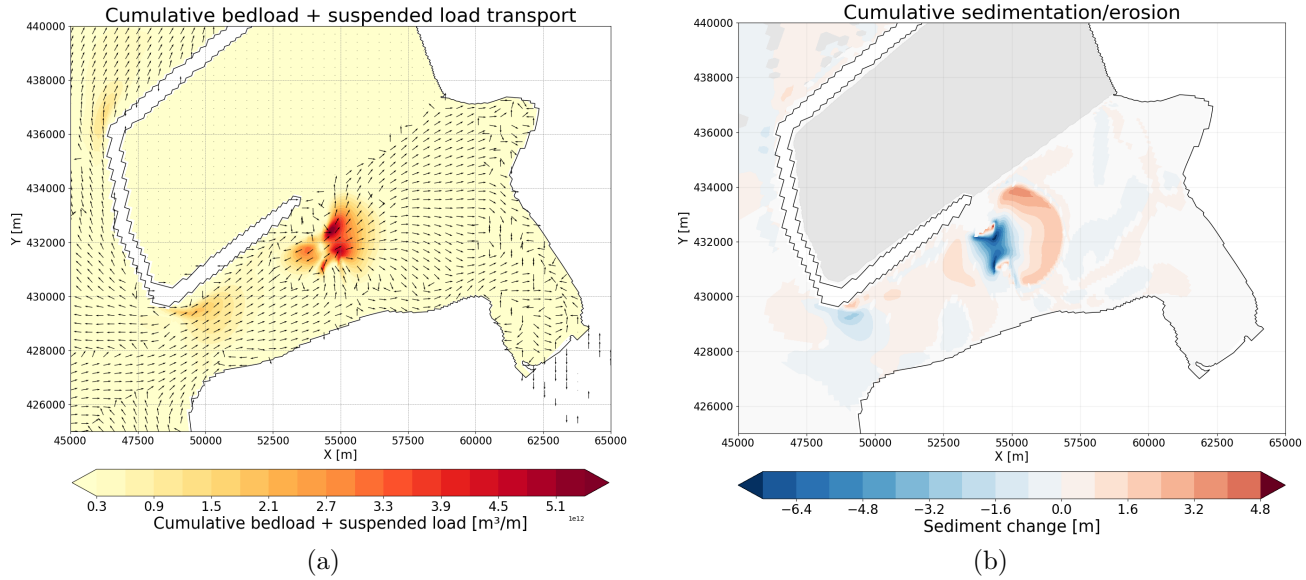

Figure 6.15: Morphological analyses for the Delta21 construction without pumps/turbines and river discharge (a) Total sediment transport over one morphological year (b) Total erosion and sedimentation over one morphological year

What can be concluded is that the implementation of the Delta21 construction into the system leads to high erosion patterns inside the tidal inlet and deposition around the tidal inlet. The erosion in the inlet leads to a depth increase of around 5 m, increasing the inlet cross-section. Because of this excessive erosion moving sediment out of the inlet in both directions, no sediment is able to be transported from outside the system into the tidal lake.

6.3. Model schematization 3: including pumps/turbines

Effect of pumps and turbines

In the next schematization the pumps/turbines are added to the system. The pumps and turbines are operating at predefined time slots and are not considered as a variable in this study, resulting in constant discharges. Inside the energy storage lake there is an observation point placed to monitor the water level. In Figure 6.16 the effect of the pumps/turbines can be seen changing the water level 5 m up and down once a day.

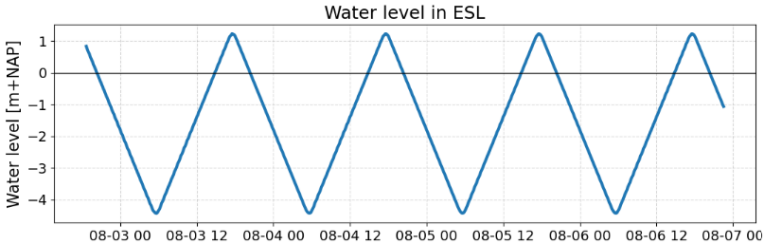

Figure 6.16: water level inside energy storage lake

To quickly check if this water level variation makes sense compared to the pumping discharge, a simple calculation can be done. There are 100 pumps connected to the energy storage lake which together can discharge 10 000 m^3/s. These pumps have an operational time of 12 hours where they fill and empty the basin. This means that after these 12 hours, a volume of 432 000 000 m^3 is pumped out of the energy storage lake. If this results to a water level change in the energy storage lake of 5 m, the area of the energy storage lake should be 86.4 km^2. We can conclude that the use of pumps and turbines in the model works correctly.

To see the effect of the pumps and turbines outside of the energy storage lake, the water level can be plotted at the six observation points. This is shown in Figure 6.17. The blue line represents the water level outside of the Delta21 construction where the effect of the pumps/turbines are negligible. This water level is steady as it repeats with the same shape every tidal cycle. The tidal wave shape at the other observation points however, do show some effect of the pumps when compared to the tidal wave shape without pumps shown in Figure 6.11. We can notice that the water level compared to the steady blue water level deviates when the tidal wave propagates into the tidal lake as the effect of the pumps becomes visible. Figure 6.17 has vertical dashed lines that show when the energy storage lake is filling or emptying by the pumps. Because of this extra discharge, the peak of the water level is higher during pumping of the energy storage lake and lower during filling of the energy storage lake. The filling and emptying of the energy storage lake has effect on the water level and flow velocity in the tidal lake as 1/4th of the pumps/turbines are directly connected to the tidal lake.

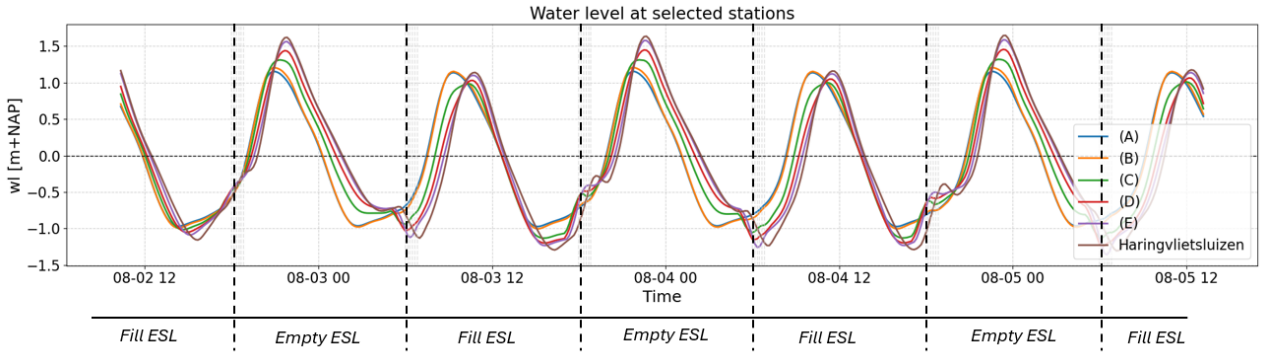

Figure 6.17: water levels at observation points when the pumps/turbines are included. Location (A) is offshore of the Delta21 construction and is not influenced by the pumps/turbines. Vertical dashed lines indicate if the energy storage lake is filling or emptying

This deviation at each time step of the tidal cycle does vary over time as one tidal cycle does not fit perfectly in 12 hours. This means that the pumping and turbining are not aligned with the tidal wave, creating a difference in water level and flow velocity each tidal cycle. To make this deviation visible, comparison is made for the water level and flow velocity in the case with and without pumps. Figure 6.18 shows these differences over the simulation time of one month. This figure shows the outcome at observation point (D), inside the inlet where the flow velocities are maximum. During one month there are over 60 tidal cycles. As the M2 tide is dominant and has a duration of approximately 12 hours and 30 minutes, the peak of the tidal wave shifts every tidal cycle half an hour. So in 24 days we should see another cycle where the pumping and tidal cycle align again and are more or less comparable.

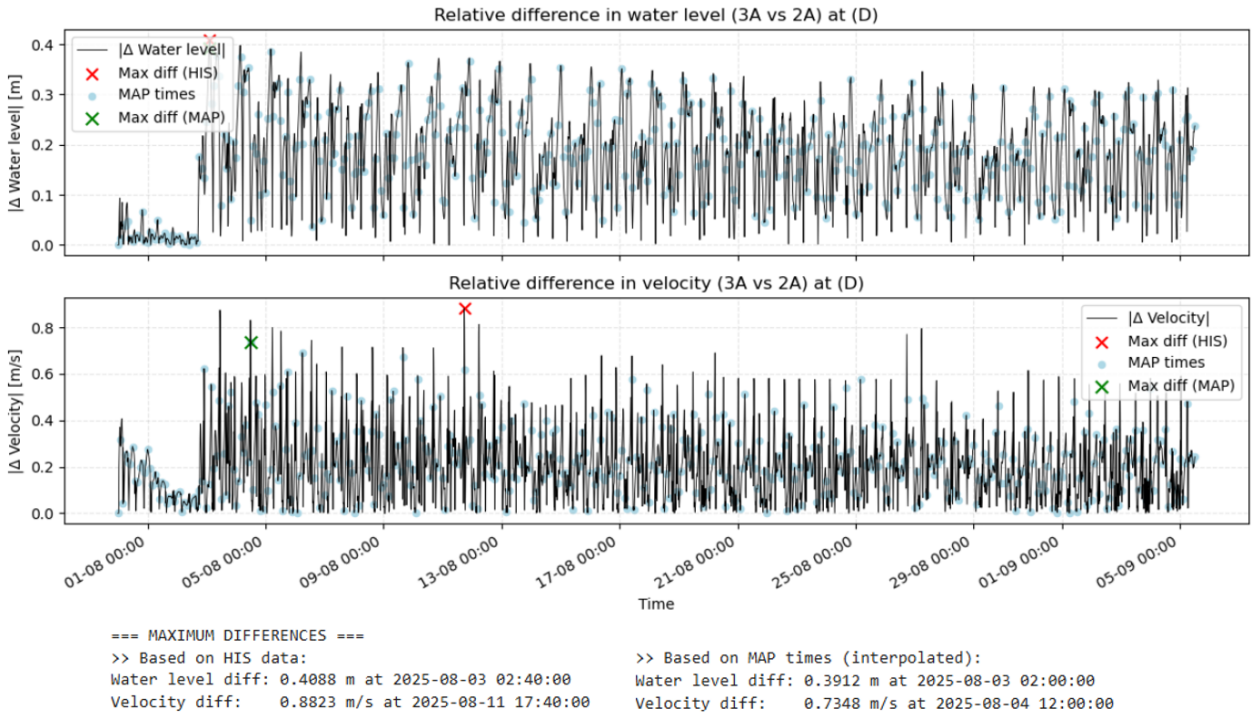

Figure 6.18: Relative differences in water level and depth averaged velocity for the case with and without pumps/turbines. The date and time when the maximum difference occurs are found by these graphs for two different locations: inside the tidal inlet and inside the tidal lake.

In the graph of Figure 6.18 the maximum deviation is marked with a blue or red cross depending on the data used. Delft3D knows two output files, namely MAP and Hist. MAP data is used visualize the output in 2D using a time interval of two hours on each grid point. The HIS output data contains the 1D results at observation points using a shorter time interval of ten minutes. The water level will deviate around 0.25 m from the case without using pumps with a maximum deviation of around 0.4 m. The flow velocity will deviate around 0.5 m/s with a maximum deviation of around 0.9 m/s. To make this maximum deviation of flow velocity visible, the MAP data is used. In the next two figures, Figure 6.19, schematization 2A and 3A are compared to each other where the only difference is the implementation of the pumps and turbines. The time step is chosen by the graph of Figure 6.18 where the maximum deviation in flow velocity is in point (D) inside the inlet. So, this graph does not show the maximum flow velocities for the given schematization but the maximum difference of the flow velocity.

On the left plot of the figure, the water is flowing out during ebb emptying the tidal lake. On the right plot of the figure, the turbines are used to fill the energy storage lake with water to produce energy. A part of the volume of water leaves the tidal lake via the turbines and therefore less water volume flows through the inlet. This results in a decrease of flow velocity in the inlet and less sediment transport at this specific timestep.

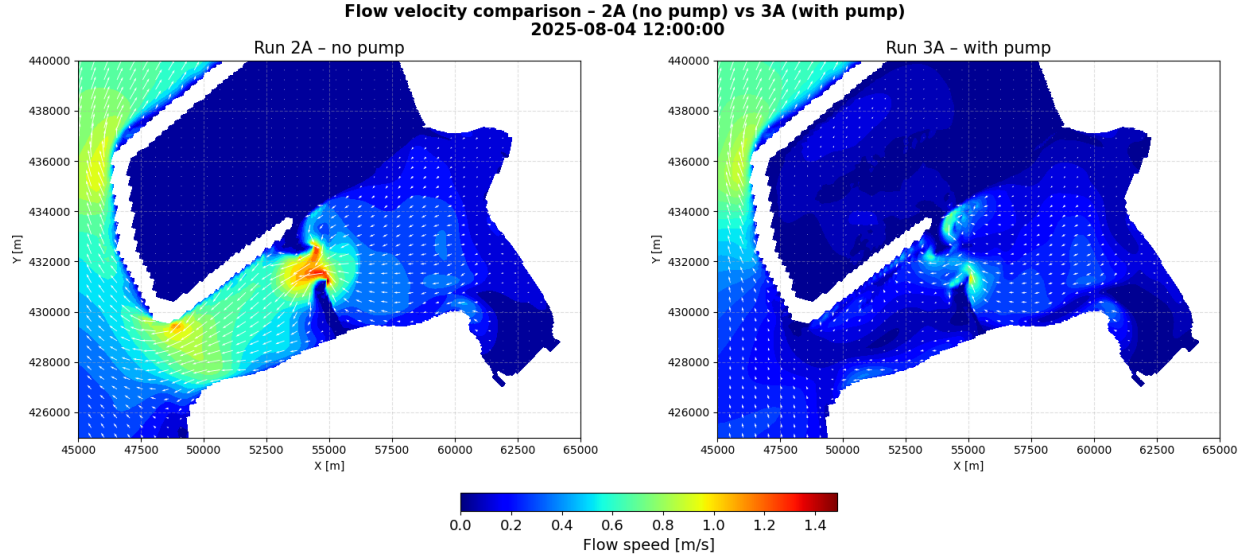

Figure 6.19: Maximum difference of the flow velocity inside the tidal inlet.

This analysis is repeated but now for the maximum flow velocity deviation at point (E) inside the tidal lake. The result is shown in Figure 6.20. On the left plot, when the pumps are not included yet, the water level is around its lowest. This can be noticed because no water is flowing over the intertidal sandbank: Hinterplaat. Water flow inside the tidal inlet is outward so the tidal lake is still emptying. In the right plot of the figure, much larger flow velocities can be found. The water level in this plot is still low as the Hinterplaat reaches above water level. At this timestep (06:00) there is a switch of pumping water into the tidal lake to filling the energy storage lake. The effect in the plot is therefore still the pumping of water from the energy storage lake into the tidal lake. Because the water level inside the tidal lake was already low, the influence of the discharge by the pumps is relatively large. The tidal lake needs to discharge the discharge of the pumps and the discharge due to the tide combined.

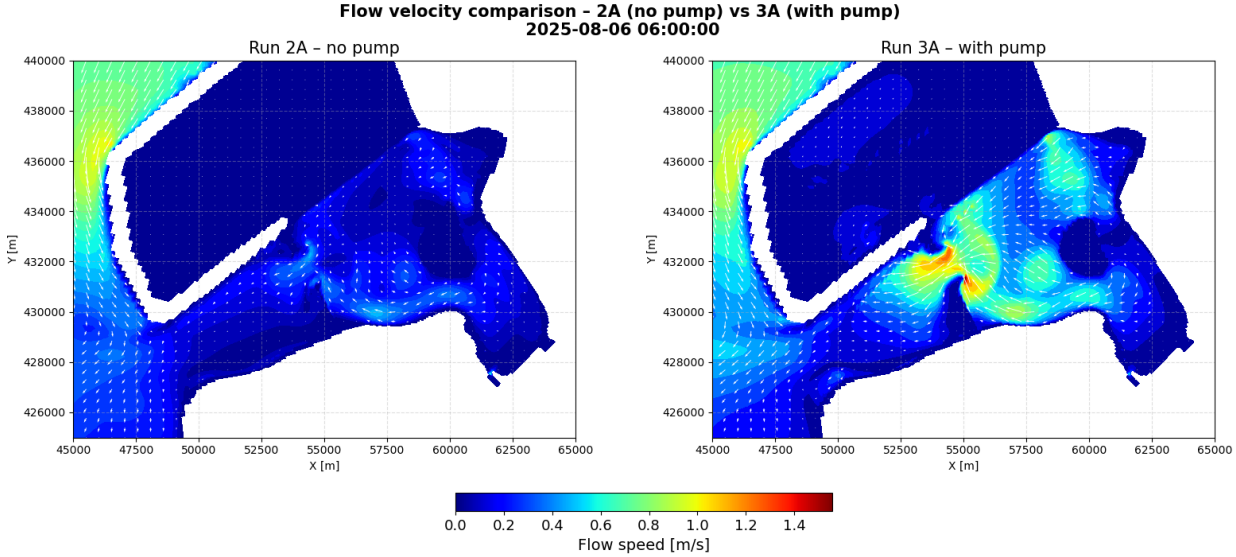

Figure 6.20: Maximum difference of the flow velocity inside the tidal lake.

The conclusion can be made that the flow velocities and water levels inside or around the tidal lake are strongly dependent on the combination of the pumps/turbines and the tide.

Comparison of different inlet widths

The next step is to analyze the effect of the inlet width. The following three inlet widths are compared: 1500 m, 2000 m and 1000 m. For each situation the bed level is set to 6 m. This results in a cross-section of respectively: 9000 m^2, 12 000 m^2 and 6000 m^2. The depth averaged flow velocity for each inlet size is shown in Figure 6.21. The effect of the inlet width to the velocity is visible. An increase of the inlet width leads to a decrease of flow velocities where a decrease of the inlet width leads to an increase of flow velocities.

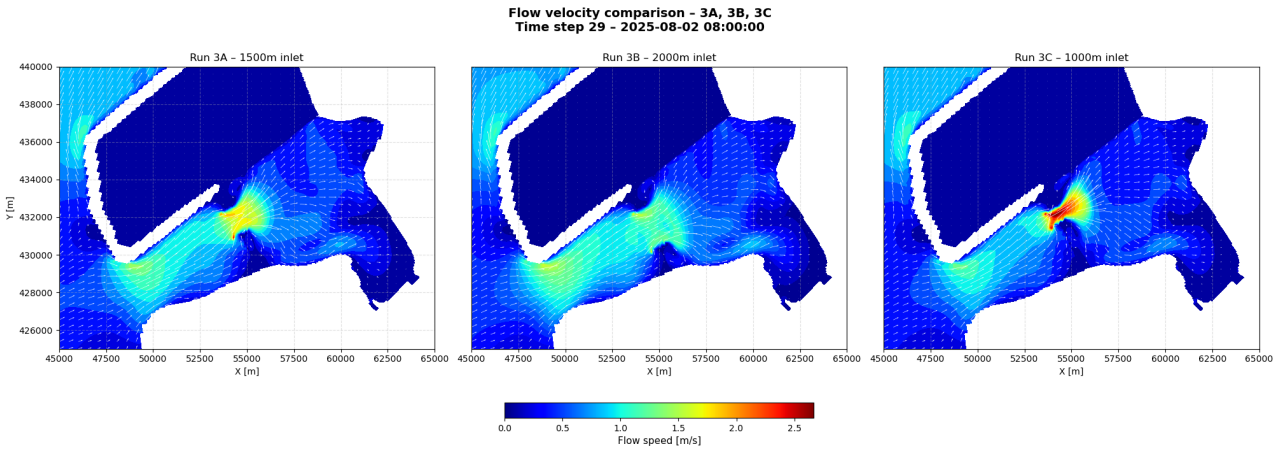

Figure 6.21: Comparison of depth averaged flow velocities for three different inlet widths: 1500 m, 2000 m and 1000 m.

One other way to make a comparison is by plotting the velocity graphs inside the inlet for each inlet size. The result is shown in Figure 6.22. The blue line represents the case without pumps/turbines and an inlet size of 1500 m. The water levels show similar results (when ignoring the effect of the pumps and turbines). The effect of squeezing described in the theory of Chapter 2 can be seen very subtile. The range in water level does decrease when the inlet size becomes smaller. At the other hand, a clear deviation in the flow velocities can be

observed. The velocities of the smallest inlet size, indicated as a red line, are reaching values that are over the 2.5 m/s. In a natural system the inlet size would grow to reduce the flow velocities. If a strong bed protection is used, this growth can be reduced. The other two inlet sizes have their maximum velocities around 1.0 m/s. This can result in some sediment transport when these maximum values are reached.

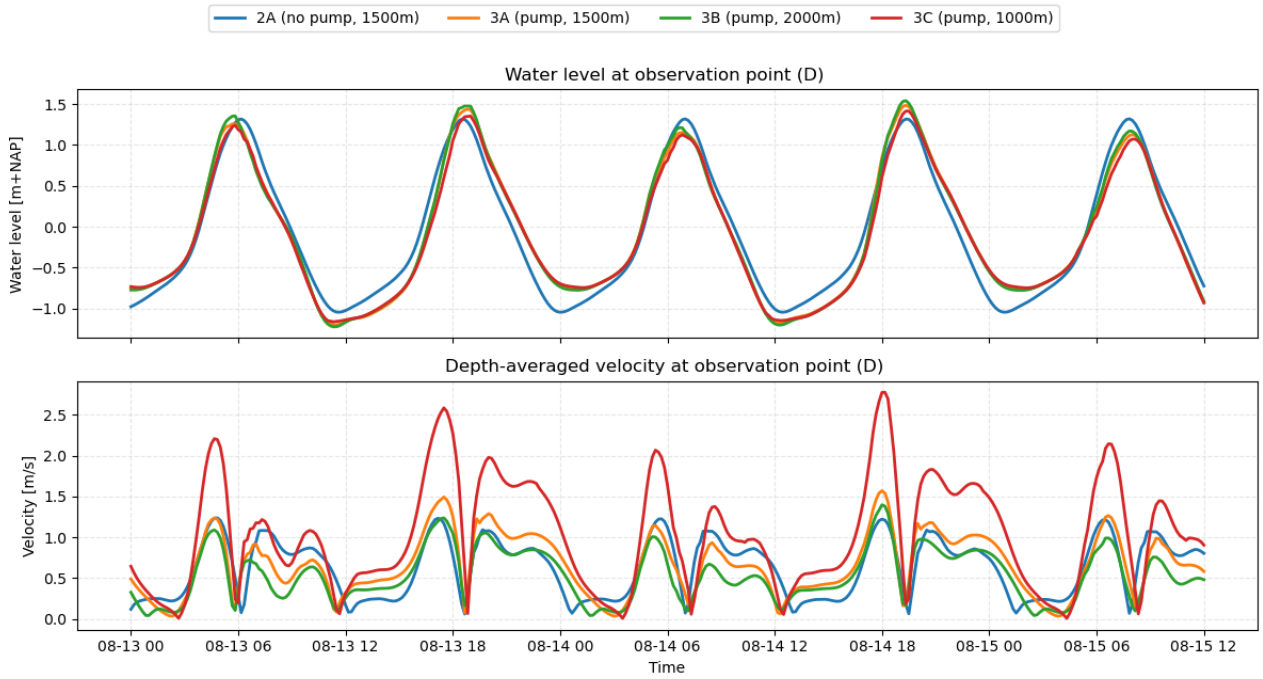

Figure 6.22: Water level and flow velocities inside the Tidal Lake. The blue line represents the case without pumps compared to three different inlet widths: 1500 m, 2000 m and 1000 m.

To see the effect after one morphological year, the cumulative erosion and sedimentation for each inlet width is plotted in Figure 6.23. For this case there is no bed protection implemented yet because we are interested in the natural response to the system. It is clear that the inlet size of 1000 m results in large flow velocities and therefore erosion.

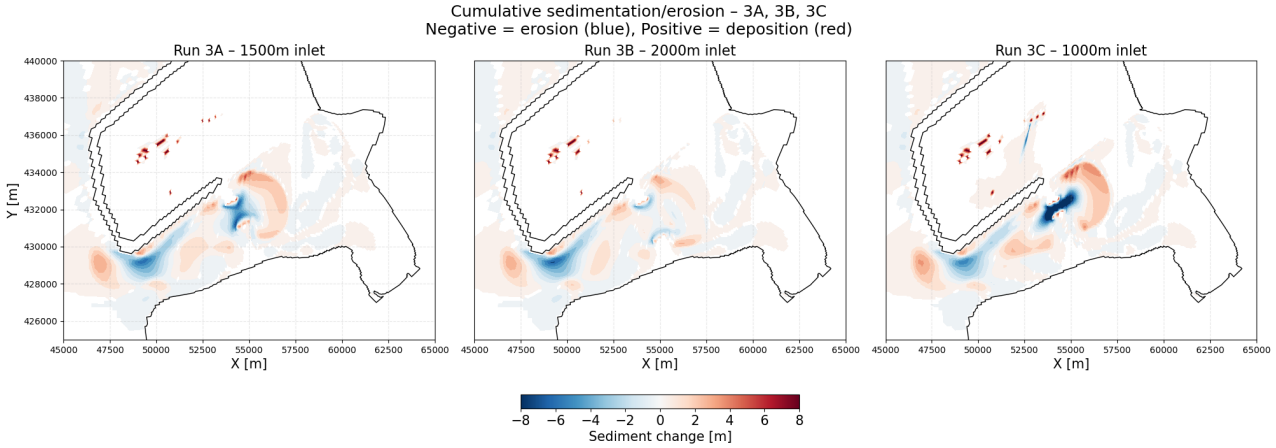

Figure 6.23: Comparison of cumulative sedimentation/erosion patterns for three different inlet widths: 1500 m, 2000 m and 1000 m.

To further investigate the effect of the different inlet widths and the effect of the pumps, the depth in the entrance of the tidal lake (inlet) can be analyzed. The flow velocity increases in the case of a contraction which will cause sediment to move in the direction of the flow. When the contraction stops, the flow velocity decreases again and sediment starts to settle. This is exactly what can be observed in the cumulative sedimentation and erosion pattern of Figure 6.21. The flow velocity and erosion through the narrowest inlet are highest. The inlet will erode as much until it reaches an equilibrium value where the sediment stops moving. It is therefore interesting to create a plot of the depth inside the inlet over time. Figure 6.24 shows the inlet depth over time for the case without pumps/turbines and the three inlet widths with pumps/turbines.

In the first comparison of the situation with and without pumps for an inlet width of 1500 m, a difference in the initial bed level can be found. The case without pumps (blue line) starts at the original bed level and the

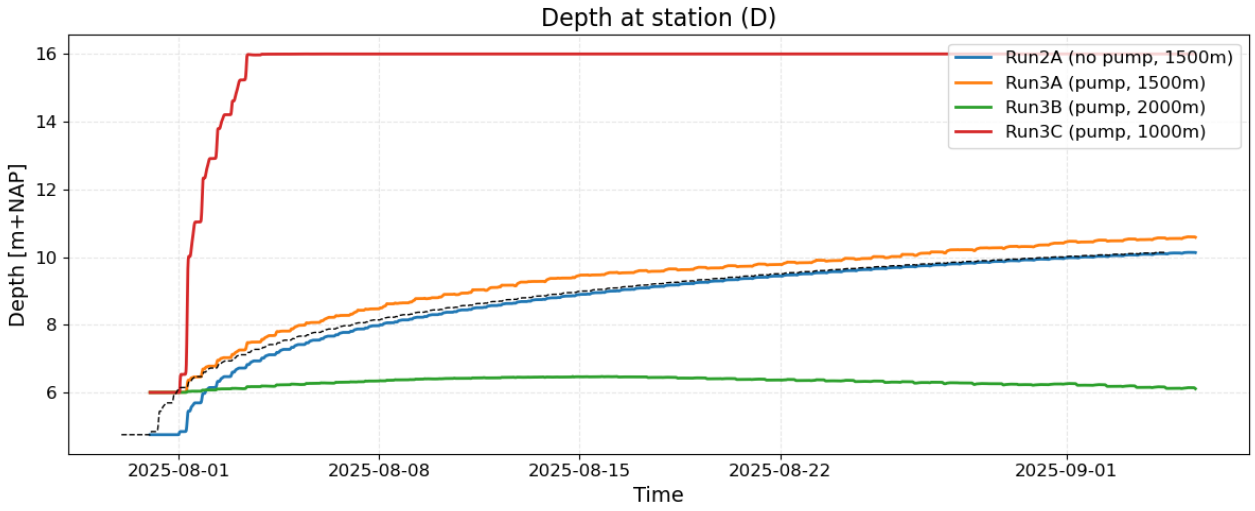

Figure 6.24: Inlet depth in time for the case without pumps and the three inlet widths: 1500 m, 2000 m and 1000 m

cases with pumps (orange line), the bed is first dredged to a uniform bed level of 6 m. To solve this problem and to see comparable results, this blue line is shifted one day in time (dashed line) so all lines start at 6 m the first of August. For the case with and without pumps (and the same inlet width of 1500 m) the depth increase follows the same shape but has an offset of half a meter. This can be explained by the extra volume of water that needs to flow through the inlet due to the pumps. What is interesting is that the graph shows the behavior of almost reaching its equilibrium condition as the change in depth decreases in time. From this graphs it looks like the depth will never reach the 12 m.

When the inlet width is decreased to 1000 m, the velocity increases and the bed starts eroding fast. The red line shows this fast increase in depth inside the inlet. The increase in depth even reached its numerical maximum value as it is set as a boundary in the model. For the same case with pumps but a larger inlet width of 2000 m, another behavior can be observed. The depth stays stable around 6 m. As already seen in Figure 6.23, there is almost no erosion in the middle of the inlet, only at the edges. We can assume that the inlet has reached its equilibrium state as there is no excessive erosion or sedimentation.

From this graph, a difference in cross-section after reaching equilibrium depth can be observed. For example in the case of 2000 m an equilibrium depth of 6 m is found which results in an equilibrium cross-section of 12000 m^2. If the water depth would be dependent on the total area of the cross section (12 000 m^2), the 1500 m width inlet would lead to a depth of 8 m and the 1000 m width to 12 m. As shown in the plot of Figure 6.24 this is not the case. This can be explained by the erosion and sedimentation plots of Figure 6.23 and the location of the observation points used for the graph of Figure 6.24. Because of the sudden contraction, flow is accelerated at the edges inside the inlet which leads to erosion. The sedimentation and erosion patterns show that in case of a 2000 m inlet width, the effect of contraction does not have influence on the middle part of the inlet, only along the edges. This leads to differences in the final bed level inside the inlet. When the inlet width is decreased to 1500 m and 1000 m, extra erosion due to contraction can be found over the entire inlet width. It can therefore be concluded that decreasing the inlet width leads to extra erosion throughout the inlet due to the effect of contraction.

The cumulative sediment transport with direction is also plotted for the three different inlet sizes shown in Figure 6.25. What can be seen is that for the inlet width of 2000 m sediment is transported from outside the system, into the tidal lake. The arrows are directed from outside the system towards the tidal lake. This is the only inlet size width where this behavior is being observed. The import of sediment indicates that the tidal lake has a characteristic of being a flood dominant system for cumulative sediment transport. As described for the other two inlet sizes, the bed erodes until the equilibrium depth is reached. Due to this erosion, cumulative sediment transport shows an increase in transport inside the inlet.

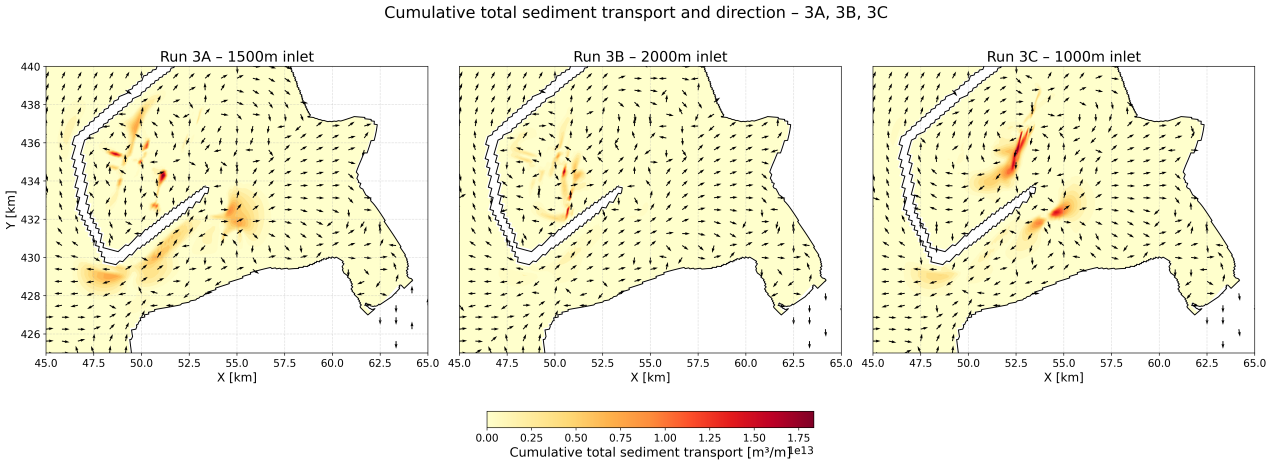

Figure 6.25: Cumulative sediment transport for the three inlet widths: 1500 m, 2000 m and 1000 m

Effect of Sea Level Rise

For the tidal inlet width of 1500 m, inclusion of pumps/turbines and no river discharge, the effect of sea level rise is investigated. As described in Chapter 3, the KNMI'23 scenarios project a regional rise of up to 1 m by the end of the century in the Netherlands. The effect of the sea level increase on the sediment transport is shown in Figure 6.26. Figure 6.26 (a) shows the effect on the cumulative bed load transport en 6.26 (b) on the cumulative suspended load transport. The suspended load transport is a factor 10 larger that the bed load transport. The vectors in this plot are normalized and therefore only show the direction of the sediment transport.

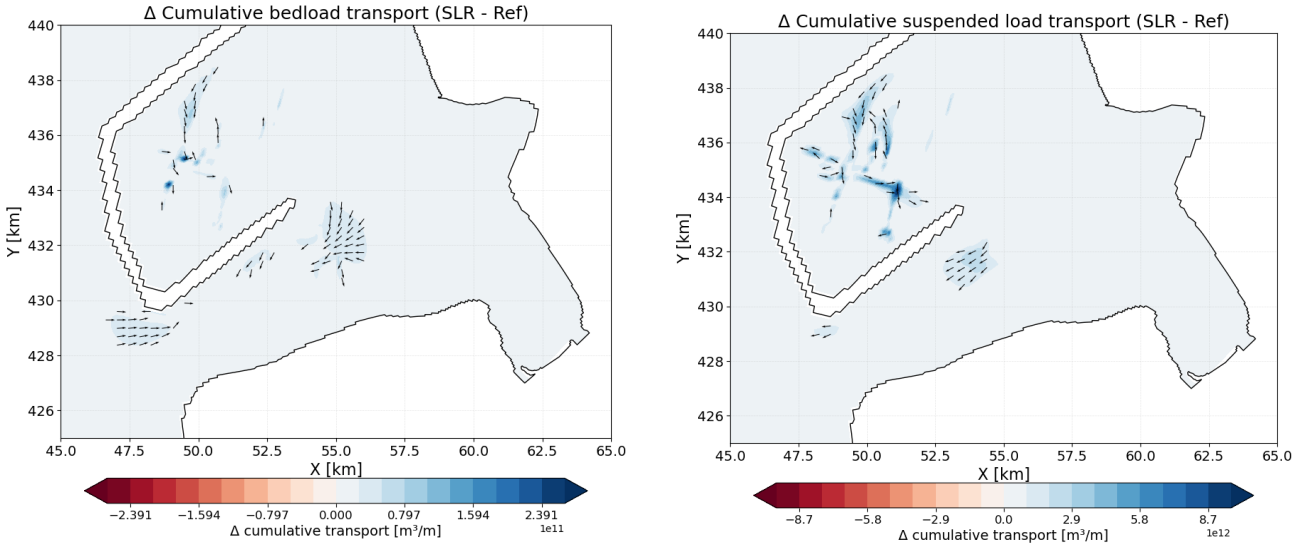

(a) (b)

Figure 6.26: Differences in cumulative sediment transport due to a 1 m sea level rise (SLR) compared to the reference scenario. (a) Bed load transport; (b) Suspended load transport. Arrow directions indicate the flow direction of transport, and arrow lengths are normalized for visualization. Color shading represents the magnitude of the difference, with red indicating an increase and blue indicating a decrease in transport

Interesting observations can be made comparing the Figure 6.26 (a) and (b). The bed load transport increases at two locations when sea level rise is included in the system. At the inland side of the tidal inlet, more sediment is transported towards the inlet. At the left corner of the energy storage lake (x=48, y=429) sediment is transported towards the tidal lake.

In the case of suspended load transport, other behavior is observed. Now the transport is increased at the offshore side of the tidal inlet in outward direction. In the same corner of the energy storage lake (x=48, y=429) a smaller amount of sediment transport is found but in the opposite direction.

The total sediment transport (bed load and suspended load) shows that sediment is transported from inside the tidal lake towards the outside. Compared to the first plot in Figure 6.25, this pattern differs. What can be concluded is that sea level rise of 1 m (in the case without river discharge and an inlet width of 1500 m) results in a net transport in ebb direction promoting ebb-dominance.

6.4. Model schematization 4: Including river discharge

General changes

In this section a moderate river discharge of Q = 1000 m^3/s is added to the system over a simulation period of 5 years. As described in Chapter 2, the river discharge will fill the basin and change the volume of water flowing in and out at the inlet. We can see in Figure 6.27 the increase in water level due to the river discharge.

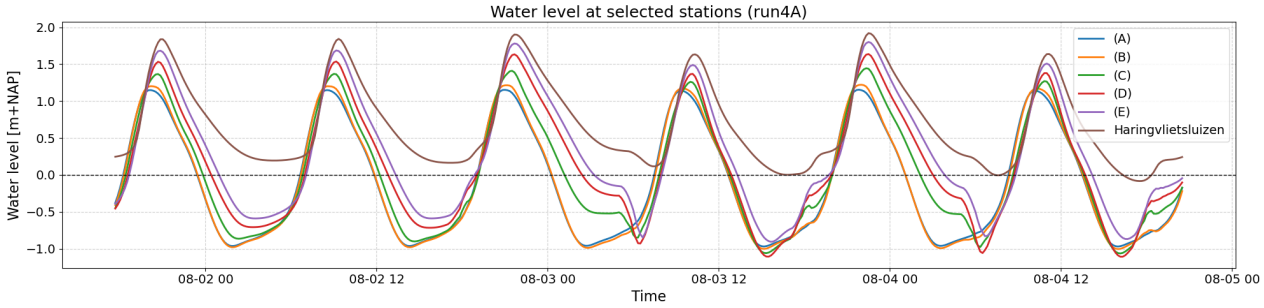

Figure 6.27: Water level at the six observation points (Locations in Figure 5.12)

The cumulative bed load and suspended load transport, Figure 6.28 (a), shows that the direction is in almost the entire tidal lake in outward direction. This is the cumulative sediment transport over a period of 5 years. It tells us that the overall sediment transport direction is in ebb direction, indicting an ebb dominant system. What can also be seen is the higher transport rates where the river discharge flows. From the Haringvliet, through the new inlet into the North Sea.

The second plot, 6.28 (b), shows the sedimentation erosion patterns. Inside the energy storage lake large values can be observed which are related to the discharges of the pumps/turbines. This is the result of large pressure in the grid cells but will not effect the results outside of the energy storage lake. What can be seen from this sedimentation erosion plot is that the new main channel is eroding and transporting sediment along the channel or pushing it offshore. In the offshore deeper parts outside the Delta21 construction, sedimentation rates above 6 m are observed. This long term river discharge changes the morphology drastically compared to the case without river discharge shown in the first plot of Figure 6.23.

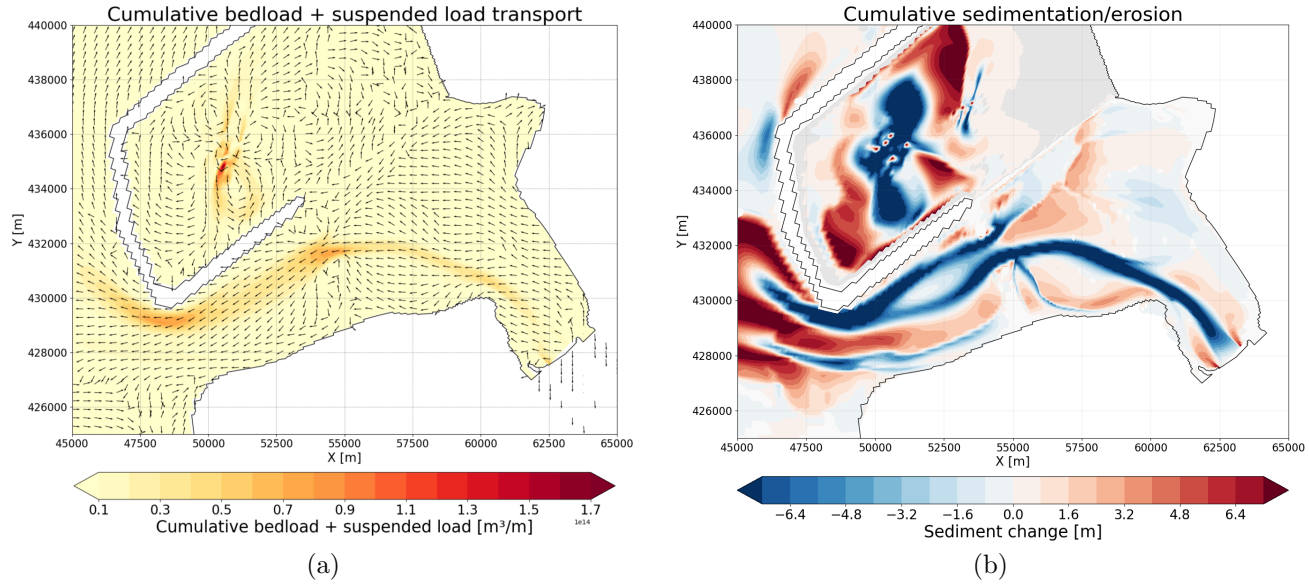

Figure 6.28: 5 year simulation with a river diascharge of Qr = 1000 m^3/s (a)cumulative bed load en suspended load transport (b) cumulative sedimentation and erosion pattern

These changes are true for all three inlet widths and therefore not shown separately. The next step is to see how the bathymetry changed over the years for each inlet width.

Inlet size 1: Moderate river discharge

Similar to Figure 3.12 at the start of this research, it is interesting to look at the bathymetry by classifying the area. The areas that we want to observe are where the deep water, shallow water and tidal flats are located. Figure 6.29 shows the initial and final state for an inlet width of 1500 m after five morphological years:

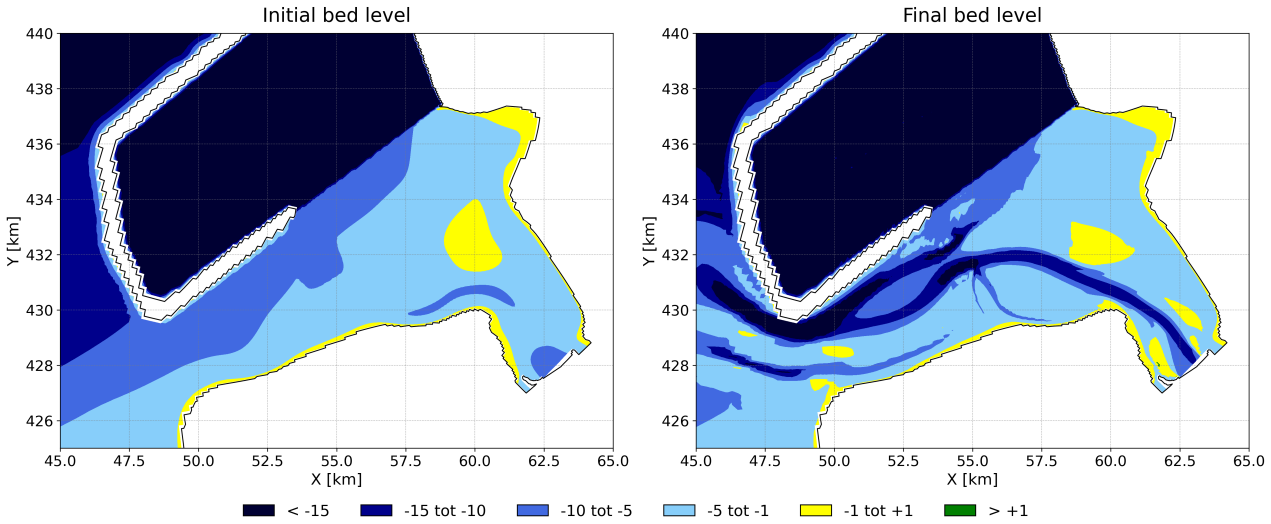

Figure 6.29: Classification of the bathymetry with an inlet width of 1500 m and a river discharge of 1000 m^3/s. On the left the initial state and on the right the final state.

These five years can be shown in six different time steps of one year. Figure 6.30 shows these steps where the year is described in the title of each plot. What can be seen is that in the first year most of the morphological changes happen. The main channel has shifted towards the new inlet location and the shape of the Hinterplaat sandbank has changed. In the following years the main channel is deepening and more tidal flats start to build up near the Haringvliet sluices.

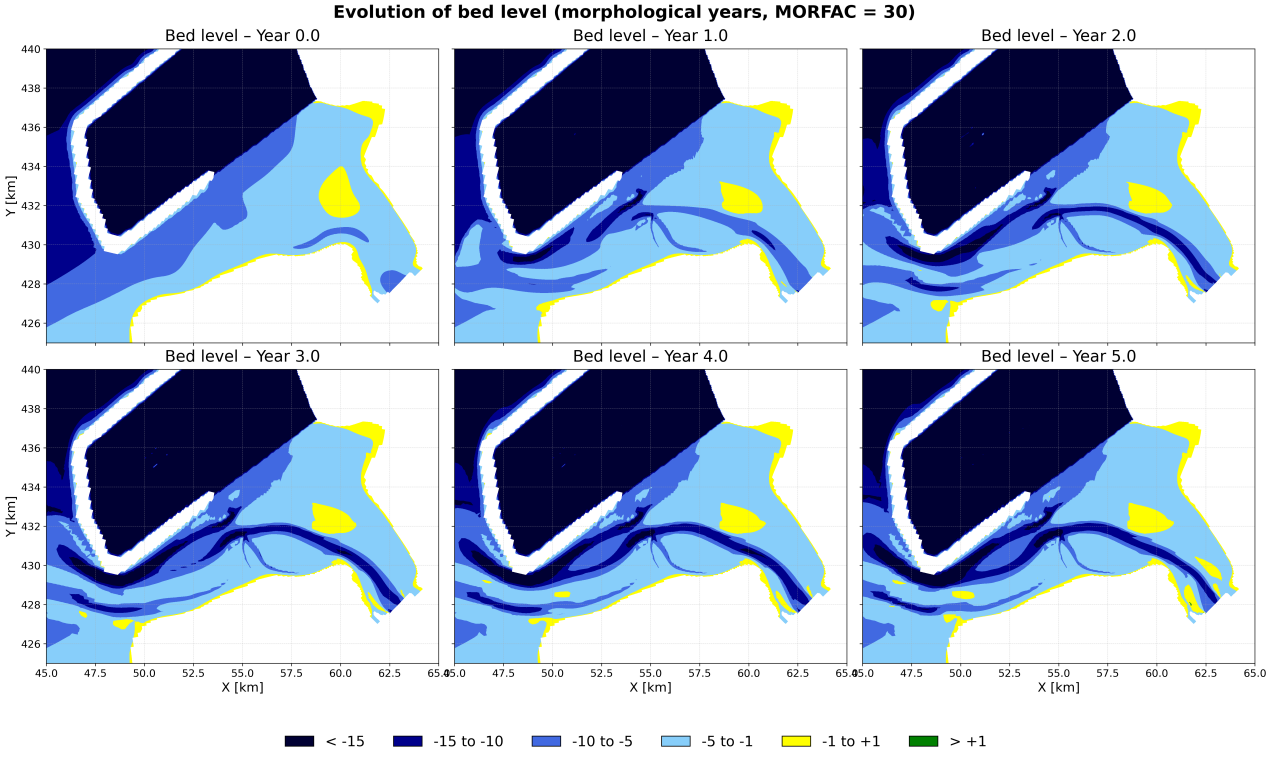

Figure 6.30: Classification of the bathymetry with an inlet width of 1500 m and a river discharge of 1000 m^3/s throughout the years

Inlet size 2: Moderate river discharge

Figure 6.31 shows the initial and final bathymetry over five morphological years for a larger inlet width of 2000 m. Comparing it to a smaller inlet width of 1500 m in Figure 6.29, there are no major changes inside the tidal lake for all three inlet sizes. Differences can be found at the offshore side of the tidal inlet. Where Figure 6.29 shows two main channels, the increase of the inlet width leads to one main channel. Also the new tidal flats (in yellow) are located on different locations.

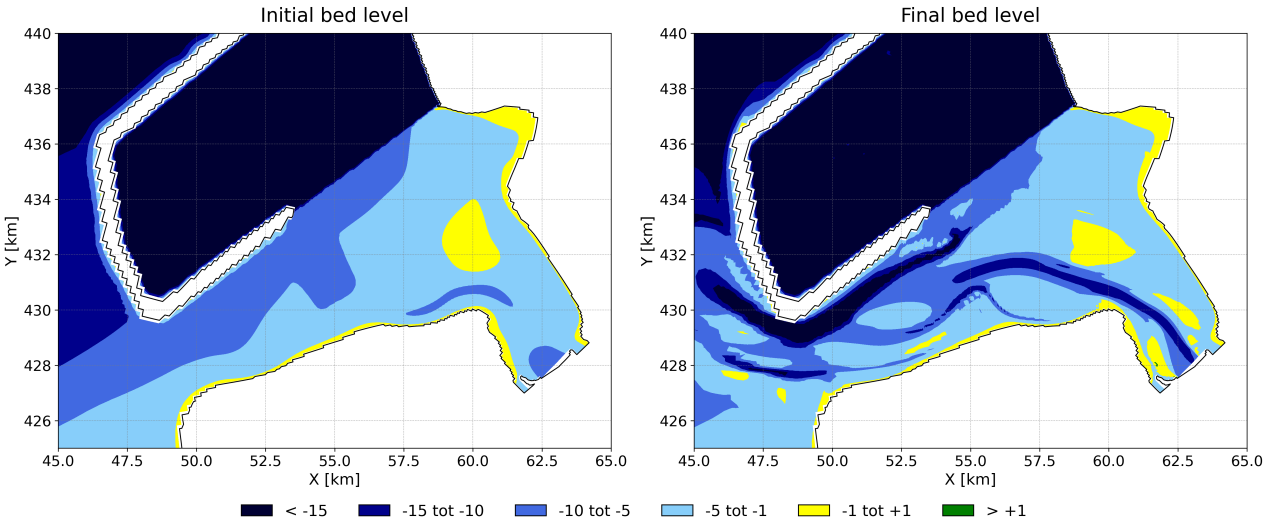

Figure 6.31: Classification of the bathymetry with an inlet width of 2000 m and a river discharge of 1000 m^3/s. On the left the initial state and on the right the final state.

Inlet size 3: Moderate river discharge

Figure 6.32 shows the initial and final bathymetry over five morphological years for a smaller inlet width of 1000 m. Also in this case, the area inside the tidal lake is not changing when the inlet width is decreased. Because of the high flow velocities related to the smaller inlet width, a formation of a large main channel can be found in the final bed level. What is interesting about the final situation is that it looks like an ebb tidal delta has formed in the lower left corner of the plot. Sediment is deposited when the water is reaching the North sea leading to creation of tidal flats. Even the smaller channels in between the tidal flats are created.

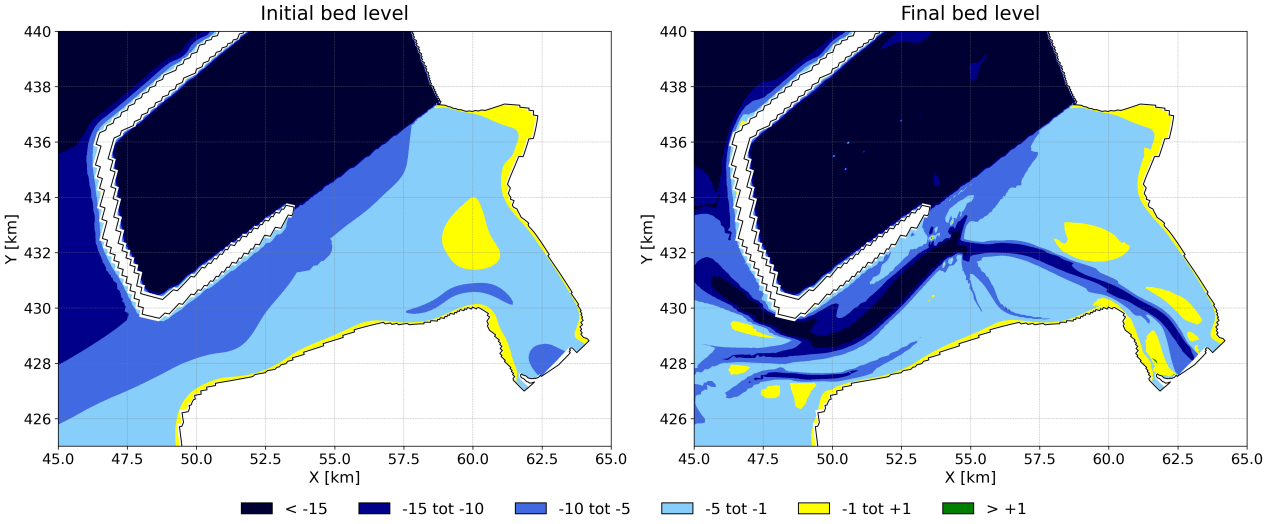

Figure 6.32: Classification of the bathymetry with an inlet width of 1000 m and a river discharge of 1000 m^3/s. On the left the initial state and on the right the final state.

A conclusion for the long term morphological changes in the case of a moderate river discharge is that the morphology does not change drastically inside the Tidal lake. This is true for all three inlet widths. The location where morphological changes can be expected is offshore of the inlet where the pattern also changes for different inlet widths.

Extreme river discharge

In this part of the research the focus is on the response of the system to an extreme discharge. Relative to the previous model, where a moderate discharge of 1000 m^3/s is used over a period of five years, we now look at an 11 day constant discharge of 5000 m^3/s. During the first simulation day, the discharge will build up to the discharge of 5000 m^3/s to avoid extreme sudden velocity changes. The simulation therefore starts at 31 07 2025 00 00 00 and ends 11 08 2025 00 00 00.

For this simulation the pumps and turbines will still operate in the given time schedule so just the effect of an increased discharge will be visible. The extreme discharge will be computed for the three cases with different inlet sizes. Figure 6.33 shows the water level at the six observation points when the inlet width is 1500 m. Because of this high river discharge, the water level increase is visible in the plot. The closer the observation point is located at the Haringvliet sluices, the more water level increase is observed. Point (A) and (B) are located outside the tidal lake and point (C) in the tidal inlet. The water level is increasing because the inlet is not capable to discharge the extreme discharge which results in filling of the basin.

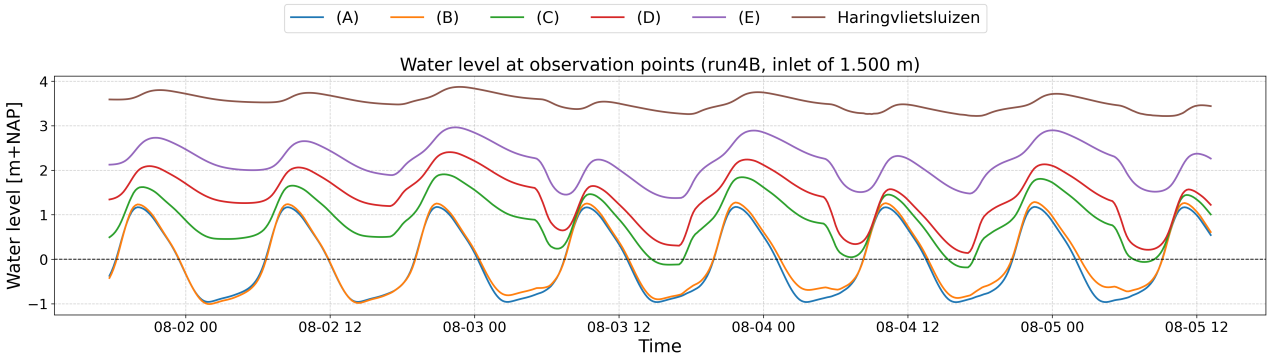

Figure 6.33: Water level at the six observation points (Locations in Figure 5.12)

Again, the sediment transport (bed load and suspended load) are shown in Figure 6.34 (a) and the erosion and sedimentation patterns in Figure 6.34 (b). Compared to Figure 6.28 where the discharge was 1000 m^3/s, the direction of the sediment transport is the same. However, the sediment erosion plot shows a different pattern.

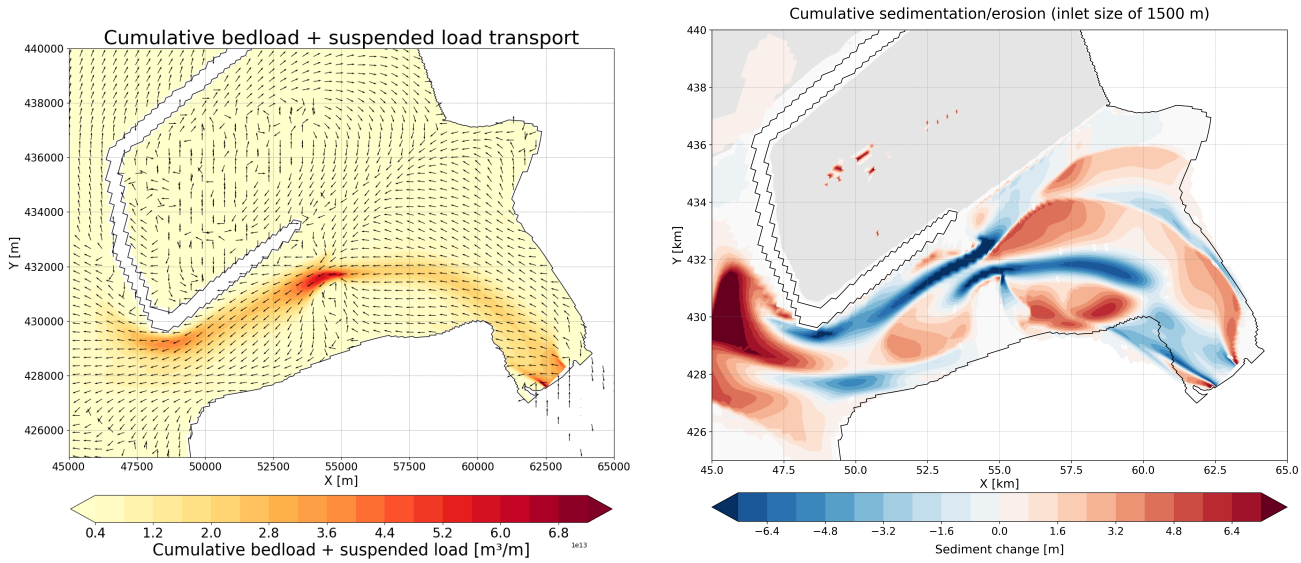

(a) (b)

Figure 6.34: Morphological analyses for the Delta21 construction without pumps/turbines and extreme river discharge (a) Total sediment transport over one morphological year (b) Total erosion and sedimentation over one morphological year

To see the morphological evolution over time from the initial until the final bed level, Figure 6.35 is created. Because the extreme river discharge is simulated for eleven days, the time frame is different than compared to the plots of moderate discharge (Figure 6.30). The dates and times are indicated in the title of each plot.

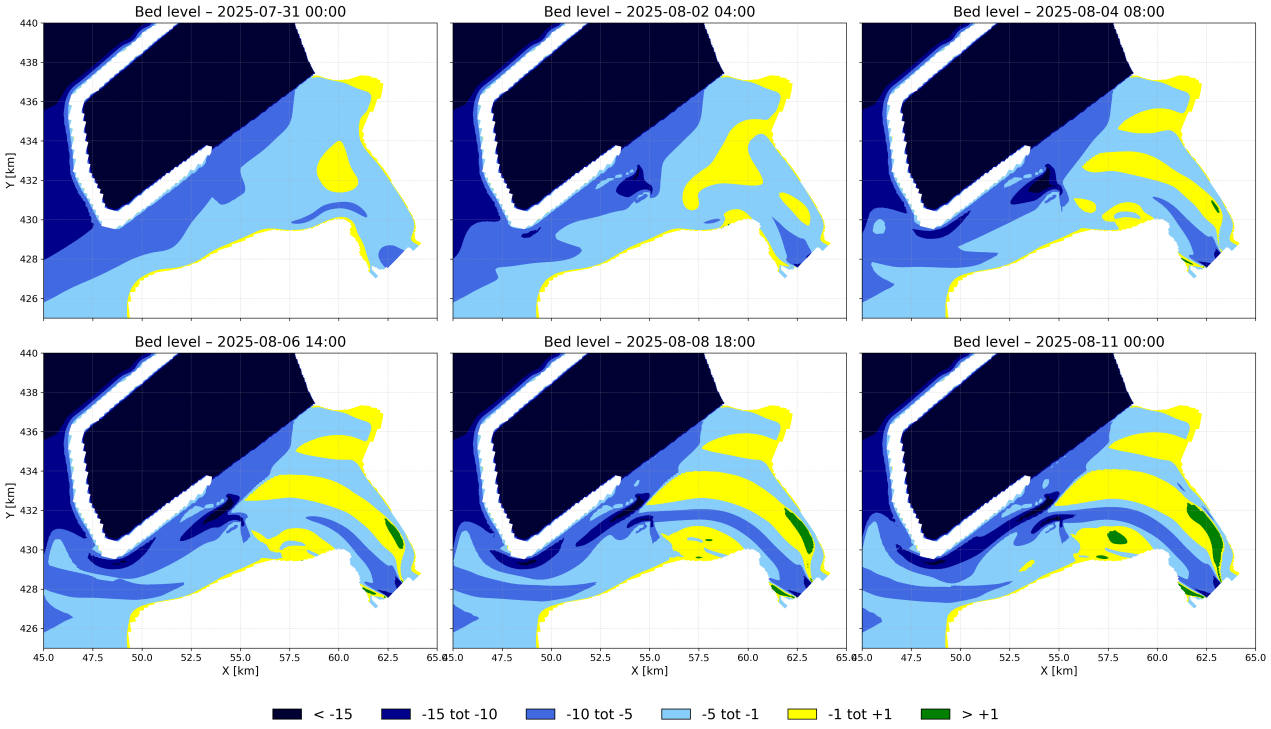

Figure 6.35: Classification of the bathymetry with an inlet width of 1500 m and a river discharge of 5000 m^3/s for 11 days.

The morphological evolutions show very different behavior and large scale creation of tidal flats. It looks like the volume of sediment increased inside the tidal lake. This can not be from imported sediment out of the tidal lake because Figure 6.34 (a) clearly shows a ebb dominant system where the dominant sediment transport is in ebb direction. One way to explain this is that the coastline (in the tidal lake) is eroding and redistributing its sediment inside the tidal lake.

7
Discussion

In this chapter a critical reflection on the research is presented. The limitations of the model are discussed including the influence on the model results. This reflection is necessary to establish correct conclusions presented in the next chapter.

7.1. Model limitations

Waves
One of the main factors to keep in mind is that this model is created using only the FLOW module of Delft3D, as the main focus is on the deformation of the tidal wave. Wind and waves are excluded from the system, resulting in simulations that only represent sedimentation and erosion driven by flow. The exclusion of waves at the offshore boundary is not expected to lead to major differences, because the Delta21 construction blocks incoming waves from entering the tidal lake.

Wind
Wind, on the other hand, can influence the results within the tidal lake. Wind forcing may alter flow velocities and directions, particularly because the basin contains large shallow areas. Wind can also generate waves due to the long fetch distances that can develop across the tidal lake, which covers an area of approximately 65 km^2. Waves mostly contribute in bringing sediment into suspension whereas the tide is responsible for most of the transport of sediment in the horizontal axis. In general, tides promote the formation of intertidal areas, whereas waves tend to erode these sandbanks.

Tide
In the model, a representative tide is imposed, meaning that variations associated with the spring–neap tidal cycle are not included. In reality, the tidal range fluctuates because it consists of multiple harmonic constituents. As a result, actual water levels and flow velocities may differ from the simulated conditions. For example, an increase in tidal range leads to a larger tidal prism, requiring more water to enter and leave the system, which produces higher flow velocities in the inlet. Within the tidal lake, differences in water level influence the duration of inundation and exposure of shallow areas. Using a representative tide is common practice to capture the general morphodynamic trends. However, the absence of spring–neap variability may lead to an underestimation of peak hydrodynamic conditions and the associated extreme sediment transport events. These tidal limitations also interact with sediment transport, as flow velocities and inundation patterns directly control where and when sand and fines are deposited.

Bed material composition
The model is setup for sand with a median grain size of 160 µm only, meaning that mud and finer sediments are not included. In the tidal lake, fine-grained material can accumulate in sheltered, low-velocity areas, and its transport and deposition are influenced by processes such as flocculation and density-driven currents. These processes are not represented in the current model setup, implying that the dynamics of fines and their potential interactions with sand are neglected. Furthermore, the model uses a single hydrodynamic layer and one active sediment layer, which limits the vertical resolution of both flow and sediment dynamics. As a result, the model approximates deposition of fines solely based on low-flow areas, without capturing potential feedback's on local flow and erosion patterns. This limitation should be considered when interpreting the predicted spatial distribution and magnitude of sedimentation within the tidal lake.

River discharge
The river discharge in the model is set as a constant value. In reality, the river discharge varies considerably: during low-flow periods, the discharge can drop to zero for extended periods, while at other times it can reach up to 200 m^3/s. This small variability is neglected in the current study, as the focus is on the larger-scale effects of hydraulic forces. For normal river conditions, a constant discharge of 1000 m^3/s is applied, which does not represent the full range of observed variability. River discharge depends strongly on rainfall in the catchment area, and therefore fluctuates over time. By using a constant discharge, the model does not capture short-term variations in flow, which may lead to over- or underestimation of velocities, water levels, and sediment transport in certain areas.

Pumps/turbines operation
Similarly, the operation of pumps and turbines is simplified. In reality, inflow and outflow through these structures depend on the availability of excess green energy and the daily energy demand, meaning that discharges fluctuate over time. In the model, maximum discharges are applied consistently, without capturing the temporal variations. This simplification limits the representation of different flow patterns that result from variable pumping and turbine operations, which may affect the timing and location of erosion or deposition, especially in areas close to these structures.

Overall, these simplifications mean that the model provides a general picture of the hydrodynamic and morphodynamic response, but small-scale, short-term effects caused by fluctuating river discharge and operational discharges of pumps and turbines are not resolved.

7.2. Result interpretation

Based on the limitations of the model, the results must be interpreted qualitatively. The research builds on theoretical background mainly derived from natural coastal systems. While these theories cannot be directly applied to a man-made, engineered hydraulic system, they provide useful insights into the underlying behavior of such systems. Understanding these natural principles can help interpret the dynamics of the newly created tidal lake, and if the design aligns closely with natural behavior, it may reduce the need for maintenance in the long term.

The system is simplified to include only three hydraulic forces: tides, pumps and turbines, and river discharge. These forces are added to the model incrementally, allowing for relative comparison. This approach enables the evaluation of the effect of each individual hydraulic force on the system's behavior. While this simplification does not produce a detailed, fully representative schematization of the real situation, it provides an overall understanding of the system dynamics and the relative contribution of each hydraulic component.

One of the findings of this research is the effect of changing the inlet width. The inlet width is a hard structure where the bed is dredged to a water depth of 6 m and no bed protection is used to allow erosion. The results presented in this study, such as patterns of erosion, sedimentation, and sediment transport, are cumulative over the entire simulation period. Consequently, they do not capture temporal changes in these patterns. For instance, the system may shift from ebb- to flood-dominant conditions in the later stages of the simulation, yet the cumulative results could still indicate an overall ebb-dominant behavior. When plotting the depth increase (due to erosion) in time inside the inlet, the equilibrium depth is revealed. When this depth is achieved, it is possible that the velocities decrease to the threshold value to stop eroding and import sediment form the outside. This will then lead to a shift to a flood dominant system.

8
Conclusions and Recommendations

This final chapter provides, based on the findings in the previous chapters, an answer to the main research question of this thesis. The first section formulates a conclusion by answering both the main research question and the sub-questions. The second section offers recommendations for applying the results and gives suggestions for future work.

8.1. Conclusions

Answer to research-based sub-questions

1. How does inlet width influence flow velocities and sediment transport capacity in human-made tidal basins?

The model results show that the inlet width strongly controls flow velocities, sediment transport, and morphological change in the tidal lake. Because the inlet is a fixed hard structure, the width cannot adapt. therefore, the system increases its cross-sectional area only through erosion of the inlet bed. Narrow inlets (1000 m and 1500 m) produce high velocities and strong initial erosion, indicating that their cross-sections are too small for the imposed tidal prism. This erosion continues until the inlet approaches an equilibrium depth, where velocities decrease toward the sediment motion threshold.

Only the 2000 m inlet without river discharge reached a state close to equilibrium and showed flood-dominant cumulative sediment transport, indicating sediment import into the tidal lake. The 1500 m inlet deepened toward an equilibrium depth, but cumulative transport over the full simulation period remained ebb-dominant due to early-stage erosion. The 1000 m inlet did not reach equilibrium within the model domain.

When river discharge is included, all inlet sizes lead to an ebb-dominant system that exports sediment regardless of width. This shows that river discharge is a decisive factor in determining the net sediment balance and can suppress flood dominance even when the inlet geometry is favorable.

In summary, wider inlets reduce velocities and allow the system to approach morphodynamic equilibrium, while narrower inlets continue to erode. Flood dominance was observed only for the 2000 m inlet without river discharge, whereas any river inflow shifts the system toward ebb-dominant behavior.

2. How do future developments (sea level rise and extreme river discharge events) impact the morphological stability of the lake?

Future boundary conditions strongly influence the morphological stability of the tidal lake. Sea level rise increases water depth, reduces bottom friction, and allows the tide to propagate further, leading to enhanced ebb-directed sediment transport. For example, a 1 m sea level rise (inlet width 1500 m, no river discharge) results in net sediment loss from the basin, potentially deepening the lake and eroding tidal flats over the long term.

Extreme river discharges cause short-term morphological responses. Limited inlet capacity leads to temporary water level rise, increasing flow velocities and shear stresses near the inlet and inner shorelines. This produces local erosion and sediment redistribution, forming new shallow areas, while net transport remains ebb-dominant.

In summary, sea level rise drives long-term sediment loss, whereas extreme river discharges induce short-term redistribution. These findings highlight the sensitivity of the tidal lake to hydrodynamic forcing and the need to account for future conditions when designing stable inlet dimensions.

3. What combination of inlet dimensions and sediment placement leads to the fastest development toward a stable tidal system?

The tidal lake naturally tends toward an equilibrium state in which approximately 88 % of the area would be tidal flats, whereas currently less than 20 % of the basin consists of tidal flats. Achieving this equilibrium requires importing sediment from outside the system. Cumulative sediment transport analysis shows that only the 2000 m inlet without river discharge allows sediment import, while narrower inlets and all scenarios with river inflow remain ebb-dominant, exporting sediment.

To reach the equilibrium condition and preferred final scenario, it may be possible to apply sediment at the deeper locations. Figure 8.1 shows on the left the current bathymetry and on the right after sediment placement. From an ecological point of view, shallow waters up to 5 m depth are preferred. The bathymetry shows that there is an area next to the energy storage lake where the depth reaches approximately -10 m.

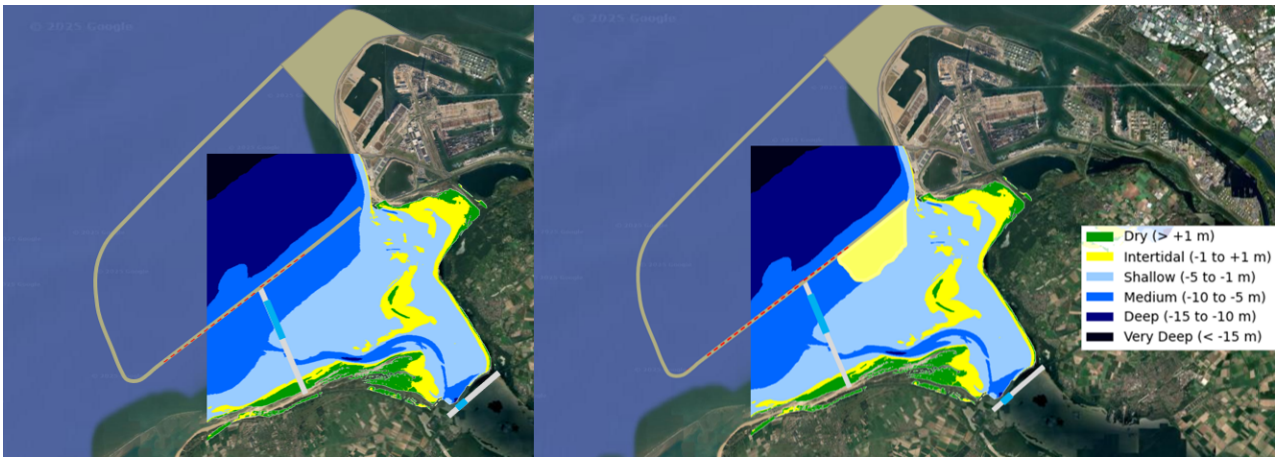

Figure 8.1: Potential sediment placement locations to stimulate tidal flat development in deeper areas of the basin.

Although sediment placement inside the tidal lake was not tested in this study, it could be considered as a measure to increase the fraction of tidal flats and accelerate morphological development toward equilibrium. The magnitude, timing, and effectiveness of such interventions remain uncertain, particularly under conditions with river discharge, which may shift the system back toward ebb dominance.

Answer to main research question

"How can a dynamically stable tidal lake be developed in the Delta21 project by optimizing inlet (storm surge barrier) size considering long-term morphological evolution under sea level rise and varying river discharge?"

A dynamically stable tidal lake within the Delta21 project can be developed only when the inlet is designed wide enough to allow the system to import sediment and adjust toward an equilibrium state. The results show that an inlet width of approximately 2000 m is required to approach such stability. Narrower inlets remain ebb-dominant and continue exporting sediment, preventing the system from developing toward a sustainable morphological configuration. Managing river discharge is equally important, as the presence of river inflow reinforces ebb dominance and limits the capacity of the lake to retain sediment. When river discharge cannot be avoided, additional sediment management becomes necessary to counteract the resulting sediment deficit.

Sea level rise further strengthens the long-term tendency for sediment loss, while extreme river discharges mainly cause short-term redistribution without altering the net export of sediment. This behavior highlights the limited ability of the system to naturally evolve toward a dynamic equilibrium under the combined influence of sea level rise and variable river inflow.

Because the system's natural equilibrium would contain roughly 88% tidal flats (far more than the current 20%) active intervention is required to accelerate morphological development. Targeted sediment placement in deeper areas can stimulate tidal flat formation and help guide the system toward its equilibrium state, even when river discharge or inlet geometry restrict natural development.

In practice, achieving a dynamically stable tidal lake therefore requires a combination of measures: designing a wide inlet that maintains flow velocities near the threshold for sediment transport, limiting or compensating river inflow, and strategically placing sediment to support tidal flat growth. Together, these actions create the conditions under which the tidal lake can evolve toward long-term morphological stability despite sea level rise and variable hydrodynamic forcing.

8.2. Recommendations

This thesis is finalized with a number of suggestions for potential future work. Future research on the Delta21 tidal lake should focus on both improving the modeling approach and enhancing the understanding of key morphological and hydrodynamic processes that were simplified in this study.

Use of 3D-model
One of the most significant improvements would be the implementation of a three-dimensional model. The current depth-averaged approach limits the representation of vertical stratification, density-driven flows, and detailed velocity profiles. A three-dimensional model would also allow the inclusion of multiple 10 layers and grain sizes, which is increasingly relevant as mud content becomes more significant in the tidal lake. This approach would enable a more realistic simulation of cohesive and non-cohesive sediment interactions and improve predictions of channel stability and tidal flat development.

The tidal forcing applied in this research was simplified, lacking spring-neap cycles and higher-order constituents. Introducing a complete tidal signal, including seasonal and extreme variations, would improve the accuracy of modeled flow velocities and sediment transport patterns. Similarly, incorporating realistic, time-varying river discharges, including sediment loads, would better represent the hydrodynamic forcing on the system. Local wind and wave conditions, which were neglected in this study, can significantly affect sediment resuspension, sandbank stability, and intertidal flat development. Coupling a hydrodynamic model with a wave model under representative wind conditions would provide a more realistic representation of local morphodynamic processes.

Explore alternative inlet lay-outs
From a design perspective, further studies should explore alternative inlet layouts, including more onshore locations, multiple inlets, or variable cross-sections. These variations could improve morphodynamic stability, optimize tidal exchange, and reduce maintenance dredging. The interaction between inlet design and sediment placement strategies should also be investigated in detail to accelerate tidal flat growth in deeper parts of the lake. High-resolution modeling of morphological features such as ebb- and flood-tidal deltas, sandbanks, and channels is recommended, using grid resolutions of 10x10 m^2 or finer. Such detailed studies would allow for better evaluation of small-scale processes that are critical for the ecological functioning of the Natura2000 area. Sensitivity analyses of observation point placement and grid alignment should also be performed, as local sediment transport patterns can vary significantly with small changes in model setup.

Evaluate operational strategies
Operational strategies, such as the use of pumps, should be further evaluated. Water levels in the tidal lake during extreme river discharges could potentially be managed by the pumps, and future studies should quantify the capacity required and optimal timing to mitigate flooding or high-velocity erosion near the inlet. Similarly, the timing and location of sediment placement should be explored in more detail. Placing sediment in deeper areas can accelerate tidal flat development, but the effectiveness of these interventions depends on hydrodynamic conditions and the presence of river discharge, which can shift the system toward net sediment export. Understanding the interactions between inlet width, flow velocities, and sediment placement is crucial to guide the system toward its equilibrium state.

Overall, these recommendations highlight key areas where further research and more detailed modeling could improve understanding of the Delta21 tidal lake's morphodynamics and inform design decisions. By addressing the modeling simplifications, testing alternative inlet configurations, and investigating operational and sediment management strategies, future studies can provide guidance for the long-term development and management of the tidal lake.

References

Arcadis, Bureau Stroming, & OAK Consultants. (2024). Preverkenning biesbosch rijn-maasmonding. *Stroming*. https://open.rijkswaterstaat.nl/@270705/systeemanalyse-pagw-biesbosch-rijn/

Bosboom, J., & Stive, M. (2023). *Coastal dynamics* (version 1.2). TU Delft Open.

Colina Alonso, A. (2018). *Morphodynamics of the haringvliet ebb-tidal delta* [Master's Thesis]. Delft University of Technology. https://repository.tudelft.nl/record/uuid:f46c3394-ac26-43b5-9338-21b202703961

de Vries, M. J. (2007). *Morphological modelling of the haringvlietmonding using delft3d* [Master's Thesis]. Delft University of Technology.

Delta21. (2023). *Stand van zaken delta21* (tech. rep.). Delta21.

Deltares. (2025, October). *Delft3d-flow: Simulation of multi-dimensional hydrodynamic flows and transport phenomena, including sediments. user manual: Hydro-morphodynamics* [DRAFT version]. Version 4.07.01. Deltares. Delft, The Netherlands. https://oss.deltares.nl/web/delft3d/manuals

Dronkers, J. (1986). Tidal asymmetry and estuarine morphology. *Netherlands Journal of Sea Research*, *20*(2-3), 117–131. https://doi.org/10.1016/0077-7579(86)90015-3

Dronkers, J. (2005). *Dynamics of coastal systems* (Vol. 25). World Scientific.

Escoffier, F. (1940). The stability of tidal inlets. *Shore and Beach*, *8*, 111–114. https://scispace.com/pdf/the-stability-of-tidal-inlets-4mfb0sx50f.pdf

Eysink, W. D., & Biegel, E. J. (1992). *Impact of sea level rise on the morphology of the wadden sea in the scope of its ecological function* (Technical Report No. H1300) (ISOS*2 Project, Phase 2). Delft Hydraulics. Delft.

Friedrichs, C. T., & Aubrey, D. G. (1988). Non-linear tidal distortion in shallow well-mixed estuaries: A synthesis. *Estuarine, Coastal and Shelf Science*, *27*(5), 521–545. https://doi.org/10.1016/0272-7714(88)90082-0

Google LLC. (2025). Google earth [Accessed: 2025-05-14].

KNMI. (2023, October). *KNMI'23 klimaatscenario's voor Nederland. Gebruikersrapport* (KNMI-publicatie No. 23-03) (Eindredactie: B. Overbeek en R. van Dorland. Gepubliceerd op 9 oktober 2023.). Koninklijk Nederlands Meteorologisch Instituut (KNMI). De Bilt, Nederland. https://www.knmi.nl/klimaatscenarios

Masson-Delmotte, V., Zhai, P., Pirani, A., Connors, S. L., Péan, C., Berger, S., Caud, N., Chen, Y., Goldfarb, L., Gomis, M. I., Huang, M., Leitzell, K., Lonnoy, E., Matthews, J. B. R., Maycock, T. K., Waterfield, T., Yelekçi, O., Yu, R., & Zhou, B. (Eds.). (2021). *Climate change 2021: The physical science basis* [Contribution of Working Group I to the Sixth Assessment Report of the Intergovernmental Panel on Climate Change]. Cambridge University Press. https://doi.org/10.1017/9781009157896

Rijkswaterstaat. (2015). *Deltawerk haringvlietsluizen* [Last modified on 2025-03-03]. Retrieved June 23, 2025, from https://www.rijkswaterstaat.nl/water/waterbeheer/bescherming-tegen-het-water/waterkeringen/deltawerken/haringvlietsluizen

Rijkswaterstaat. (2024). Bathymetrie nederland – binnenwateren 1 mtr. [Retrieved July 22, 2025 from https://geoweb.rijkswaterstaat.nl/ModuleViewer/?app=d22bec5b3e3244b19cdd20b308442683].

Rijkswaterstaat. (2025a). *Matroos timeseries viewer* [Accessed: June 24, 2025]. https://noos.matroos.rws.nl/timeseries/start/

Rijkswaterstaat. (2025b). Rijkswaterstaat waterwebservices – getijgegevens [Toegang via Waterinfo; CC0-licentie. Zie "WATHTBRKD" grootheid voor astronomisch getij.]. https://waterwebservices.rijkswaterstaat.nl/

Rijkswaterstaat. (2025c, January). Bathymetrie nederland – kust en vaklodingen 20 mtr [Gebaseerd op metingen tot en met 2024, $RD_N AP - cordinaten. Opgevraagdjuli 22, 2025$]. https://maps.rijkswaterstaat.nl/dataregister-publicatie/srv/eng/catalog.search#/metadata/4f208f35-1ca6-4558-9498-0eabf845a92e

Roelvink, J. (1999). *Kleinschalig morfologisch onderzoek mv2 fase 1b: Gevoeligheidsonderzoek* (Technical report). WL Delft Hydraulics, TU Delft. https://repository.tudelft.nl/file/File_3d53acbf-0432-4401-8b50-f18e7821701e

Steijn, R., Eysink, W., van Holland, G., & van de Graaff, J. (2001). *Bandbreedte morfologische effectvoorspelling – mv2: Een onderzoek ten behoeve van natuurtypering* (Technical report). Alkyon, WL Delft Hydraulics.

Storm, K., Kuijpers, J., & Harmsen, C. (2006). Eb… en weer vloed in het haringvliet. *Landschap*, *23*(4), 198–207. https://www.landschap.nl/wp-content/uploads/2006-4_198-207.pdf

van Cappellen, L., Bakker, C., Bongaerts, M., Bouwman, P., & Vendrik, J. (2024, February). *Delta21: Energetisch-economische analyse. valmeer als onderdeel van duurzaam energiesysteem* (tech. rep. No. 23.230192.182)

(Opdrachtgevers: Verboon Maasland (2023), Provincie Zuid-Holland (2024)). CE Delft. Delft. https://www.ce.nl

van Horick, Q. R. B. (2023, January). *Design of the navigation and discharge channel in the tidal lake of the delta21 project: A design and morphological modelling study* [Master's Thesis]. Delft University of Technology. https://repository.tudelft.nl/record/uuid:c3a7d367-3627-4e7d-93a3-1d9f4b565643

Van De Kreeke, J., & Robaczewska, K. (1993). Tide-induced residual transport of coarse sediment; application to the ems estuary. *Estuarine, Coastal and Shelf Science*, *31*(3), 209–220. https://doi.org/10.1016/0077-7579(93)90022-K

Van Rijn, L. C. (2007a). Unified view of sediment transport by currents and waves. i: Initiation of motion, bed roughness, and bed-load transport. *Journal of Hydraulic Engineering*, *133*(6), 649–667. https://doi.org/10.1061/(ASCE)0733-9429(2007)133:6(649)

Van Rijn, L. C. (2007b). Unified view of sediment transport by currents and waves. ii: Suspended transport. *Journal of Hydraulic Engineering*, *133*(6), 668–689. https://doi.org/10.1061/(ASCE)0733-9429(2007)133:6(668)

Van Vessem, P. (1998). *Morphological modelling of the haringvliet mouth using delft3d* (tech. rep.). WL | Delft Hydraulics. Delft, The Netherlands.

Wateren and Programmatische Aanpak Grote. (2024). Analyse van het ecologische systeem van de biesbosch rijn-maasmonding.

Waterwet Overheid. (2024). Besluit beheer haringvlietsluizen [Geraadpleegd op 23 juni 2025 via wetten.overheid.nl].

Wit, J. d., Chamuleau, T., Winter, H., Breukelaar, A., Beijk, V., & Goes, R. (2011). *Andere mogelijkheden voor het besluit beheer haringvlietsluizen: Een verkennende studie naar verbetering van de vismigratie tussen de noordzee en het rijn- en maasstroomgebied bij het intrekken van het kierbesluit* (tech. rep. No. 438070) (Met lit. opg.; WD0511ZH038). Ministerie van Infrastructuur en Milieu / Rijkswaterstaat, Waterdienst; IMARES, Wageningen UR. https://zoek.officielebekendmakingen.nl/blg-120660.pdf

Zaldivar Piña, M. I. (2020, October). *Stability of intertidal and subtidal areas after delta21 plan: Evaluating the consequences for the morphological development produced by the intervention* [Master's thesis]. Delft University of Technology. http://repository.tudelft.nl/

A
Model results

In this appendix, additional Delft3D output figures and supplementary graphs are presented. These figures were not included in the main research report but serve as supporting material to substantiate the analyses and conclusions.

Schematization 1B

Full 366 days run with a morphological factor of 1. No Delta21 construction and no river discharge.

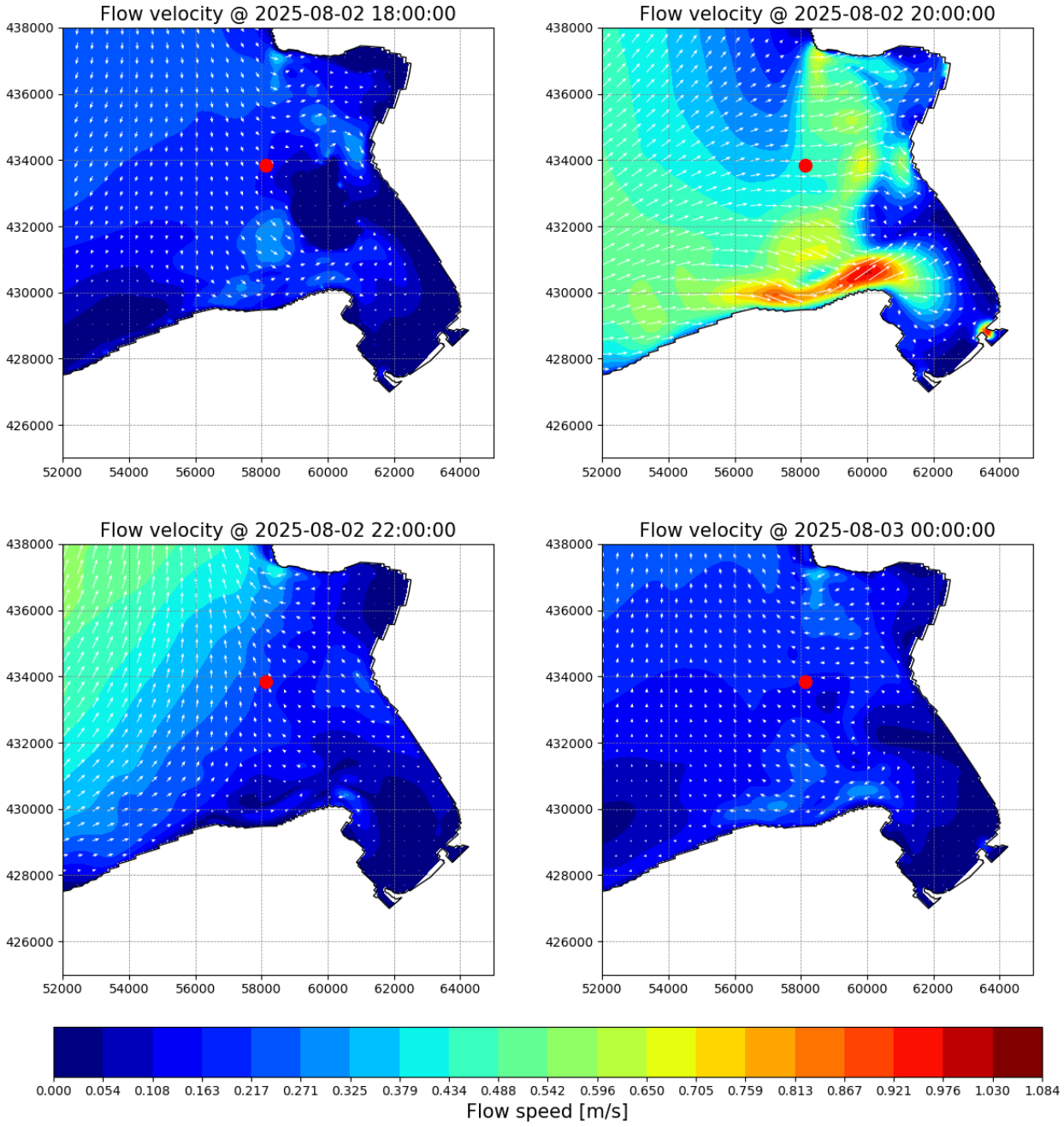

Figure A.1: Four different phases in one tidal cycle of run 1B

Schematization 1A

37.5 days run with a morphological factor of 10. No Delta21 construction and no river discharge.

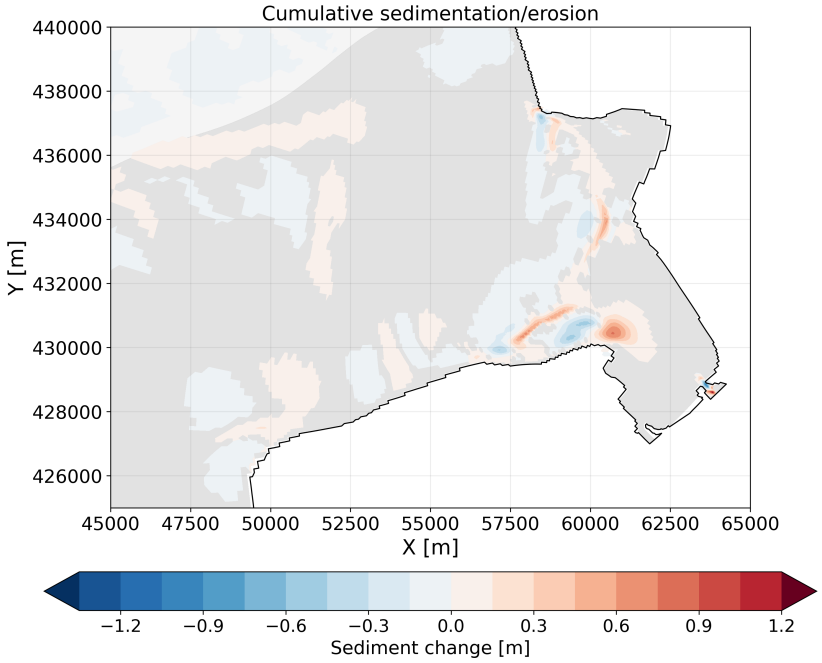

Figure A.2: Cumulative sedimentation and erosion pattern of run 1A

Schematization 1B

366 days run with a morphological factor of 1. No Delta21 construction and no river discharge.

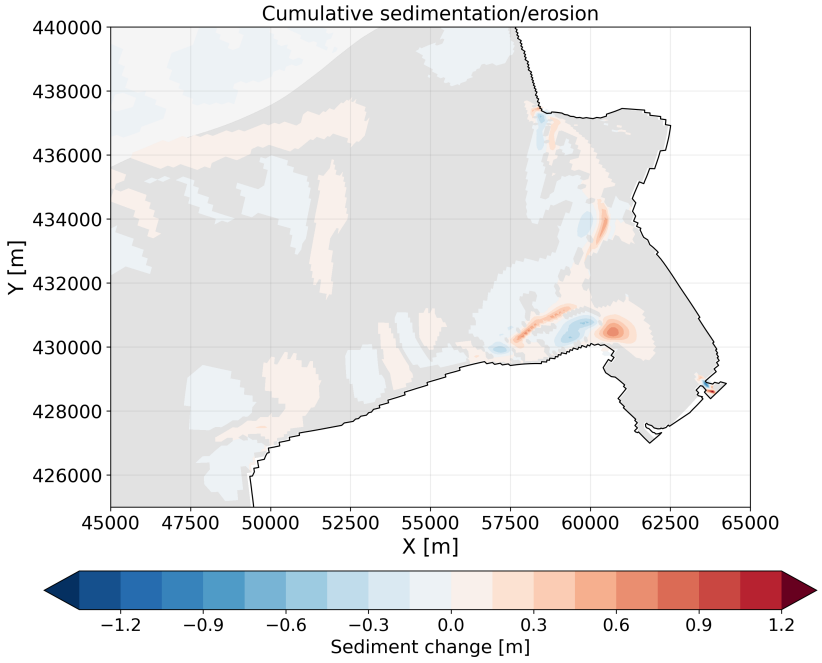

Figure A.3: Cumulative sedimentation and erosion pattern of run 1B

Schematization 1C

12.2 days run with a morphological factor of 30. No Delta21 construction and no river discharge.

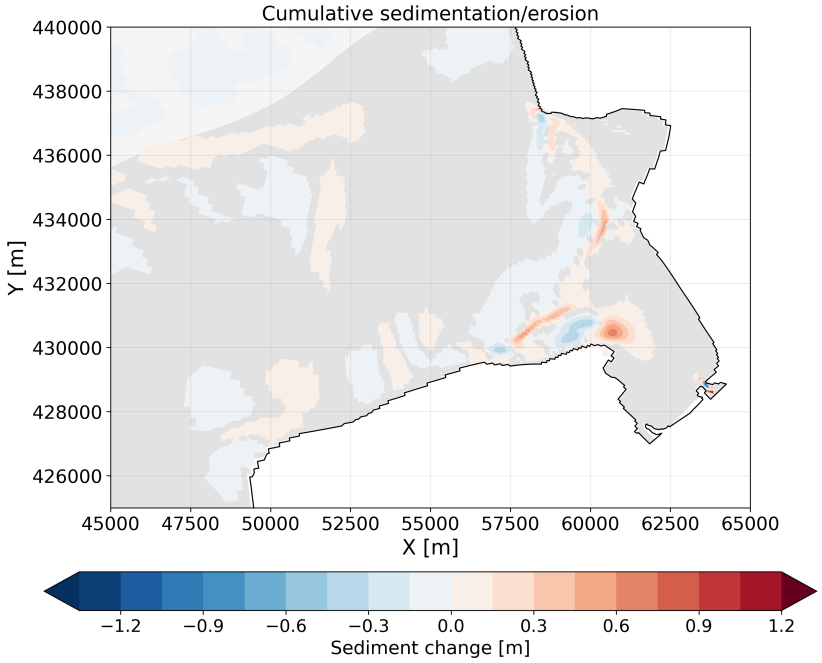

Figure A.4: Cumulative sedimentation and erosion pattern of run 1C

Schematization 1D

7.3 days run with a morphological factor of 50. No Delta21 construction and no river discharge.

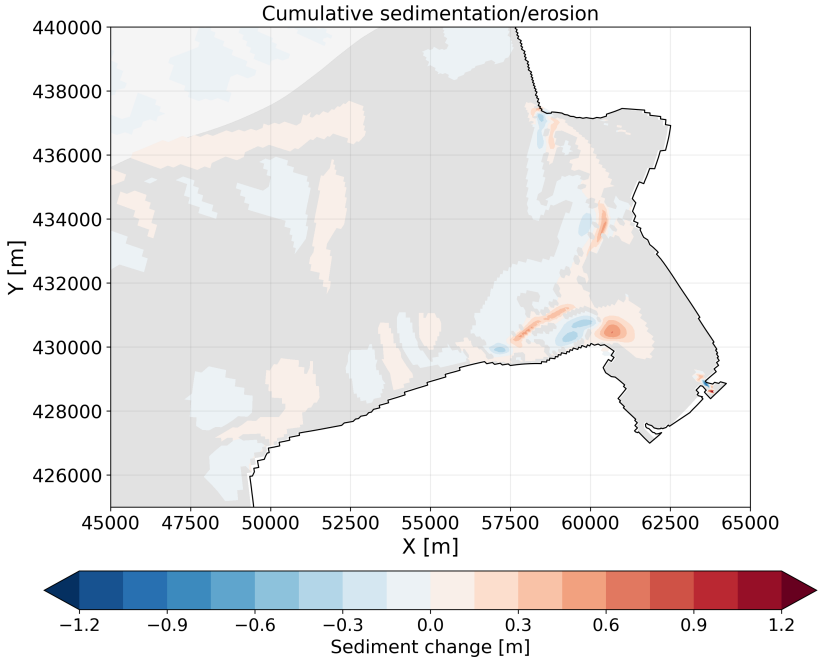

Figure A.5: Cumulative sedimentation and erosion pattern of run 1D

Schematization 2A

37.5 days run with a morphological factor of 10. Including the Delta21 construction with an inlet width of 1500 m and no river discharge.

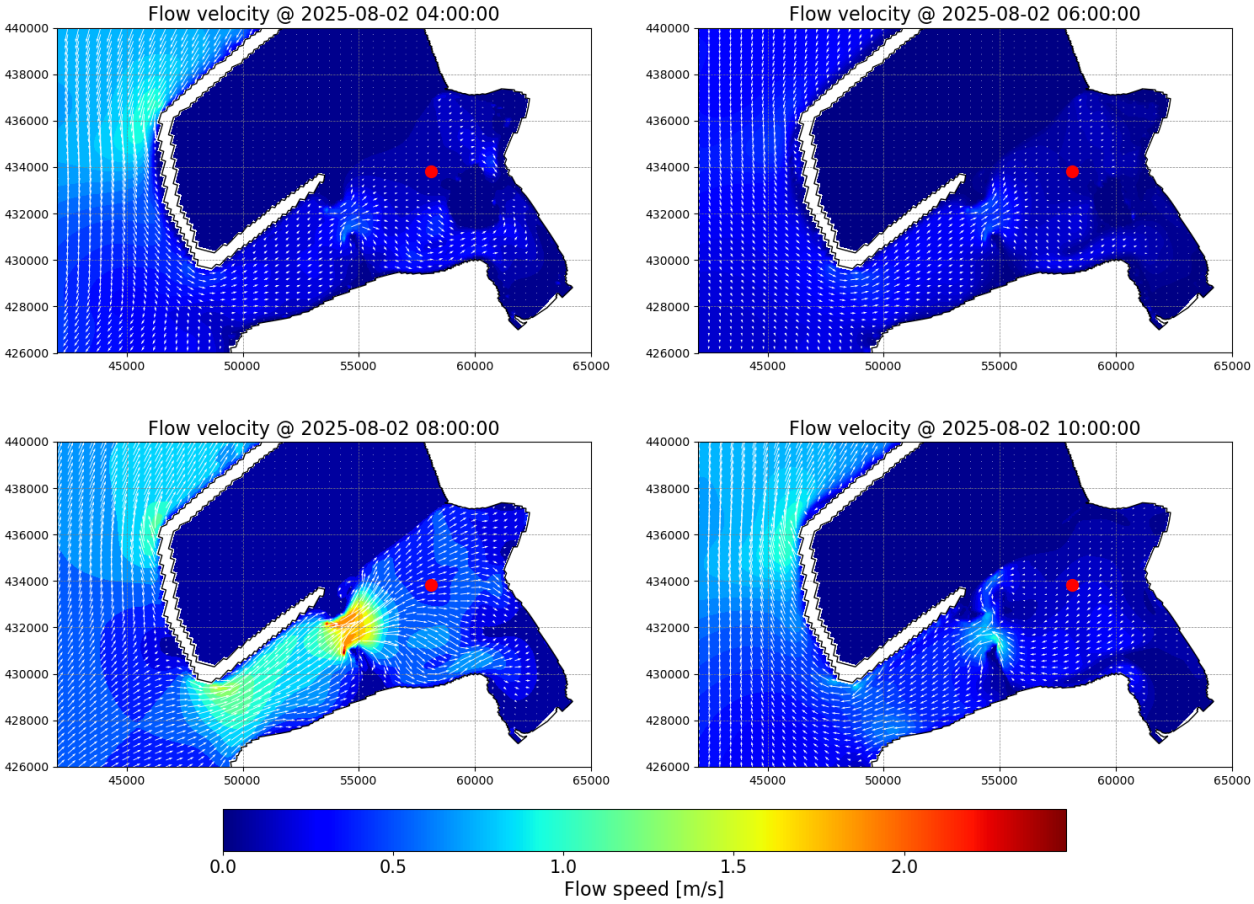

Figure A.6: Four different phases in one tidal cycle of run 2A

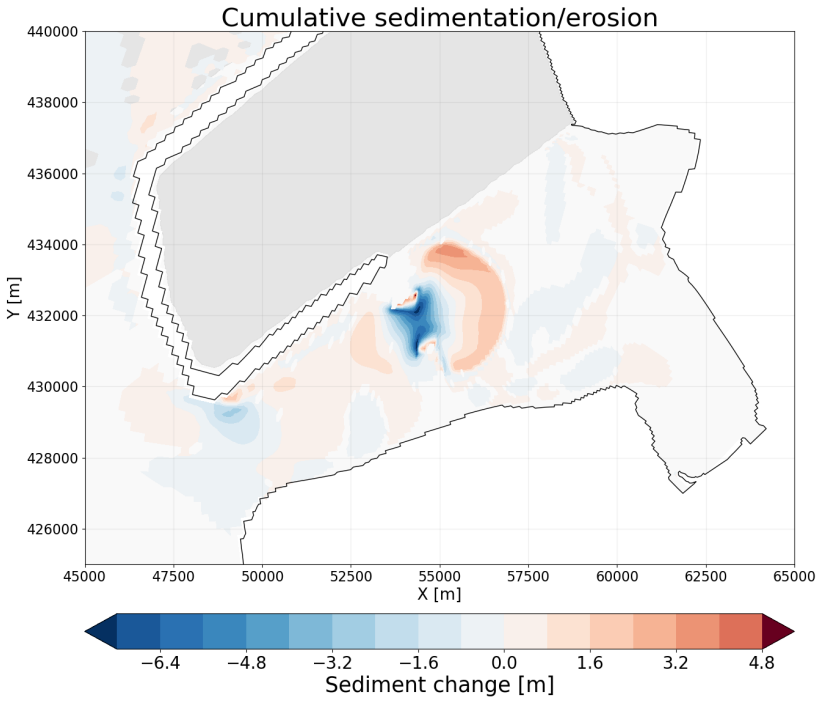

Figure A.7: Cumulative sedimentation and erosion pattern of run 2A

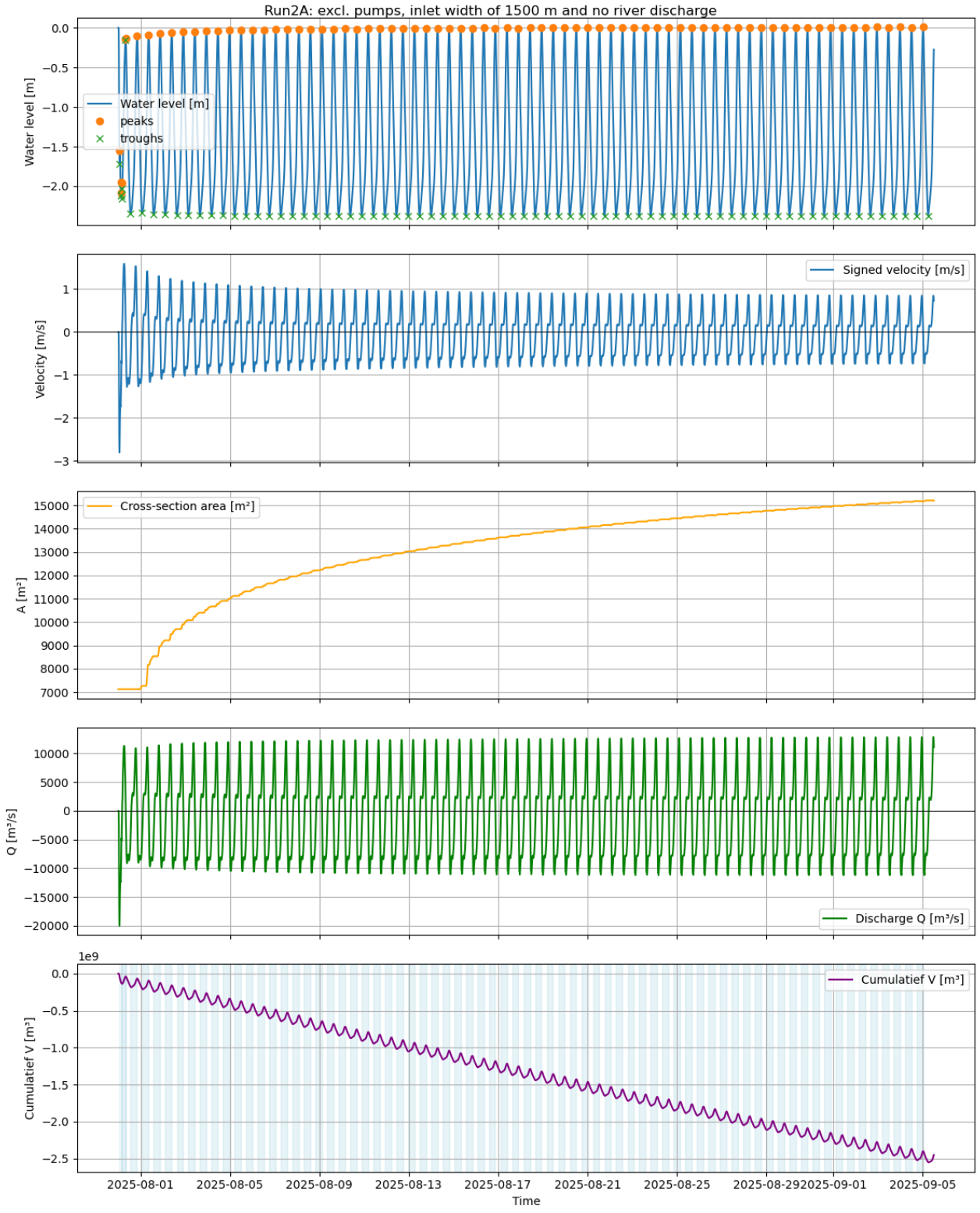

Figure A.8: Full analysis

Schematization 3A

37.5 days run with a morphological factor of 10. Including the Delta21 construction with an inlet width of 1500 m, pumps and turbines and no river discharge.

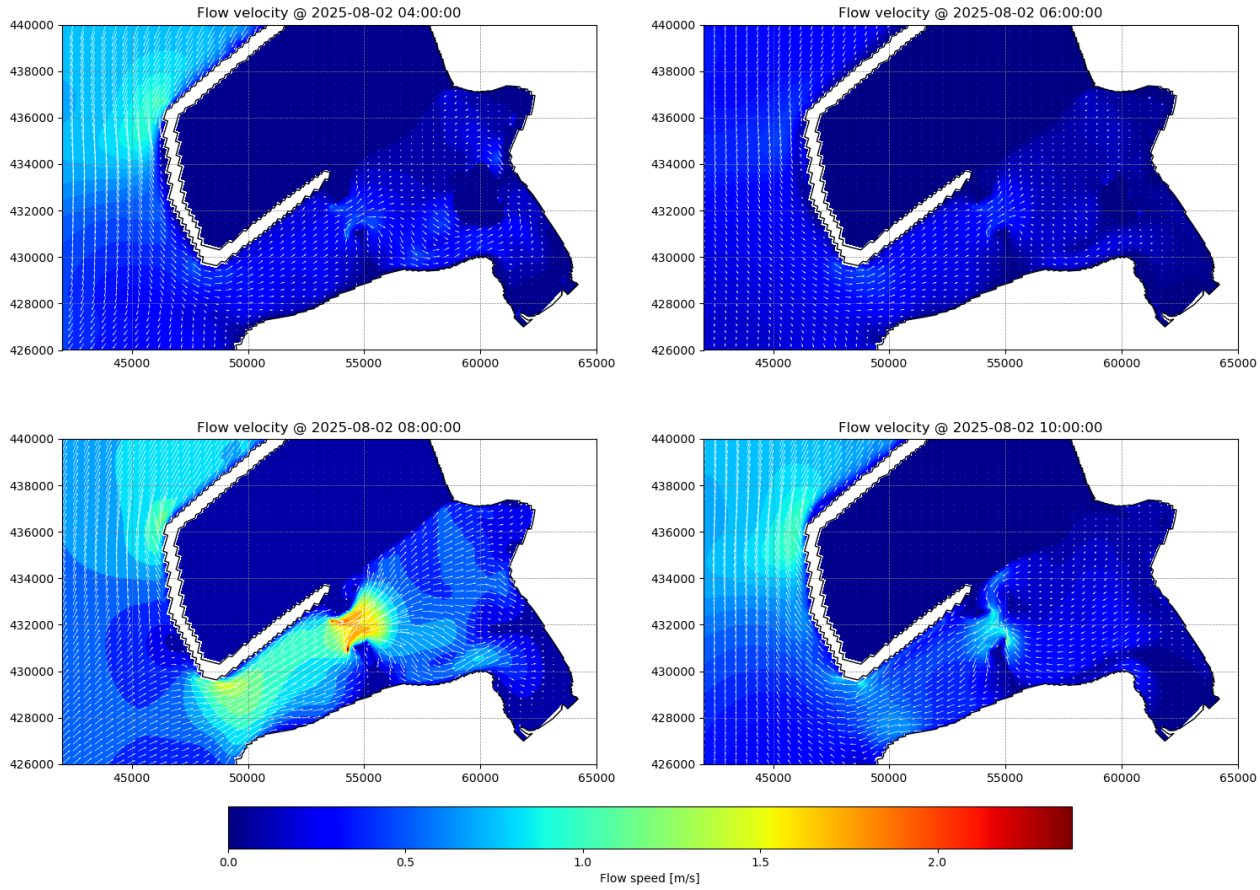

Figure A.9: Four different phases in one tidal cycle of run 3A

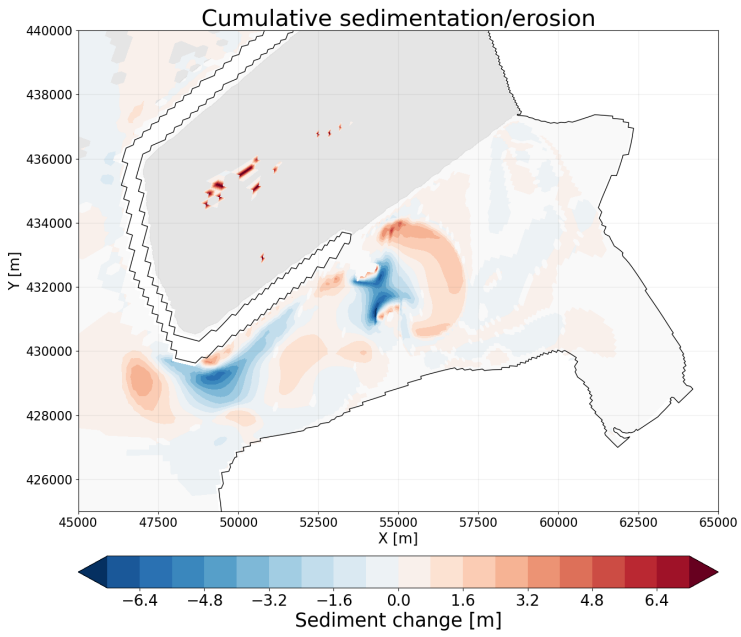

Figure A.10: Cumulative sedimentation and erosion pattern of run 3A

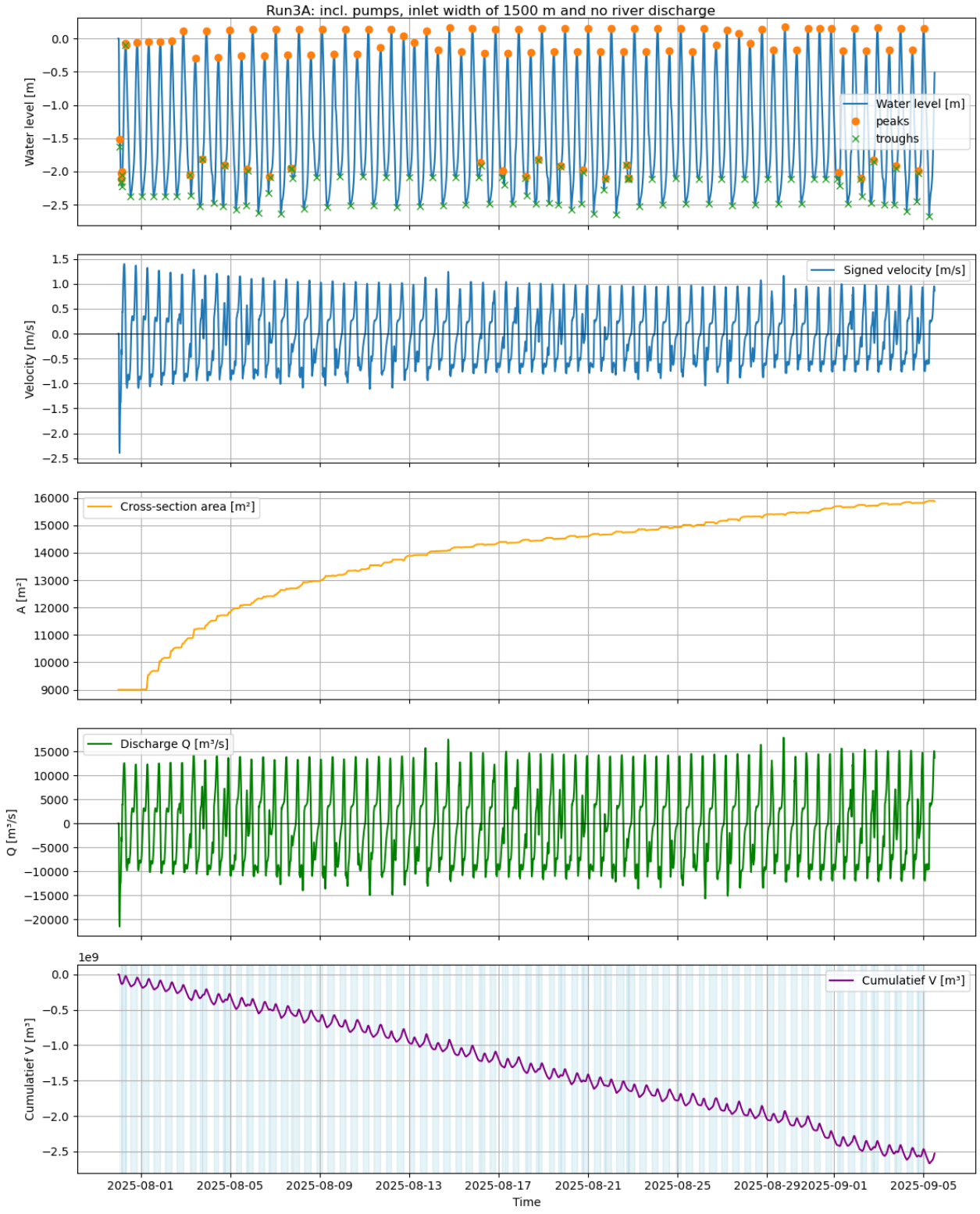

Figure A.11: Full analysis

Schematization 3B

37.5 days run with a morphological factor of 10. Including the Delta21 construction with an inlet width of 2000 m, pumps and turbines and no river discharge.

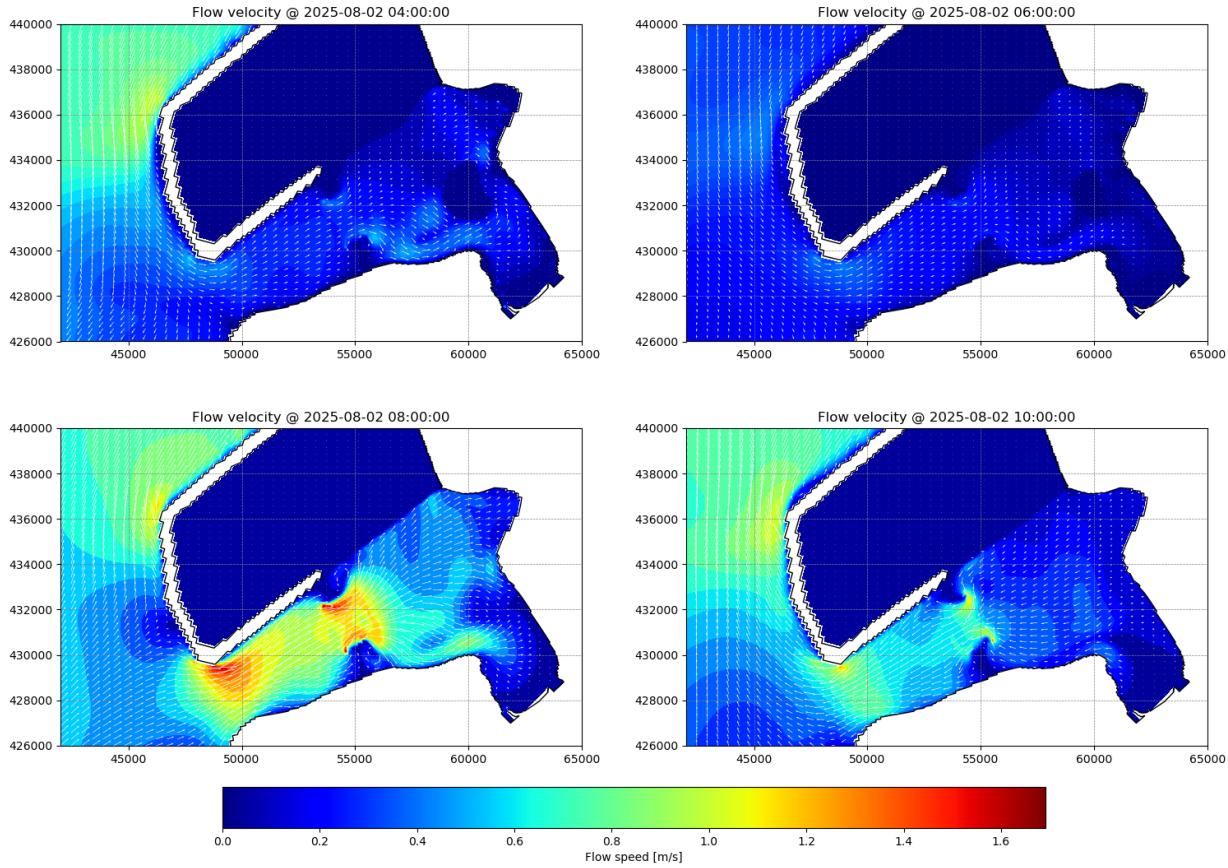

Figure A.12: Four different phases in one tidal cycle of run 3B

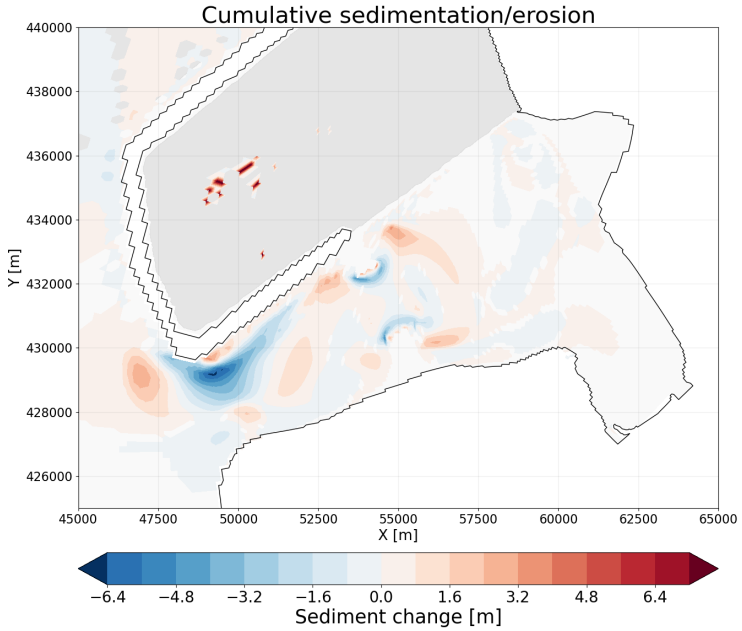

Figure A.13: Cumulative sedimentation and erosion pattern of run 3B

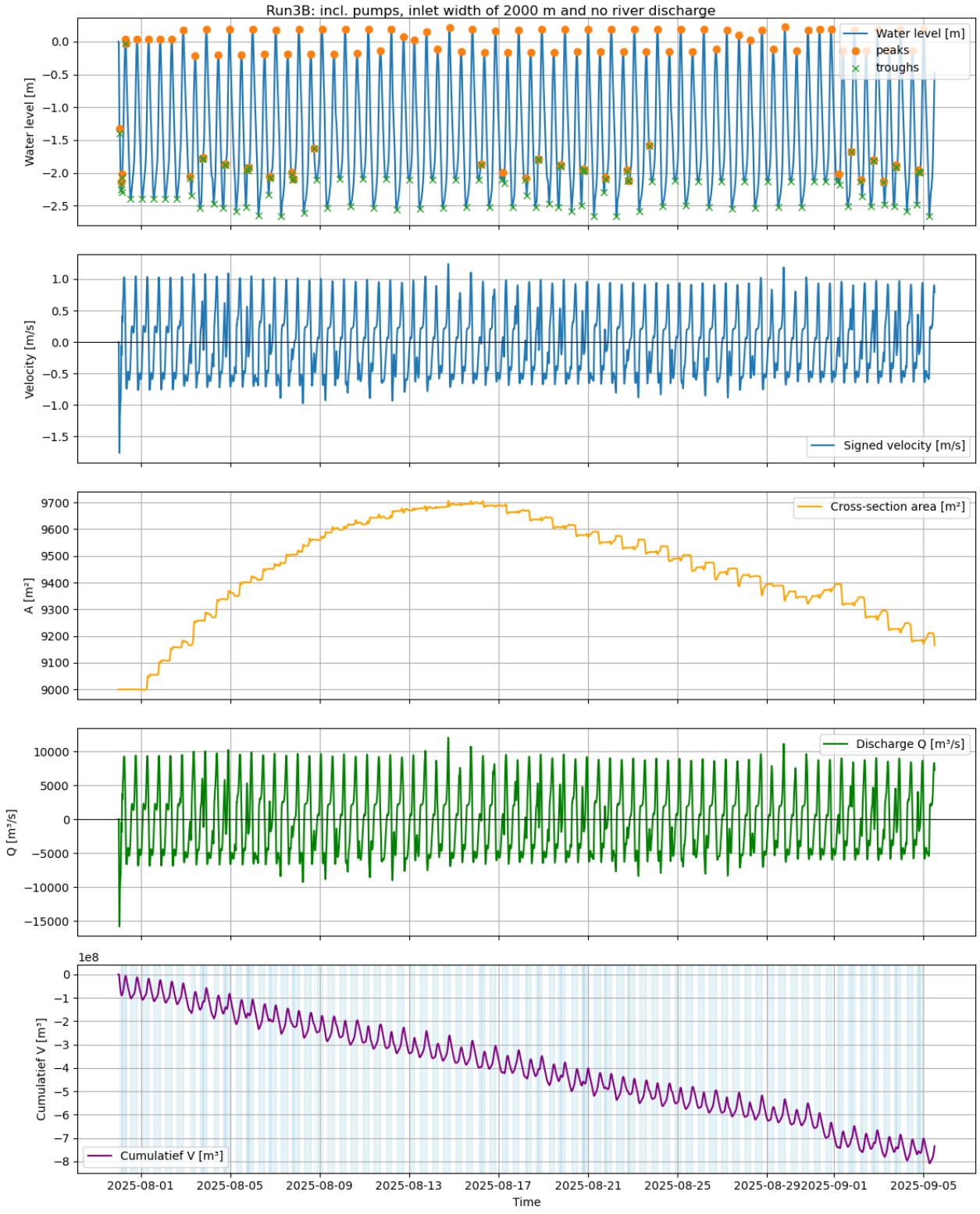

Figure A.14: Full analysis

Schematization 3C

37.5 days run with a morphological factor of 10. Including the Delta21 construction with an inlet width of 1000 m, pumps and turbines and no river discharge.

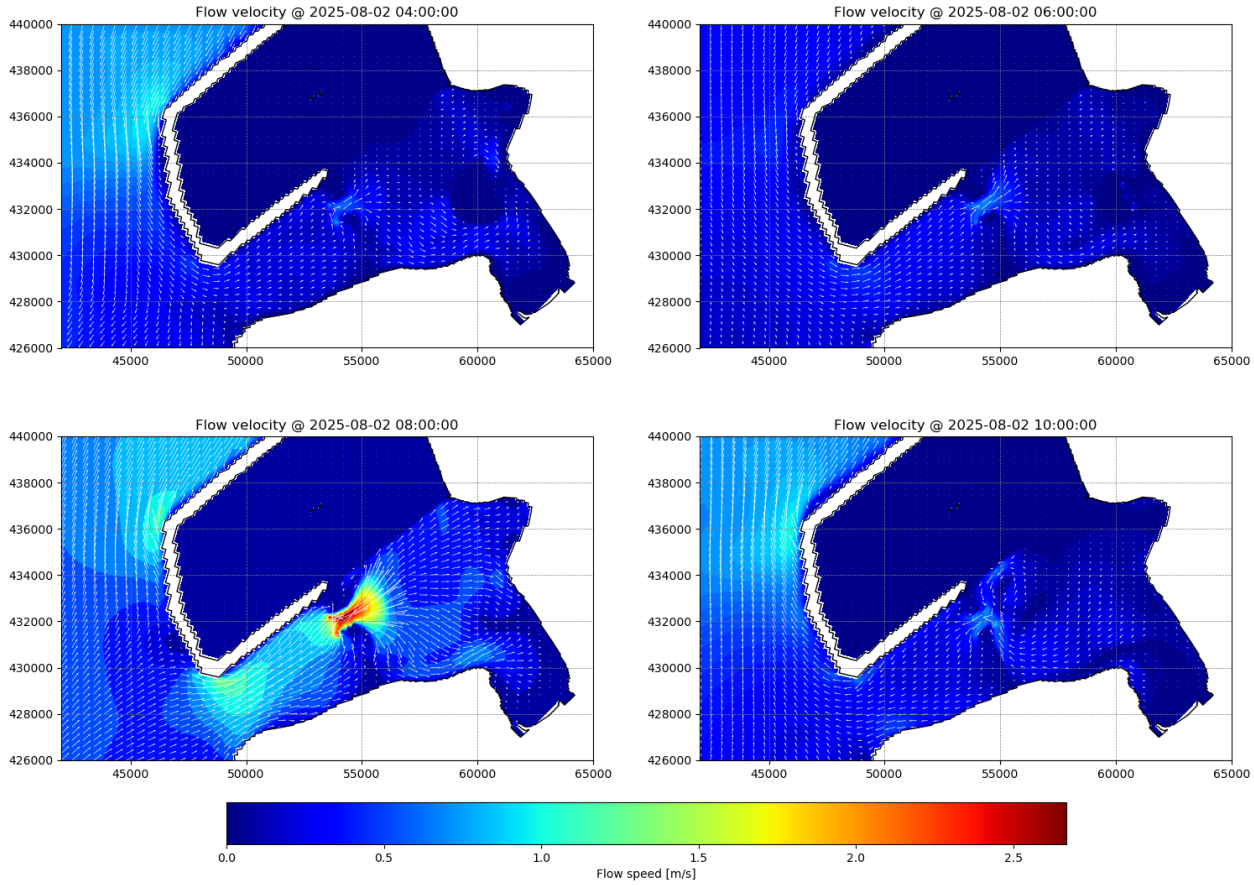

Figure A.15: Four different phases in one tidal cycle of run 3C

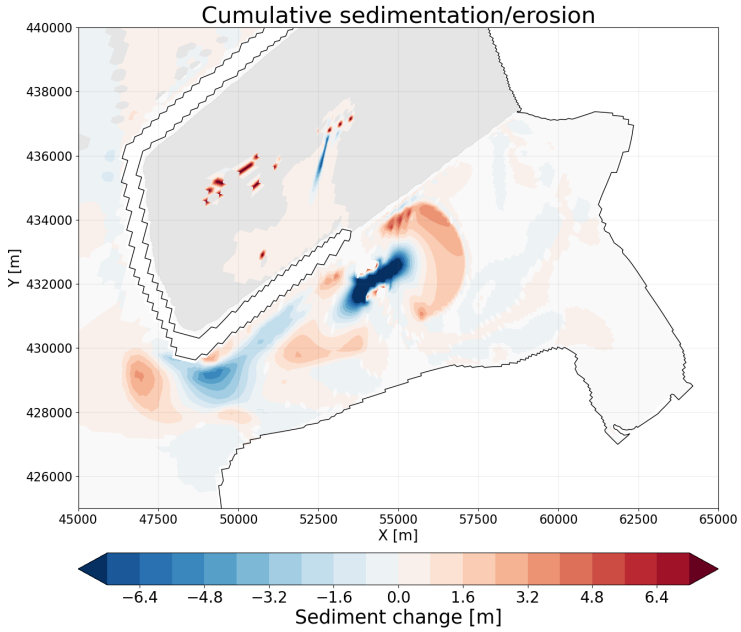

Figure A.16: Cumulative sedimentation and erosion pattern of run 3C

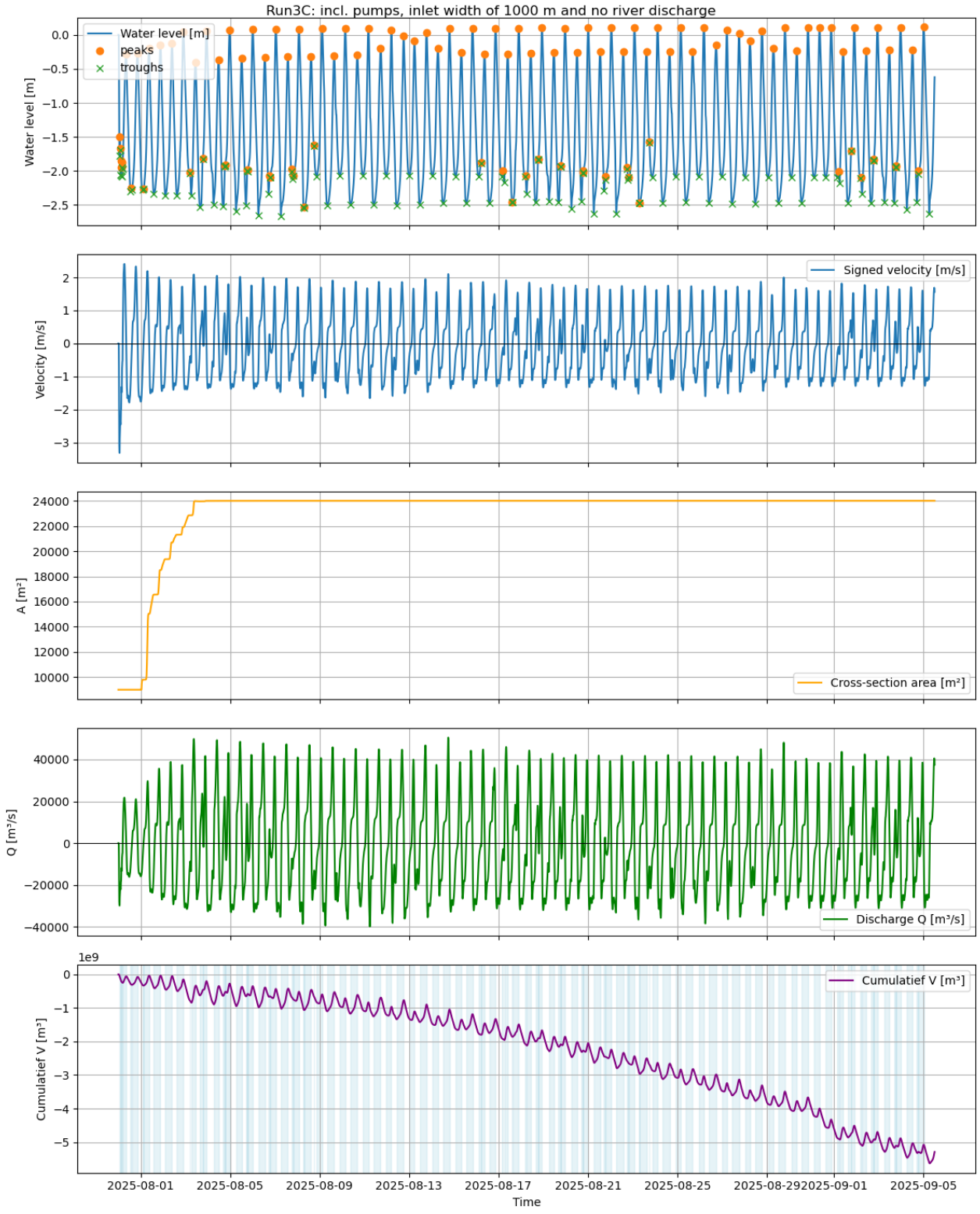

Figure A.17: Full analysis

Schematization 4A

37.5 days run with a morphological factor of 10. Including the Delta21 construction with an inlet width of 1500 m, pumps and turbines and a river discharge of 1000 m^3/s.

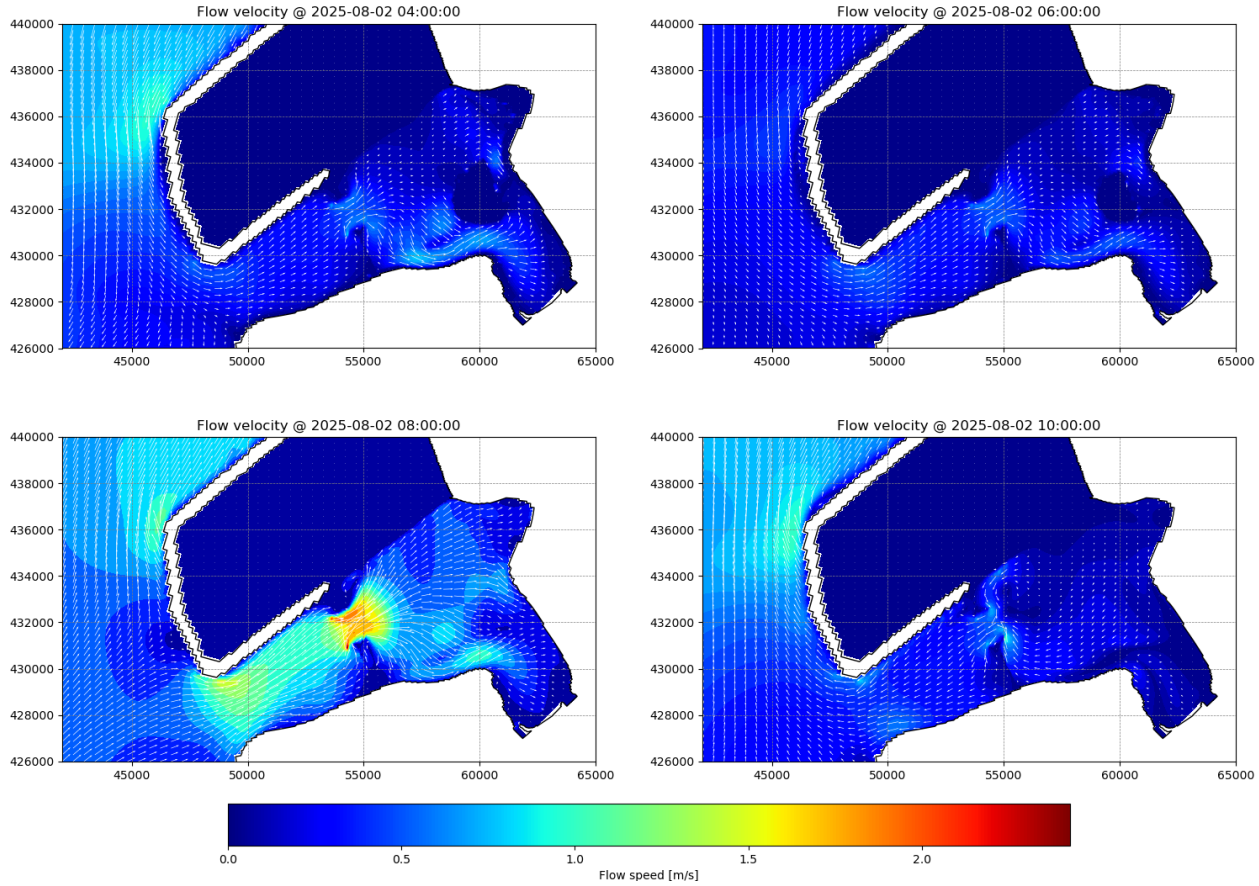

Figure A.18: Four different phases in one tidal cycle of run 4A

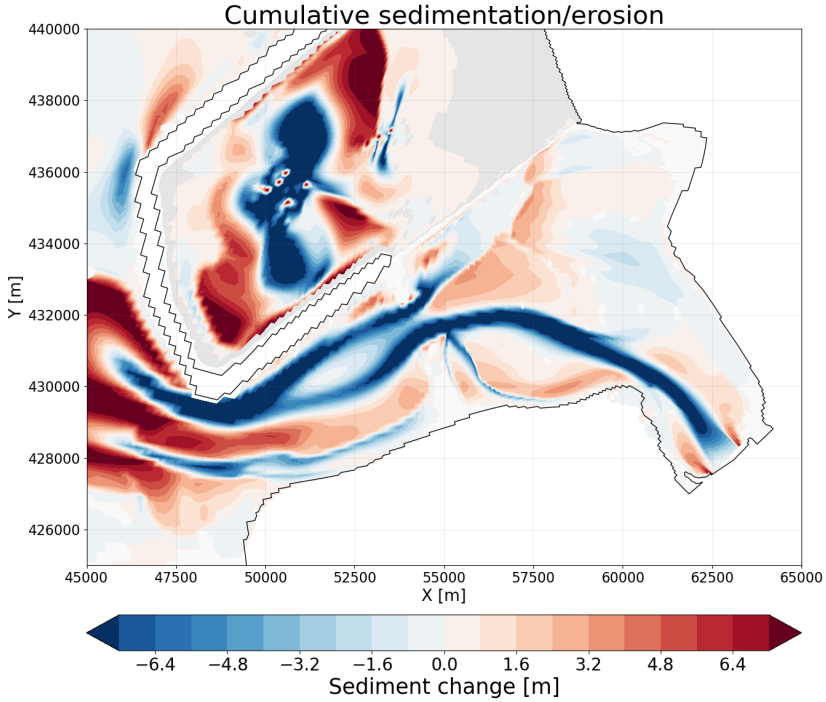

Figure A.19: Cumulative sedimentation and erosion pattern of run 4A

Schematization 4B

11 days run with a morphological factor of 1. Including the Delta21 construction with an inlet width of 1500 m, pumps and turbines and a river discharge of 5000 m^3/s.

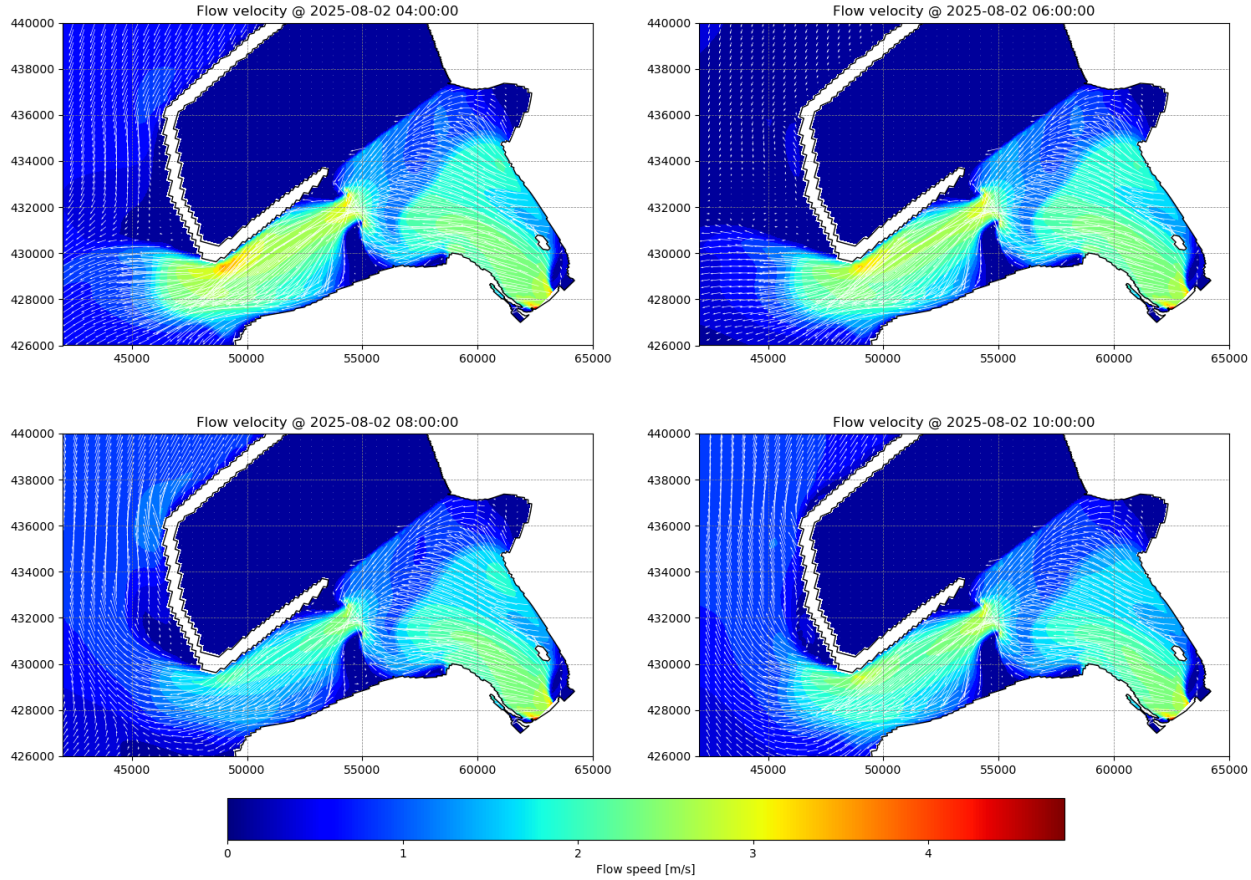

Figure A.20: Four different phases in one tidal cycle of run 4B

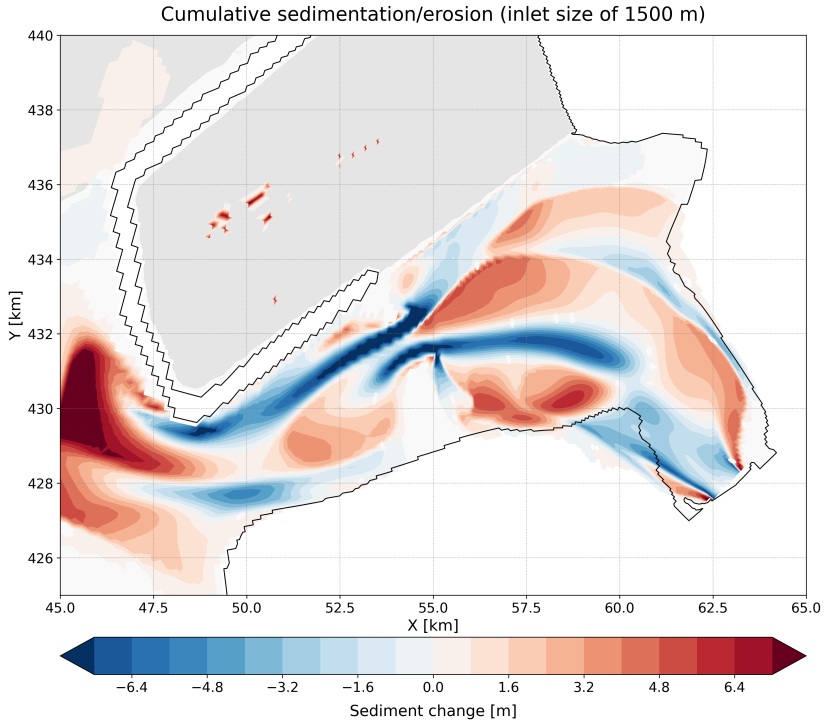

Figure A.21: Cumulative sedimentation and erosion pattern of run 4B

Schematization 4C

37.5 days run with a morphological factor of 10. Including the Delta21 construction with an inlet width of 2000 m, pumps and turbines and a river discharge of 1000 m^3/s.

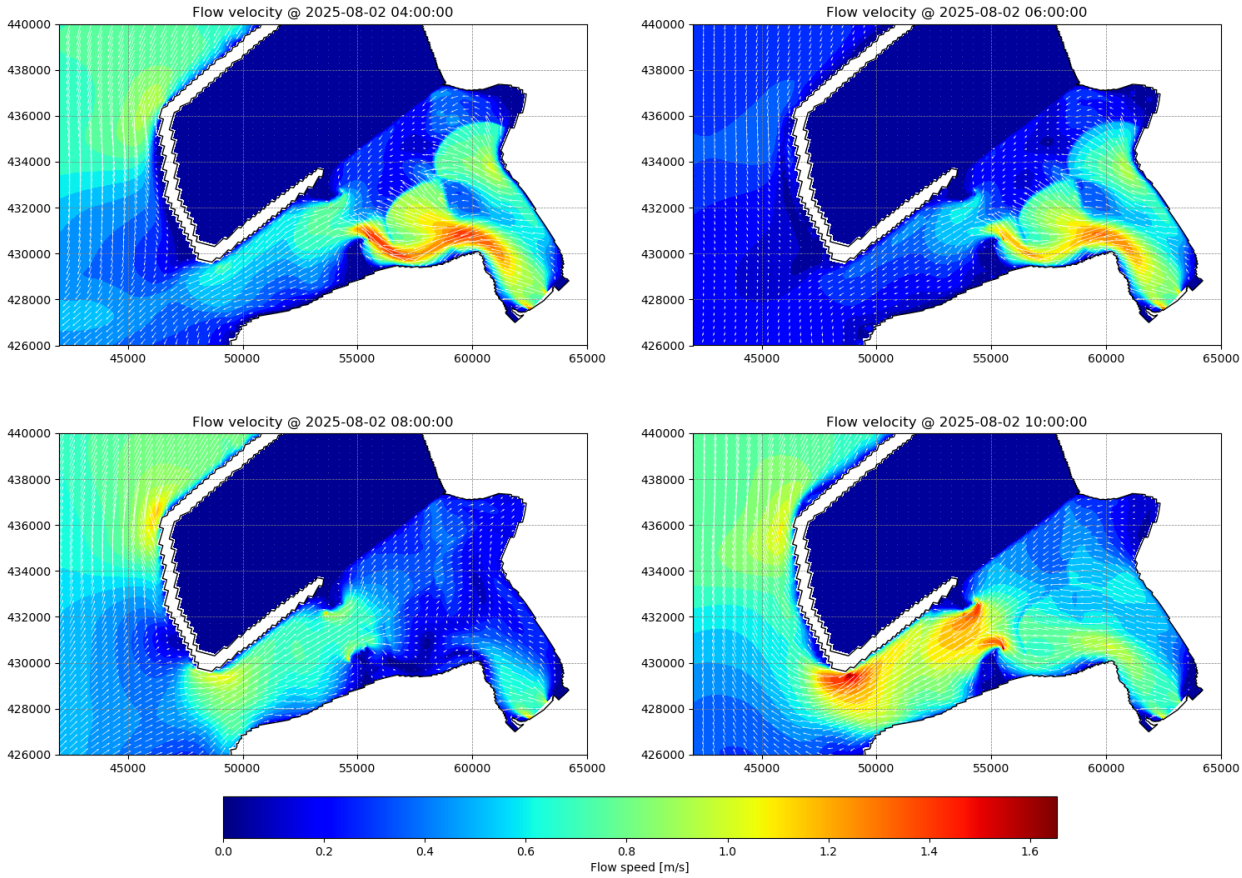

Figure A.22: Four different phases in one tidal cycle of run 4C

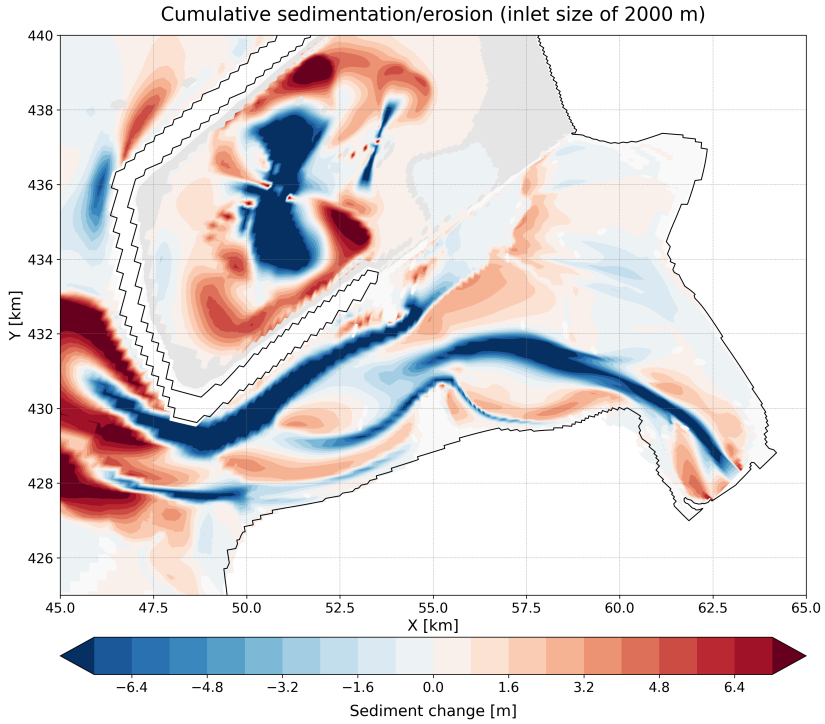

Figure A.23: Cumulative sedimentation and erosion pattern of run 4C

Schematization 4E

37.5 days run with a morphological factor of 10. Including the Delta21 construction with an inlet width of 1000 m, pumps and turbines and a river discharge of 1000 m^3/s.

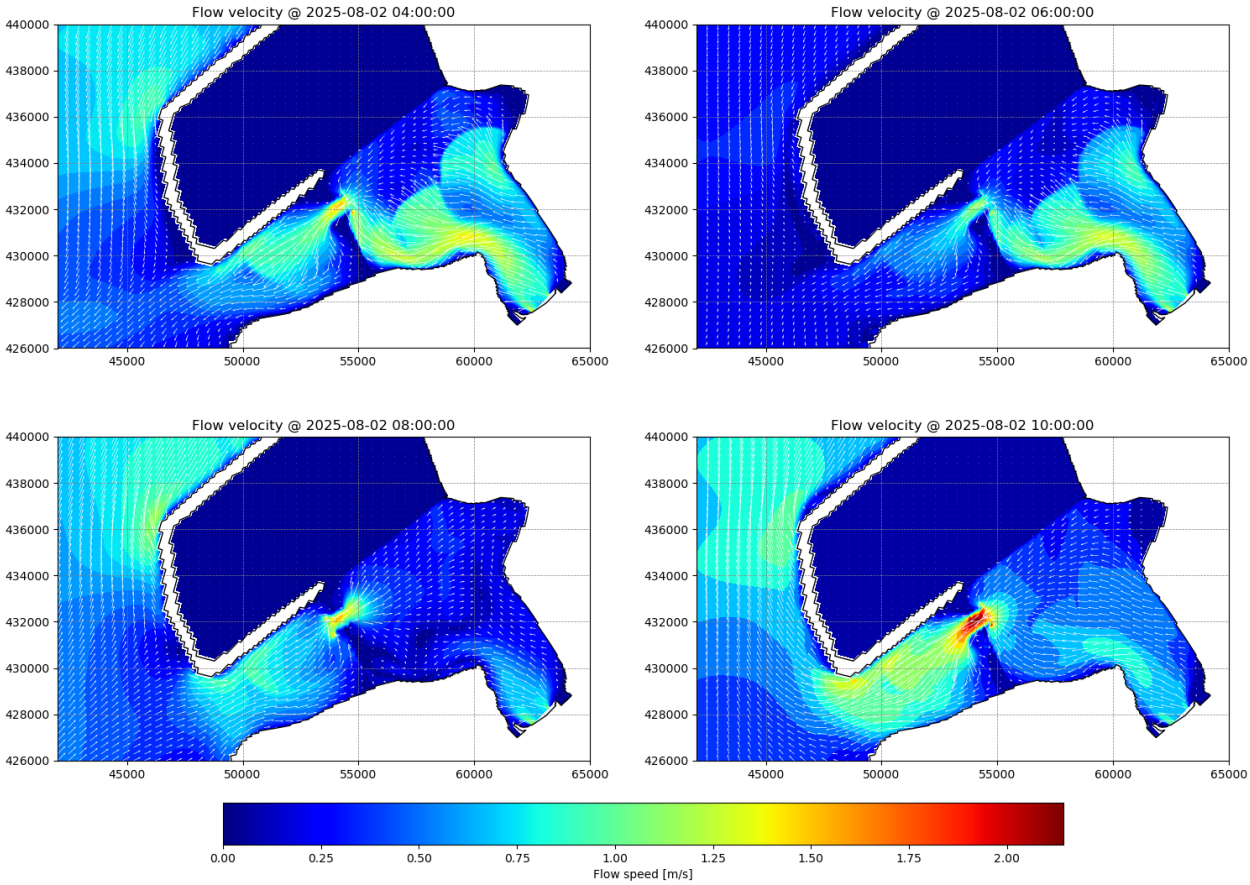

Figure A.24: Four different phases in one tidal cycle of run 4E

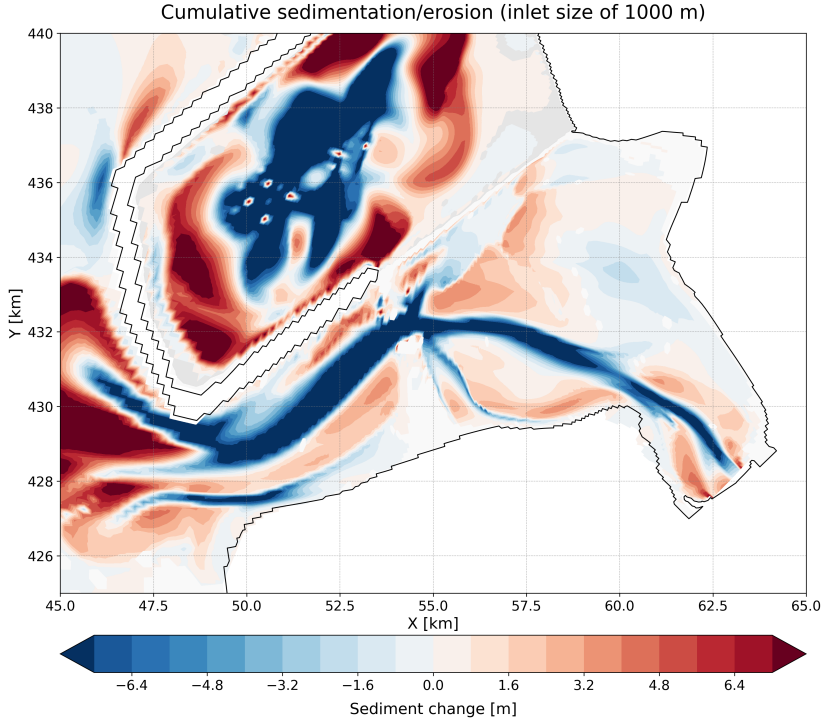

Figure A.25: Cumulative sedimentation and erosion pattern of run 4E